Control System for Doubly Fed Induction Generator Based Wind Energy Conversion System

by

Aman Abdulla Tanvir

A Thesis Submitted to
Saint Mary's University, Halifax, Nova Scotia
in Partial Fulfillment of the Requirements for
the Degree of Masters of Science in Applied Science

June, 2016, Halifax, Nova Scotia

Approved:	Dr. Adel Merabet Supervisor
Approved:	Dr. Rachid Beguenane Co-Supervisor
Approved:	Dr. Jason Gu Examiner
Approved:	Dr. Jason Rhinelander Reader
Date:	June 30, 2016

Abstract

Control System for Doubly Fed Induction Generator

Based Wind Energy Conversion System

by Aman Abdulla Tanvir

Abstract: This thesis deals with the analysis, modeling, and control of the doubly-fed induction machine used as a wind turbine generator. The energy efficiency of wind turbine systems equipped with doubly-fed induction generators are compared to other wind turbine generator systems. Moreover, two controlling methods of variable-speed wind turbine system using a doubly-fed induction generator are analyzed and validated experimentally. In addition, artificial neural network (ANN) is used to estimate the rotor position in model reference adaptive system (MRAS) based speed estimation technique.

June 30, 2016.

Acknowledgement

The author is obliged to his supervisor Dr. Adel Merabet for his diligent guidance, inspiration and patience all through the dissertation work. Special thanks are due to Canada Foundation of Innovation for the Grant 30527; Faculty of Graduate Studies and Research, Saint Mary's University for funding the research and Government of Nova Scotia for Nova Scotia Graduate Scholarship.

The author records his sincere thanks to his co-supervisor Dr. Rachid Beguenane and committee member Dr. Jayson Rhinelander for providing support and carefully reviewing this dissertation.

The author is indebted to his family and friends who have been a source of encouragement and motivation to complete this work. He wants to dedicate the effort done in this dissertation to his late grandmother who always loved him and sheltered him.

Table of Contents

List of Illustration

List of Abbreviation

Acronyms	Description
IM	Induction Machine
DFIM	Doubly Fed Induction Machine
DFIG	Doubly Fed Induction Generator
SCIG	Squirrel Cage Induction Generator
MRAS	Model Reference Adaptive System
ANN	Artificial Neural Network
PJ	Peta Joules
kW	Kilo Watt
GW	Giga Watt
PWM	Pulse Width Modulation
DPC	Direct Power Control
DTC	Direct Torque Control
PDPC	Predictive Direct Power Control
PDTC	Predictive Direct Torque Control
IVS-DTC	Integral Variable Structure-Direct Power Control
AVR/PSS	Automatic Voltage Regulator/Power System Stabilizer
FRT	Fault Ride Through
IGBT	Insulated Gate Bipolar Transistor
FPGA	Field Programmable Gate Array
PI	Proportional Integral
RTS	Real Time Simulation
RCP	Rapid Control Prototyping
HIL	Hardware in the Loop
PS	Pure Simulation
WT	Wind Turbine
WECS	Wind Energy Conversion System

Chapter 1

Introduction

1.1. Background and Motivation

Future trend of energy production is moving towards a higher share of renewable energy sources driven by global warming issues and the desire to reduce dependence on fossil fuels. Wind energy (on shore) is becoming competitive with fossil fuels. Taking into account the fuel cost and CO_2 cost, wind energy costs less than energy generated by coal and gas and it considerably cheaper than nuclear [1]. Furthermore, among the possible renewable energy sources, wind power generation is one of the most attractive options. The availability in different areas and more favorable economics of generating large scale power from wind makes wind power generation a commercially viable option. National Energy Board of Canada published the total end-use (or secondary) energy demand is 11151.3 Peta Joules (PJ) in 2016 and more than 23% of current demand will be increased by 2035. End-use energy demand includes energy used in the residential, commercial, industrial and transportation sectors. This includes non-energy and feedstock demands [2]. The need to upgrade the generating capacity and meet new demand offers an opportunity to transition to renewable energy sources. This demand can be met more realistically with wind power among other renewable sources, due to favorable wind

profiles in many locations in Canada and the well matured technology of wind turbines that provide more reliable solution for grid integration. 433Giga Watt (GW) of harvesting capacity installed worldwide [3] and turbines that increased in power by a factor of 100 over the last two decades [1] are valid proof that wind power is on an ascending trend that no other source of renewable energy has seen before.

Wind power generation operates on the principle of energy conversion in air mass particle movement with linear kinetic energy which is converted from mechanical energy into electrical energy using wind turbines and electrical generators. Wind power generators are mainly asynchronous machines which have the advantage of being cheaper, low maintenance, and is highly suitable for large scale wind applications for its variable speed operation i.e. Doubly Fed Induction Generators (DFIGs). There are several reasons for using variable-speed operation of wind turbines; among those are possibilities to reduce stresses of the mechanical structure, acoustic noise reduction and the possibility to control active and reactive power [4]. Most of the major wind turbine manufactures are developing new larger wind turbines in the 3-to-7-MW range [1, 5]. These large wind turbines are all based on variable-speed operation with pitch control using a direct-driven synchronous generator (without gearbox) or a DFIG. Fixed-speed induction generators with stall control are regarded as unfeasible [5] for these large wind turbines. Today, doubly-fed induction generators are commonly used by the wind turbine industry for larger wind turbines [1, 6, 7].

The major advantage of the doubly-fed induction generator, is that the power electronic equipment only has to handle a fraction (20–30%) of the total system power [8, 9]. This means that the losses in the power electronic equipment (AC-DC-AC converters) can be reduced in comparison to power electronic equipment that has to handle the total system power as for a direct-driven synchronous generator, apart from the cost saving of using a smaller converter.

1.2. Literature Review

According to a survey done by O. Carlson et al [10] the energy production can be increased by 2-6 % for a variable-speed wind turbine in comparison to a fixed-speed wind turbine, while in D.S Zinger et al [11] stated that the increase in energy can be 39 %. In German booklet et al [12] show that the gain in energy generation of the variable-speed wind turbine compared to the most simple fixed-speed wind turbine can vary between 3-28 % depending on the site conditions and design parameters. Calculations of the energy efficiency of the doubly-fed induction generator system, has been presented in several papers [13, 14, 15]. A comparison to other electrical systems for wind turbines is, however, harder to find. One exception, where R. Datta et al [16] have made a comparison of the energy capture for different schemes of the electrical configuration, i.e., fixed-speed wind turbine using an induction generator, full variable-speed wind turbine using an inverter-fed induction generator, and a variable-speed wind turbine using a doubly-fed induction generator. The energy capture can be significantly enhanced by

using a doubly-fed induction machine as a generator and the increased energy capture of a doubly-fed induction generator by over 20% with respect to a variable-speed system using a cage rotor induction machine and by over 60% in comparison to a fixed-speed system [16]. Aspects such as the wind distribution, electrical and mechanical losses of the systems were neglected in R. Datta et al [16] study.

When the idea of wind power generation by using reluctance machines in doubly fed generation scheme were introduced and implemented [17, 18, 19] which led to early attempts of using wound rotor induction machines for doubly fed generation scheme. The first implementation of DFIG is recorded by R. Pena et al [20] where, the control strategy is based on PI controllers in conjunction with sinusoidal PWM that ends up with a constant switching frequency. The work is followed by more researchers in control method. The detailed model based studies on DFIG is presented by R. Pena, where the rotor position would be found through current and voltage models [21]. Another important modelling research reported by A. Peterson et al [22] where grid integration of DFIG and its operation under voltage sag is studied. Further studies on transient analysis of doubly fed induction generators followed in [23]. Implementation of current controlled methods on DFIG using a hysteresis controller to achieve better dynamics reported by Chowdhury et al [24].

In doubly-fed configuration two back-to-back connected converters as shown in Figure 1.1, provide the required magnetization current at rotor windings. In fact three phase power supply or grid connection to a three phase converter provides a stable DC

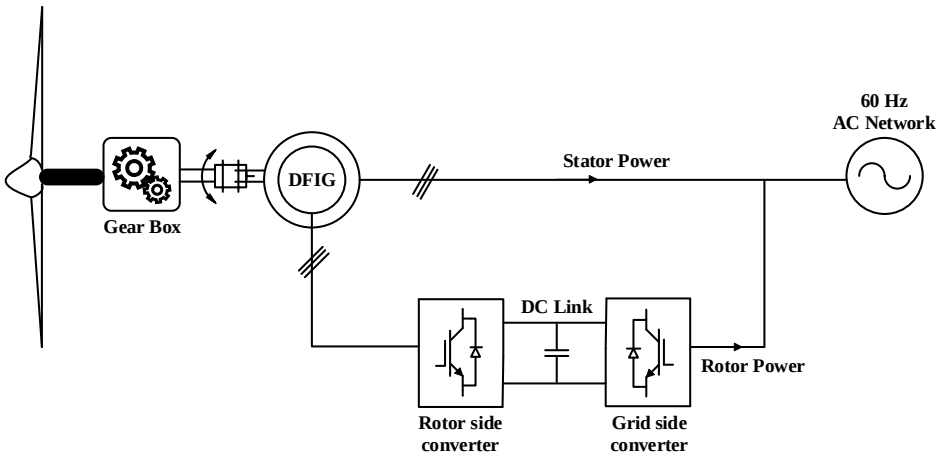

Figure 1.1: DFIG Wind Turbine System

voltage. This converter is usually called grid side converter (GSC). The DC voltage can be used for another voltage source three phase converter which is directly connected to terminals of rotor winding called Rotor Side Converter (RSC). RSC normally has the same configuration and component as the GSC, the only difference is in the control algorithm for the RSC. Although, the main task of Grid Side Converter (GSC) is to keep the dc bus voltage constant, GSC may also be used to compensate reactive power or in some cases to remove reactive power pulsation during unbalanced condition [25]. The RSC would provide the required magnetization current waveforms in rotor windings to generate required active and reactive power at stator terminals. However, as electrical torque is related to active power it is also reported in literature that in some control methods [26] the active and reactive reference values has been substituted with electrical torque and stator flux reference values.

To study the DFIG, RSC and GSC might be studied separately. In practice, as

long as a stable dc bus voltage is provided by GSC, the RSC can operate totally isolated from the GSC. M. Mesbah et al [27] provides a GSC that is able to control DC even in unbalanced grid voltage source condition. However, the solution lacks the reactive power compensation. Also, in most methods RSC operates totally isolated from the GSC and a different controller would handle the operation of each converter. On the other hand, to deal with the active power pulsations in unbalance grid voltage there is a control method reported in literature et al [25] that consider both converters in one control loop. Thus, the set points of GSC would be derived out of the RSC set points and turbine generator operating condition. The need to improve the machine performance to meet the new grid codes for fault ride through performance led to more studies [28, 29]. Some control methods have been proposed to improve fault ride capability of wind turbine generators and achieve better performance are also reported in literature such as Direct active control method et al [30], model based studies et al [31, 32], PDPC et al [33, 34], PDTC et al [35], Vector-Based Hysteresis et al [36, 37] and IVS-DTC et al [38]. Moreover, sensorless methods to have a more reliable, noise immune and less expensive system are also reported by previous researchers [39, 40, 41, 42]. A comparative study for some basic control approaches has been performed by E. Tremblay et al [43].

Several researchers are still investigating the best control strategies to improve the performance of DFIG. A feedback linearization based nonlinear voltage and slip controller is proposed by A. Balogun et al [44] for a DFIG connected to an infinite bus. A direct active and reactive power controller based on stator flux estimation is discussed by

B. Singh et al [45]. The paper uses a basic hysteresis controller. M. E. Zarei et al [46] proposed the well-known vector control and direct power control to regulate the active and reactive power generated by DFIG. DFIG control strategy that is very similar to the conventional AVR/PSS for synchronous generator is proposed by R. Dev Shukla et al [47] to support the power grid voltage and frequency.

The main drawback of the aforementioned works is their inability to cope with large changes in grid parameters. Even though, practical results in previous researches have been offered including some useful hints for hardware setup, there is not enough detailed design are documented in literature. For this reason, study of DFIG through practical implementation would help to justify various methods and ideas.

1.3. Objective & Contribution

The main purpose of this thesis is the analysis of the DFIG for a wind turbine (WT) application during steady-state operation of 2kW DFIG based wind energy conversion system emulator. In order to analyze the DFIG during steady-state and transient operation both the modeling and the control of the system is important. Hence, the control and the modeling are also important parts of the thesis. The main contribution of this thesis is dynamic and steady-state analysis of the DFIG, with details being as follows:

- An in-depth literature survey has been carried and different aspects regarding DFIG operation and control are analyzed. From all the strategies presented in the

literature the focus is set on the ones that offered a good trade-off between complexity and performance.

- An energy efficiency comparison of electrical systems for wind turbines. The investigated systems are fixed-speed induction generator system and variable-speed systems.
- Closed-loop control of a 2kW DFIG based wind turbine emulator has been successfully developed, analyzed, and implemented in real time simulation. The experimental results confirm stable operation of the generator, and successful controlling of active and reactive power. Furthermore, the results demonstrate validity of the closed-loop control with regards to the dynamic performance of the generator and stable control of the dc-link voltage, when they experienced torque disturbance from the exciter and the load machine.

1.4. Outline

This thesis is organized as follow:

Chapter 2 Description of properties of the wind and wind energy conversion system. Finally, different wind turbine concepts are compared and described.

Chapter 3 Overview of Doubly Fed Induction Generator (DFIG) based wind turbine and the dynamic modeling of DFIG in stationary & rotating reference frame for the development of machine control are presented.

Chapter 4 Control system aspects of DFIG based wind energy conversion system is presented. Advance non-linear controllers has developed based on the obtained model in Chapter 3, for controlling the machine side converter as well as grid side converter.

Chapter 5 The description of laboratory system setup and the operation procedure of 2kW DFIG based wind energy conversion system emulator is illustrated.

Chapter 6 Analysis of the graphical representation of system performances are obtained by real time experiment, providing the practical information and a deeper understanding of the machine's behavior in wind energy conversion system.

Chapter 7 The conclusion and proposed future work is presented.

Chapter 2

Wind Energy Conversion System

2.1. Introduction

Over the last twenty years, renewable energy sources have been attracting great attention due to the cost increase, limited reserves, and adverse environmental impact of fossil fuels. In the meantime, technological advancements, cost reduction, and governmental incentives have made some renewable energy sources more competitive in the market. Among them, wind energy is one of the fastest growing renewable energy sources [48].

Wind energy has been used for hundreds of years for milling grains, pumping water, and sailing the seas. The use of windmills to generate electricity can be traced back to the late nineteenth century with the development of a 12kW DC windmill generator [49]. It is, however, only since the 1980s that the technology has become sufficiently mature to produce electricity efficiently and reliably. Over the past two decades, a variety of wind power technologies have been developed, which have improved the conversion efficiency of and reduced the costs for wind energy production. The size of wind turbines has increased from a few kilowatts to several megawatts each. In addition to on-land installations, larger wind turbines have been pushed to offshore

locations to harvest more energy and reduce their impact on land use and landscape. This chapter provides an overview of wind energy conversion systems (WECS) and a background on several aspects related to this stimulating technology.

2.2. Wind Energy Conversion

In this section, properties of the wind, which are of interest in this thesis, will be described. First the wind distribution, i.e., the probability of a certain average wind speed, will be presented. The wind distribution can be used to determine the expected value of certain quantities, e.g. produced power. Then different methods to control the aerodynamic power will be described.

2.2.1. Wind Distribution

The annual average wind speed is an extremely important factor for the output power of a wind turbine. The average wind speed on a shorter time basis is, apart from the annual wind speed, also dependent on the distribution. It has been found that the wind distribution can be described by the Weibull probability density function [50]. The Weibull distribution is described by the following probability density function

$$f(\omega) = \frac{k}{c}\left(\frac{\omega}{c}\right)^{k-1} e^{-(\omega/c)^k} \tag{2.1}$$

where k is a shape parameter, c is a scale parameter, and ω is the wind speed. Thus, the average wind speed (or the expected wind speed), ϖ , can be calculated from

$$\varpi = \int_0^\infty \omega f(\omega) d\omega = \frac{c}{k}\Gamma\left(\frac{1}{k}\right) \tag{2.2}$$

where Γ is Euler's gamma function, i.e.,

$$\Gamma(z) = \int_0^\infty t^{z-1} e^{-t} dt \tag{2.3}$$

If the shape parameter equals 2, the Weibull distribution is known as the Rayleigh distribution. For the Rayleigh distribution the scale factor, *c*, given the average wind speed can be found from (*k*=2, and $\Gamma\left(\frac{1}{2}\right) = \sqrt{\pi}$)

$$c = \frac{2}{\sqrt{\pi}}\varpi \tag{2.4}$$

In figure 2.1, the wind speed probability density function of the Rayleigh distribution is plotted. The average wind speeds in the figure are 5.1 m/s, 6.5 m/s, and 8.1 m/s. A wind speed of 5-5.5 to 6.5 m/s correspond to a medium wind speed site in Halifax [51], while 8.5 to 9.5 m/s are wind speeds available at sites located in New Brunswick [52].

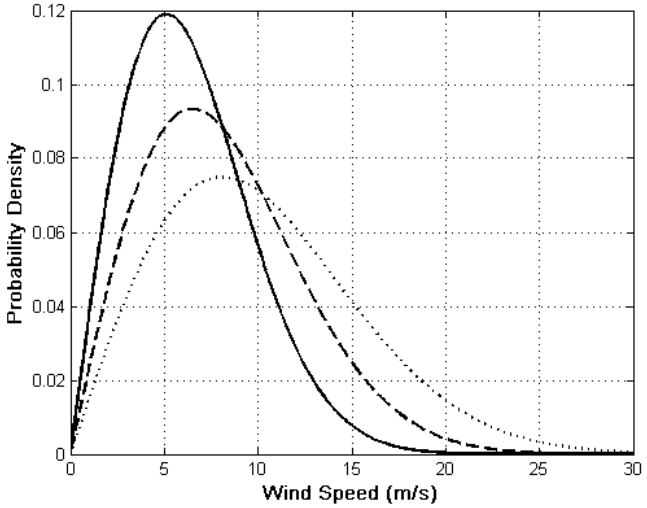

Figure 2.1: Probability density of the Rayleigh distribution. The average wind speed are 5.1 m/s (solid), 6.5 m/s (dashed) and 8.1 m/s (dotted)

2.2.2. Aerodynamic Power Control

At high wind speeds it is necessary to limit the input power to the wind turbine, i.e., aerodynamic power control. There are three major ways of performing the aerodynamic power control, i.e., by stall, pitch, or active stall control. Stall control implies that the blades are designed to stall in high wind speeds and no pitch mechanism is thus required [53].

Pitch control is the most common method of controlling the aerodynamic power generated by a turbine rotor, for newer larger wind turbines. Almost all variable-speed wind turbines use pitch control. Below rated wind speed the turbine should produce as much power as possible, i.e., using a pitch angle that maximizes the energy capture. Above rated wind speed the pitch angle is controlled in such a way that the aerodynamic power is controlled at its rated power [53]. In order to limit the aerodynamic power, at high wind speeds, the pitch angle is controlled to decrease the angle of attack, i.e., the angle between the chord line of the blade and the relative wind direction [54]. It is also possible to increase the angle of attack towards stall in order to limit the aerodynamic power. This method can be used to fine-tune the power level at high wind speeds for fixed-speed wind turbines. This control method is known as *active stall* or *combi stall* [53].

2.2.3. Aerodynamic Conversion

Some of the available power in the wind is converted by the rotor blades to mech-

-nical power acting on the rotor shaft of the wind turbine (WT). For steady-state calculations of the mechanical power from a wind turbine, the so called C_p (λ, β)-curve can be used. The mechanical power, P_{mech}, can be determined by [54]

$$P_{mech} = \frac{1}{2}\rho A_r C_p(\lambda, \beta)\omega^3 \tag{2.5}$$

$$\lambda = \frac{\Omega_r r_r}{\omega}$$

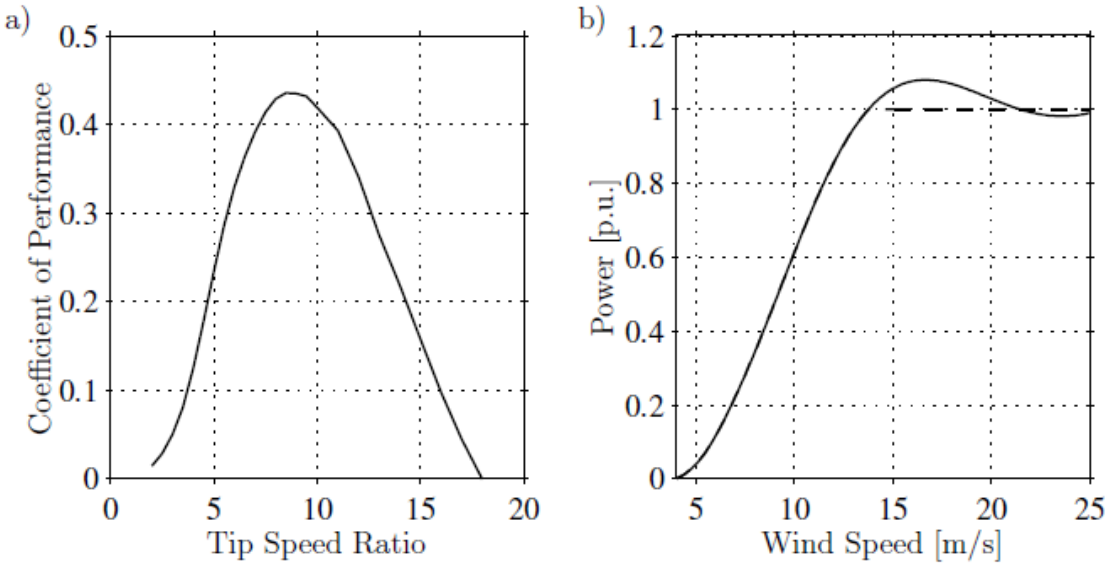

Figure 2.2: a) The power coefficient, C_p, as a function of the tip speed ratio, λ b) Mechanical power as a function of wind speed at rated rotor speed (solid line is fixed pitch angle, i.e., stall control and dashed line is active stall)

where C_p is the power coefficient, β is the pitch angle, λ is the tip speed ratio, ω is the wind speed, Ω_r is the rotor speed (on the low-speed side of the gearbox), r_r is the rotor-plane radius, ρ is the air density and A_r is the area swept by the rotor. In Figure 2.2, an example of a C_p (λ, β) curve and the shaft power as a function of the wind speed for rated rotor speed, i.e., a fixed-speed wind turbine, can be seen. In Figure 2.2b) the solid line

corresponds to a fixed pitch angle, β, while dashed line corresponds to a varying β (active stall).

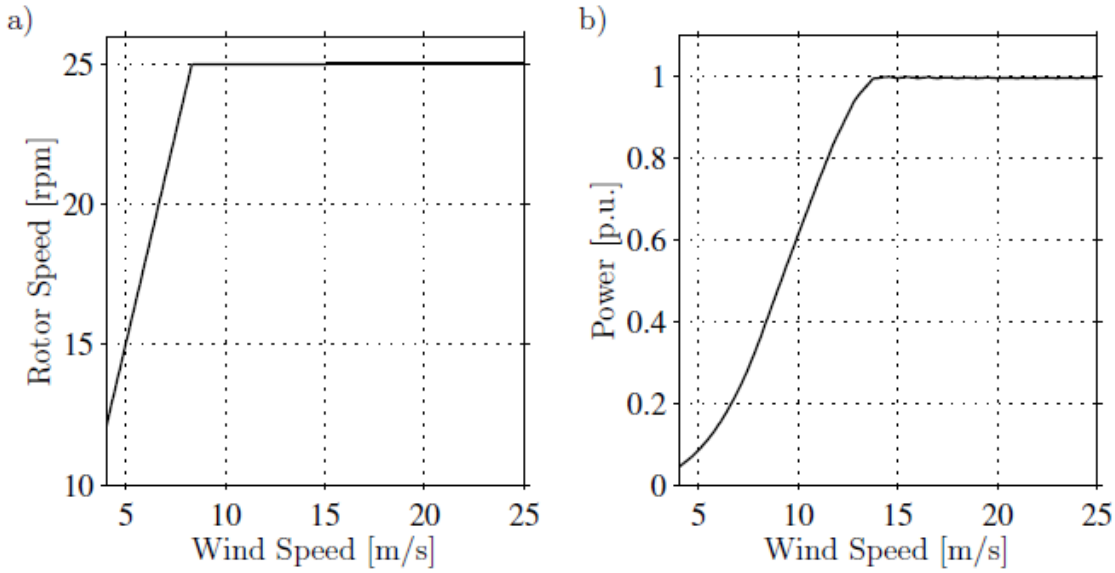

Figure 2.3: Typical characteristic for a variable speed wind turbine. a) Rotor speed as a function of wind speed. b) Mechanical power as a function of wind speed.

Figure 2.3 shows an example of how the mechanical power, derived from the C_p (λ, β) curve, and the rotor speed vary with the wind speed for a variable-speed wind turbine. The rotor speed in the variable-speed area is controlled in order to keep the optimal tip speed ratio, λ, i.e., C_p is kept at maximum as long as the power or rotor speed is below its rated values. As mentioned before, the pitch angle is at higher wind speeds controlled in order to limit the input power to the wind turbine, when the turbine has reached the rated power. As seen in Fig. 2.3b) the turbine in this example reaches the rated power, 1 p.u., at a wind speed of approximately 13 m/s. Note that there is a possibility to optimize the radius of the wind turbines rotor to suit sites with different average wind speeds. For

example, if the rotor radius, r_r, is increased, the output power of the turbine is also increased, according to (2.5). This implies that the nominal power will be reached for a lower wind speed, referred to Figure 2.3b). However, increasing the rotor radius implies that for higher wind speed the output power must be even more limited, e.g., by pitch control, so that the nominal power of the generator is not exceeded. Therefore, there is a trade-off between the rotor radius and the nominal power of the generator. This choice is to a high extent dependent on the average wind speed of the site.

2.3. Wind Energy Conversion System Configurations

The wind turbine is one of the most important elements in wind energy conversion systems. Over the years, different types of wind turbines have been developed [55]. This section provides an overview of wind turbine technologies, including fixed and variable-speed turbines.

A fundamental concept in understanding wind technology is wind energy capture. Wind holds in it a discrete amount of power at any given point in time, dependent in large part on the wind speed. As wind speed can vary greatly, wind turbines must be capable of operating over a wide wind speed range. The wind turbine can operate in one of two ways either fixed speed or variable speed. For fixed-speed wind turbines, the generator (induction generator) is directly connected to the grid. Since the speed is almost fixed to the grid frequency, and most certainly not controllable, it is not possible to store the turbulence of the wind in form of rotational energy. Therefore, for a fixed-speed system

the turbulence of the wind will result in power variations, and thus affect the power quality of the grid [56]. For a variable-speed wind turbine the generator is controlled by power electronic equipment, which makes it possible to control the rotor speed. In this way the power fluctuations caused by wind variations can be more or less absorbed by changing the rotor speed [57] and thus power variations originating from the wind conversion and the drive train can be reduced. Hence, the power quality impact caused by the wind turbine can be improved compared to a fixed-speed turbine [58].

The generator and power converter in a wind energy conversion system are the two main electrical components. Different designs and combinations of these two components lead to a wide variety of WECS configurations [55], which can be classified into three groups:

(1) fixed-speed WECS without power converter interface,

(2) WECS using reduced-capacity converters, and

(3) full-capacity converter operated WECS.

In this section the above wind turbine systems will be presented:

2.3.1. Fixed-Speed Wind Turbine

A typical configuration of WECS without a power converter interface is illustrated in Figure 2.4, where the generator is connected to the grid through a transformer. A Squirrel Cage Induction Generator (SCIG) is exclusively used in this type

of WECS, and its rotational speed is determined by the grid frequency and the number of poles of the stator winding. For a four-pole megawatt generator connected to a grid of 60 Hz, the generator operates at a speed slightly higher than 1800 rpm. At different wind speeds, the generator speed varies within 1% of its rated speed. A gearbox is normally required to match the speed difference between the turbine and generator such that the generator can deliver its rated power at the rated wind speed. This configuration requires a soft starter to limit high inrush currents during system start-up, but the soft starter is bypassed by a switch after the system is started. During normal operation, the system does not need any power converter. A three phase capacitor bank is usually required to compensate for the reactive power drawn by the induction generator.

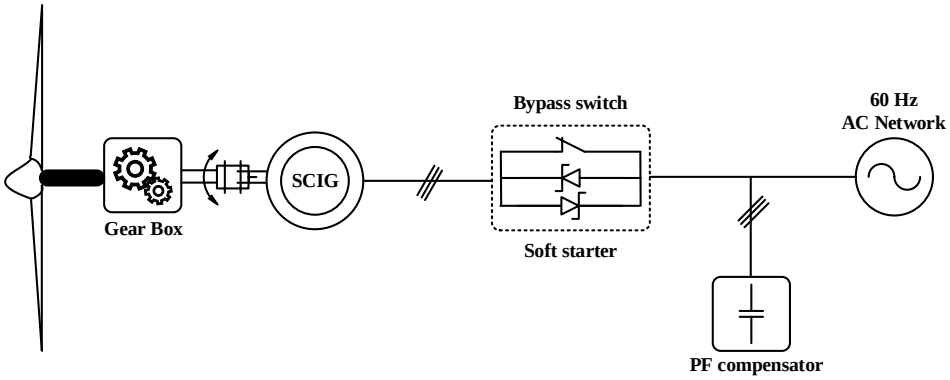

Figure 2.4: Wind energy conversion system without power converter interface

This wind energy system features simplicity, low manufacturing/maintenance costs, and reliable operation. The main drawbacks include: (1) the system delivers the rated power to the grid only at a given wind speed, leading to low energy conversion efficiency at other wind speeds; and (2) the power delivered to the grid fluctuates with the wind speed, causing disturbances to the grid. Despite its disadvantages, this wind

energy system is still widely accepted in industry with a power rating up to a couple of megawatts.

2.3.2. Variable-Speed Wind Turbine with Reduced-Capacity Converters

Variable-speed operation has a series of advantages over fixed-speed wind systems. It increases the energy conversion efficiency and reduces mechanical stress caused by wind gusts. The latter has a positive impact on the design of the structure and mechanical parts of the turbine and enables the construction of larger wind turbines. It also reduces the wear and tear on the gearbox and bearings, expanding the life cycle and reducing the maintenance requirements. The main drawback of variable-speed WECS is the need for a power converter interface to control the generator speed, which adds cost and complexity to the system. However, the power converter decouples the generator from the grid, which enables the control of the grid-side active and reactive power [59].

Variable-speed WECS can be further divided into two types based on the power rating of the converter with respect to the total power of the system: reduced-capacity power converter and full-capacity power converter. The variable-speed WECS with reduced-capacity converters are only feasible with wound-rotor induction generators (WRIG) since variable-speed operation can be achieved by controlling the rotor currents without the need to process the total power of the system. There are two designs for the WRIG configurations: one with a converter-controlled variable resistance, and the other with a four-quadrant power converter system.

2.3.2.1. Wound Rotor Induction Generator with Variable Rotor Resistance

Figure 2.5 shows a typical block diagram of the WRIG wind energy system with a variable resistance in the rotor circuit. The change in the rotor resistance affects the torque/speed characteristic of the generator, enabling variable-speed operation of the turbine. The rotor resistance is normally made adjustable by a power converter. The speed adjustment range is typically limited to about 10% above the synchronous speed of the generator [60]. With variable-speed operation, the system can capture more power from the wind, but also has energy losses in the rotor resistance. This configuration also requires a soft starter and reactive power compensation. The WRIG with variable rotor resistance has been in the market since the mid 1990s with a power rating up to a couple of megawatts.

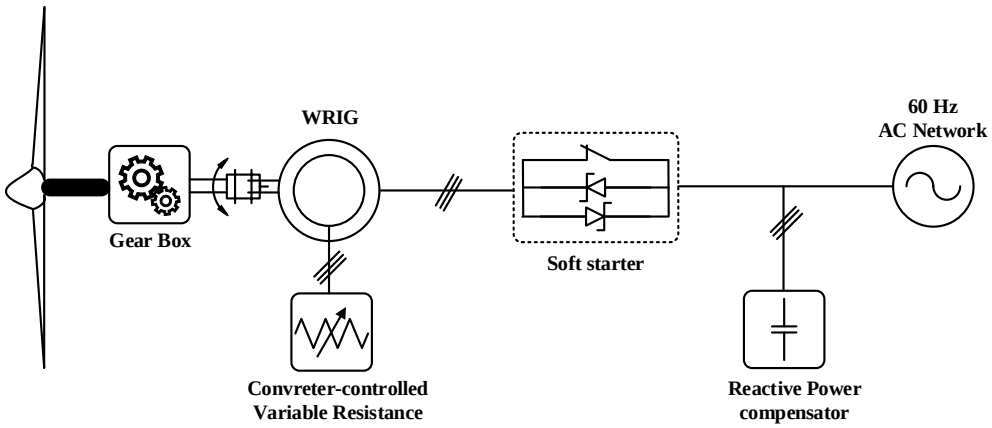

Figure 2.5: Variable-speed configuration with variable rotor resistance

2.3.2.2. Doubly Fed Induction Generator with Rotor Converter

A typical block diagram of the doubly fed induction generator (DFIG) wind energy

system is shown in figure 2.6. The configuration of this system is the same as that of the WRIG system except that (1) the variable resistance in the rotor circuit is replaced by a grid-connected power converter system, and (2) there is no need for the soft starter or reactive power compensation. The power factor of the system can be adjusted by the power converters. The converters only have to process the slip power in the rotor circuits, which is approximately 30% of the rated power of the generator, resulting in reduced converter cost in comparison to the wind energy systems using full-capacity converters [59].

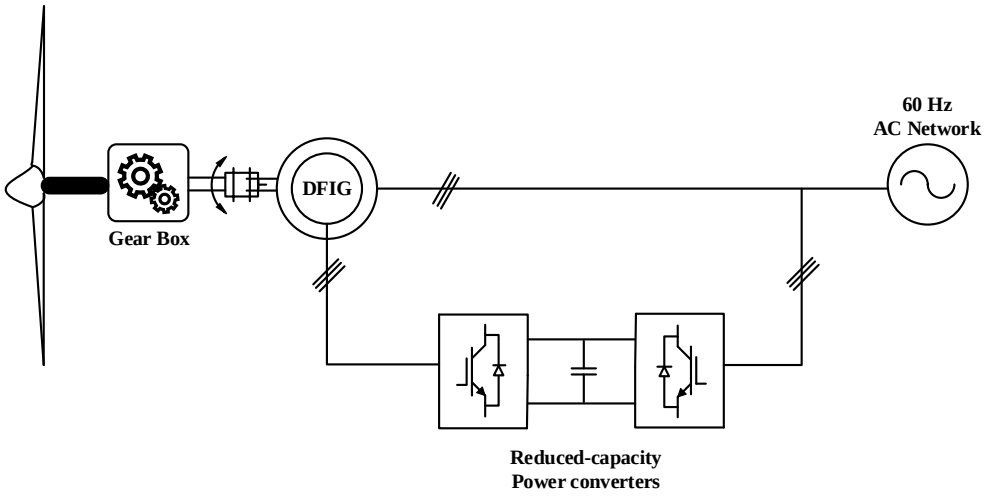

Figure 2.6: Variable-speed configuration with reduced-capacity converters

The use of the converters also allows bidirectional power flow in the rotor circuit and increases the speed range of the generator. This system features improved overall power conversion efficiency, extended generator speed range (±30%), and enhanced dynamic performance as compared to the fixed-speed WECS and the variable resistance configuration. These features have made the DFIG wind energy system widely accepted

in today's market.

2.3.3. Variable-Speed Wind Turbine with Full-Capacity Power Converters

The performance of the wind energy system can be greatly enhanced with the use of a full-capacity power converter. Figure 2.7 shows such a system in which the generator is connected to the grid via a full-capacity converter system [59]. Squirrel cage induction generators, wound rotor synchronous generators, and permanent magnet synchronous generators (PMSG) have all found applications in this type of configuration with a power rating up to several megawatts. The power rating of the converter is normally the same as that of the generator. With the use of the power converter, the generator is fully decoupled from the grid, and can operate in full speed range. This also enables the system to perform reactive power compensation and smooth the grid connection. The main drawback is a more complex system with increased costs.

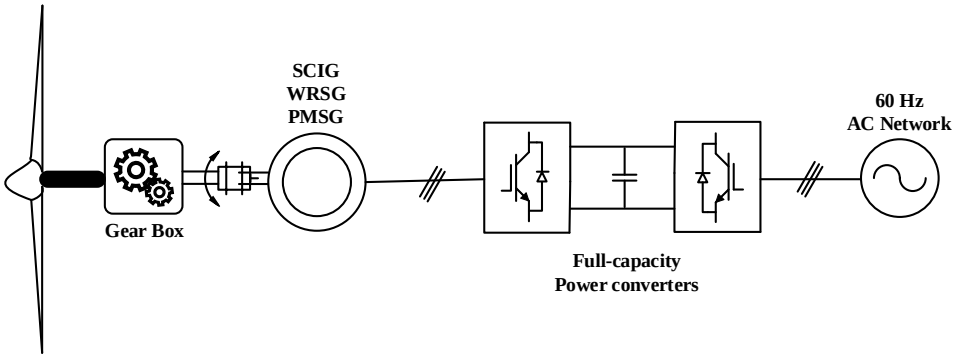

Figure 2.7: Variable-speed configurations with full-capacity converters

It is noted that the wind energy system can operate without the need for a gearbox if a low-speed synchronous generator with a large number of poles is used. The

elimination of the gearbox improves the efficiency of the system and reduces initial costs and maintenance. However, a low-speed generator has a substantially larger diameter to accommodate the large number of poles on the perimeter, which may lead to an increase in generator and installation costs.

Conclusion

This chapter provided an overview of wind energy conversion systems. The basic concepts of wind power, aerodynamic conversion, aerodynamic control, facts, current state, and market trends of wind power technology were presented. The fundamentals of wind energy systems were discussed, including fixed- and variable-speed operations which complements the in-depth analysis of wind energy systems covered in the other chapters of this thesis.

Chapter 3

Dynamic Modeling of DFIM

3.1. Introduction

Induction Machine (IM) is used in a wide variety of applications as a mean of converting electric power to mechanical work. The primary advantage of the induction machine is its rugged brushless construction and no need for separate DC field power. These machines are very economical, reliable, and are available in the ranges of fractional horse power (FHP) to multi–megawatt capacity. Also, unlike synchronous machines, induction machines can be operated at variable speeds. There are two types of induction machine based on the rotor construction namely, squirrel cage type and wound rotor type. Squirrel cage rotor construction is popular because of its ruggedness, lower cost and simplicity of construction and is widely used in stand-alone wind power generation schemes. Wound rotor machine can produce high starting torque and is the preferred choice in grid-connected wind generation scheme. Another advantage with wound rotor is its ability to extract rotor power at the added cost of power electronics in the rotor circuit [61].

The dynamic and transient behaviors of the induction machine must be examined for modeling purposes; and perhaps more importantly, for development of the subsequent

machine control. Dynamic behavior explains and defines the behavior of the machine's variables in transition periods as well as in the steady state. This dynamic behavior of machines is normally studied by a "dynamic model". By means of the dynamic model, it is possible to know at all times the continuous performance (not only at steady state) of the variables of the machine, such as torque, currents, and fluxes, under certain voltage supplying conditions [62]. In this way, by using the information provided by the dynamic model, it is possible to know how the transition from one state to another is going to be achieved, allowing one to detect unsafe behaviors, such as instabilities or high transient currents. On the other hand, the dynamic model provides additional information of the system during the steady state operation, such as dynamic oscillations, torque or current ripples etc [62].

Consequently, the dynamic model, represented in differential equation form, is structured as a compact set of model equations, allowing it to be simulated using any modeling and control software such as Simulink-MATLAB and RT-LAB and providing all the information related to the machine's variables. This is often called a "digital simulation model." It enables one to know the continuous behavior of all variables of the machine.

Thus, this chapter develops different dynamic models of the DFIM based on the space vector theory. By means of this powerful mathematical tool, the dynamic model equations (differential equations) of DFIM are derived to be used in the control system development.

3.2. Induction Machine

In this section the basics of one of the most widely used electrical machine named induction machine has discussed. The types of induction machine with advantages and comparison between types has briefly explained.

An electrical machine is such an electromechanical device which converts electrical energy into a mechanical energy or mechanical energy into electrical energy. In case of three phase AC operation, most widely used electrical machine is three phase induction machine. Almost 80% of the mechanical power used by industries is provided by three phase induction machines because of its simple and rugged construction, low cost, good operating characteristics, absence of commutator and good speed regulation [63]. In three phase induction machine, the power is transferred from the stator to the rotor winding through induction when it works as a motor and, in case of a generator, the power is transferred from the rotor to the stator. The Induction machine is also called asynchronous machine as it can runs at a speed other than the synchronous speed.

An induction machine has two major parts:

3.2.1. Stator

The stator of a three phase induction machine is made up of numbers of slots to construct a three phase winding circuit which is connected to three phase AC source. The three phase winding are arranged in such a manner in the slots that they produce a rotating ma-

-gnetic field after the three phase AC supply is given to them [64].

3.2.2. Rotor

The rotor is a rotating part of the induction machine. The rotor is connected to the mechanical load/prime mover through the shaft. Rotor of three phase induction machine consists of cylindrical laminated core with parallel slots that can carry conductors. Conductors are heavy copper or aluminum bars which fit in each slots and they are short circuited by the end rings. The slots are not exactly made parallel to the axis of the shaft but are slotted a little skewed because this arrangement reduces magnetic humming noise and can avoid stalling of machine [64].

Depending upon the type of rotor construction used the three phase induction machine are classified as:

I. Squirrel cage induction machine

II. Slip ring or wound rotor or doubly fed induction machine

The primary difference between the three-phase wound-rotor induction machines and the three-phase squirrel-cage induction machines is the design of the machine rotor. The rotor of the three-phase squirrel-cage induction machines are made of conducting bars short-circuited by rings at both ends, while the rotor of the three-phase wound-rotor induction machines consists of wire windings similar to the machine stator windings. These rotor windings are accessible through slip rings and brushes, allowing the connection of electrical components to the machine rotor [65].

Three-phase wound-rotor induction machines offer a number of advantages over other types of induction machines, most notably the ability to produce high starting torques at lower starting currents. Large three-phase wound-rotor induction machines are also easier to assemble than comparatively sized three phase squirrel-cage induction machines. Due to these advantages, three phase wound-rotor induction machines are commonly used in industry for any application requiring a large rotating machine (0.75 MW, or 1000 hp, and more). In such cases, the ability to produce a high starting torque with a reasonable starting current is crucial [62].

Another particularity of three-phase wound-rotor induction machines is the possibility to adjust the machine operating speed by controlling the rotor currents. Due to this feature, three-phase wound-rotor induction machines were traditionally used in applications requiring a rotating machine to run over a wide range of speeds. Today, however, the ability to adjust the speed of three-phase wound-rotor induction machines is used less frequently because the same results can be achieved more efficiently by controlling the speed of three-phase squirrel-cage induction machines using variable-frequency motor drives.

3.3. Classification of Induction Generators

This section presents the classification of induction generators which are using in wind energy conversion system. Depending on the wind speed and the availability of electrical network, induction generators are classified.

On the basis of rotor construction, induction generators are two types i.e., the wound rotor induction generator and squirrel cage induction generator. Depending upon the prime movers used (constant speed or variable speed) and their locations (near to the power network or at isolated places), generating schemes can be broadly classified as under [66]:

A. Constant-Speed Constant Frequency (CSCF)

In this scheme, the prime mover speed is held constant by continuously adjusting the blade pitch and/or generator characteristics. An induction generator can operate on an infinite bus bar at a slip of 1% to 5% above the synchronous speed. Induction generators are simpler than synchronous generators. They are easier to operate, control, and maintain, do not have any synchronization problems, and are economical.

B. Variable-Speed Constant Frequency (VSCF)

The variable-speed operation of wind electric system yields higher output for both low and high wind speeds. This results in higher annual energy yields per rated installed capacity. Both horizontal and vertical axis wind turbines exhibit this gain under variable-speed operation. Popular schemes to obtain constant frequency output from variable speed are as shown.

I. AC–DC–AC Link:

With the advent of high-powered thyristors, the ac output of the three-phase alternator is rectified by using a bridge rectifier and then converted back to ac using line-

commutated inverters. Since the frequency is automatically fixed by the power line, they are also known as synchronous inverters.

II. Doubly Fed Induction Generator (DFIG):

The DFIG consists of a three-phase wound rotor induction machine that is mechanically coupled to either a wind or hydro turbine, whose stator terminals are connected to a constant voltage constant frequency utility grid. The variable frequency output is fed into the ac supply by an ac–dc–ac link converter consisting of either a full-wave diode bridge rectifier and thyristor inverter combination or current source inverter (CSI)-thyristor converter link. One of the outstanding advantages of DFIG in wind energy conversion systems is that it is the only scheme in which the generated power is more than the rating of the machine. It can feedback the grid by providing reactive power when grid requires. However, due to lack of control and operational disadvantages, the DFIG scheme could not be used extensively in standalone application.

C. Variable-Speed Variable Frequency (VSVF)

With variable prime mover speed, the performance of synchronous generators can be affected. For variable speed corresponding to the changing derived speed, self-excited induction generator (SEIG) can be conveniently used for resistive heating loads, which are essentially frequency insensitive. This scheme is gaining importance for stand-alone wind power applications.

3.4. Overview of Doubly Fed Induction Generator

A wound rotor induction generator is composed by a stator and a rotor. In the case of a DFIG, both stator and rotor have three sinusoidally distributed windings, corresponding to three phases, displaced by 120º. The three phases are called *a, b* and *c*. The stator has *p* pairs of poles.

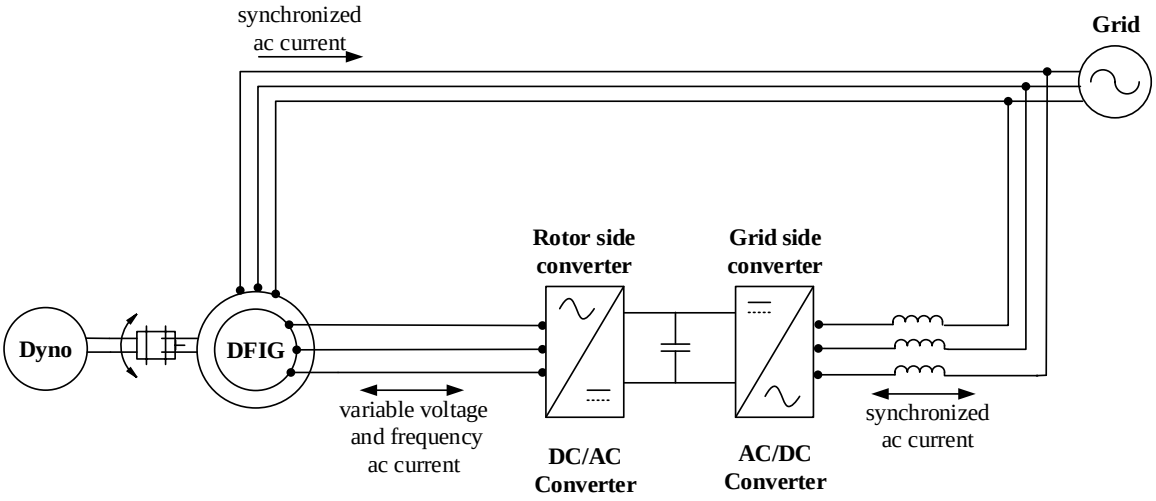

Figure 3.1: Schematic of DFIG configuration

The rotor is connected to the grid through converters. A schematic of such a system is presented in Figure 3.1. When the machine produces energy, less than 30% of the power is handled by the rotor windings which flows from the rotor to the grid. The converters can then be chosen in accordance with this small rotor power. The minimization of the converter volume and cost is assured. This is in contrast with past techniques like the squirrel cage induction generator where the converter had to cope with the full load power increasing the cost of the assembly significantly. The actual

percentage is an outcome of the fact the since the stator windings are connected directly to the grid they are the ones handling most of the transferred power.

The stator windings are connected to the grid which imposes the stator current frequency f_e. The stator currents create a rotating magnetic field in the air gap. The rotational speed of this field, ω_e, is proportional to f_e:

$$\omega_e = 2\pi f_e. \tag{3.1}$$

If the rotor spins at a speed different from that of the rotational field, it sees a variation of magnetic flux. Therefore, by Faraday's law of induction, currents are induced in the rotor windings. Let us define ω_m the rotor mechanical speed and ω_r the rotor electrical speed by

$$\omega_r = P\omega_m. \tag{3.2}$$

The flux linked by the rotor windings change with time if $\omega_r \neq \omega_e$. The machine operates usually as a generator if $\omega_r > \omega_e$ and as a motor otherwise. In the case of the DFIG however, it can operate in sub-synchronous mode as a generator. The slip, s, defines the relative speed of the rotor compared with that of the stator:

$$s = \frac{\omega_e - \omega_r}{\omega_e} \tag{3.3}$$

The slip is usually negative for a generator and positive for a motor. The currents induced in the rotor windings pulse at an angular speed defined by the difference between the synchronous speed and the rotor speed. Indeed, the stator currents at ω_r sees the

rotating magnetic field created by the stator pulsating at $\omega_e - \omega_r$. It means the frequency of the rotor currents, f_r is

$$f_r = s\, f_e. \tag{3.4}$$

If the rotor were to rotate at the synchronous speed, it would not see any change in magnetic fluxes. No currents would then be induced in its windings. Therefore, the machine operates always at speeds different from synchronous speed. The rotor-side inverter controls the rotor currents. From (3.4), it can be noted that controlling the rotor currents controls the slip and so the speed of the machine.

3.5. Characteristics of DFIG

DFIG are introduced by the special characteristics of the converter controlling the generator operation, widely known as ‘frequency converter’. As mentioned it consists of two different converters linked together by a capacitance known as ‘dc link’ Figure 3.1. The main principle is to interpose a frequency converter between the variable voltage and frequency induction machine and the fixed frequency grid.

The converters are defined as the grid-side converter and the rotor-side converter. The main purpose of the grid-side one is to control the dc-link voltage so that it remains nearly constant during normal and abnormal operations. Moreover it is entrusted with the coupling between the rotor windings and the non- ideal grid. On the other hand the rotor-side converter is directly related to the rotor windings and therefore it controls the

frequency and the magnitude of rotor voltages fed to the machine. It is obvious that the frequency of the rotor windings may differ from the fundamental frequency of the grid.

Furthermore by the proper tuning of the frequency converter the whole system can operate on all 4-quadrants. This is definitely an advantage of paramount importance as the generator can either import or export reactive power from-to the grid. In other words not only the DFIG can provide active power to the grid it can also support it during system failures, short circuits with an amount of reactive power. Specifically below the synchronous speed, while in motoring mode and at super-synchronous operation, while in generating mode, the rotor-side converter operates as a rectifier, and thus slip power is fed into the grid. In contrast, at sub-synchronous speed, while in generating mode and above the synchronous speed, while in motoring mode, the grid side converter acts like a rectifier and hence the slip power is supplied to the rotor.

Installing a converter on the stator windings implies that the machine is entirely decoupled from the grid and thus it doesn’t provide any additional inertia to the power system. DFIGs on the other hand do provide a sufficient additional inertia and thus improve the fault ride through capability of the grid.

3.6. Doubly Fed Induction Machine Modeling

In this section the mathematical modelling of the DFIG is presented. In order to provide the needed feedback about the tuning of the controller the electrical equivalent of the DFIG is illustrated and analyzed. Moreover, all equations of the equivalent system are

transformed into both αβ and dq0 reference frame. Further the decoupled active and the reactive power equations are exposed in d and q axis for both the stator and the rotor.

In the stationary (*abc*) reference frame, the relationships between voltages, currents and flux linkages of each phase of the machine can be obtained by Kirchhoff's and Faraday's law [67-69] :

$$\begin{bmatrix} v_{as} \\ v_{bs} \\ v_{cs} \end{bmatrix} = R_s + \begin{bmatrix} i_{as} \\ i_{bs} \\ i_{cs} \end{bmatrix} + \frac{d}{dt} \begin{bmatrix} \lambda_{as} \\ \lambda_{bs} \\ \lambda_{cs} \end{bmatrix} \tag{3.5}$$

$$\begin{bmatrix} v_{ar} \\ v_{br} \\ v_{cr} \end{bmatrix} = R_r + \begin{bmatrix} i_{ar} \\ i_{br} \\ i_{cr} \end{bmatrix} + \frac{d}{dt} \begin{bmatrix} \lambda_{ar} \\ \lambda_{br} \\ \lambda_{cr} \end{bmatrix} \tag{3.6}$$

The subscripts *r* and *s* denote rotor and stator quantities, respectively. The subscripts *a, b* and *c* are used for phases *a, b* and *c* quantities, respectively. The symbols *v* and *i* are for voltages and currents and λ represents flux linkages.

The stator and rotor winding resistances are R_s and R_r. They are assumed to be equal for all phase windings.

The flux linkages are coupled to the currents by the inductances:

$$\begin{bmatrix} \lambda_{as} \\ \lambda_{bs} \\ \lambda_{cs} \end{bmatrix} = L_s \begin{bmatrix} i_{as} \\ i_{bs} \\ i_{cs} \end{bmatrix} + L_M \begin{bmatrix} i_{ar} \\ i_{br} \\ i_{cr} \end{bmatrix} \tag{3.7}$$

$$\begin{bmatrix} \lambda_{ar} \\ \lambda_{br} \\ \lambda_{cr} \end{bmatrix} = L_r \begin{bmatrix} i_{ar} \\ i_{br} \\ i_{cr} \end{bmatrix} + L_M^T \begin{bmatrix} i_{as} \\ i_{bs} \\ i_{cs} \end{bmatrix} \tag{3.8}$$

The winding inductance matrices are defined by:

$$L_s = \begin{bmatrix} L_{ls} + L_m & -\frac{1}{2}L_m & -\frac{1}{2}L_m \\ -\frac{1}{2}L_m & L_{ls} + L_m & -\frac{1}{2}L_m \\ -\frac{1}{2}L_m & -\frac{1}{2}L_m & L_{ls} + L_m \end{bmatrix} \tag{3.9}$$

$$L_r = \begin{bmatrix} L_{lr} + L_m & -\frac{1}{2}L_m & -\frac{1}{2}L_m \\ -\frac{1}{2}L_m & L_{lr} + L_m & -\frac{1}{2}L_m \\ -\frac{1}{2}L_m & -\frac{1}{2}L_m & L_{lr} + L_m \end{bmatrix} \tag{3.10}$$

$$L_M = L_m \begin{bmatrix} \cos(\theta_r) & \cos(\theta_r + \frac{2\pi}{3}) & \cos(\theta_r - \frac{2\pi}{3}) \\ \cos(\theta_r - \frac{2\pi}{3}) & \cos(\theta_r) & \cos(\theta_r + \frac{2\pi}{3}) \\ \cos(\theta_r + \frac{2\pi}{3}) & \cos(\theta_r - \frac{2\pi}{3}) & \cos(\theta_r) \end{bmatrix} \tag{3.11}$$

The subscripts *l* and *m* relate to the leakage and magnetizing inductances, respectively. The maximum amplitude of the mutual inductance between the stator and the rotor is L_m. It must also be noted that equation (3.11) depends on the angular shift of the rotor θ_r which in turn depends on the angular speed of the rotor ω_r. The rotor electrical angular displacement regarding to the stator, defined from ω_r, the electrical rotor speed is

$$\theta_r(t) = \int_0^t \omega_r dt + \theta_r(0) \tag{3.12}$$

where θ_r (0) is the initial position of the rotor at t=0.

It can then be noted that the voltage, current and mutual inductance matrix L_M are derived in (*abc*) stationary reference frame and depends on time. Since modeling and analysis for such a system is difficult to manage, the time variant parameters can be made time invariant by transforming them into an appropriate rotating reference frame.

In order to complete the modeling, a model of the mechanical dynamics is needed. The dynamics of the generator shaft relate the rotor speed and the electromagnetic torque:

$$J \frac{d\omega_m}{dt} = T_m - T_e \tag{3.13}$$

where J is the inertia of the machine, T_m is the mechanical torque and T_e is the electromagnetic torque.

3.6.1. (*d*-*q*) Reference Frame

It has been mentioned above that the parameters of the machine need to be transformed into a suitable rotating reference frame. This aim can be achieved by defining the (*d*-*q*) reference frame, which will be rotating at the synchronous angular speed of the system. The DFIG can be regarded as a traditional induction generator with a nonzero rotor voltage. The dynamic equation of a three-phase DFIG can be written in a

synchronously rotating direct-quadrature (*d*-*q*) reference frame as [70]:

$$v_{ds} = R_s i_{ds} - \omega_e \lambda_{qs} + \frac{d\lambda_{ds}}{dt} \tag{3.14.a}$$

$$v_{qs} = R_s i_{qs} + \omega_e \lambda_{ds} + \frac{d\lambda_{qs}}{dt} \tag{3.14.b}$$

$$v_{dr} = R_r i_{dr} - \omega_s \lambda_{qr} + \frac{d\lambda_{dr}}{dt} \tag{3.15.a}$$

$$v_{qr} = R_r i_{qr} + \omega_s \lambda_{dr} + \frac{d\lambda_{qr}}{dt} \tag{3.15.b}$$

$$\lambda_{ds} = L_s i_{ds} + L_m i_{dr} \tag{3.16.a}$$

$$\lambda_{qs} = L_s i_{qs} + L_m i_{qr} \tag{3.16.b}$$

$$\lambda_{dr} = L_r i_{dr} + L_m i_{ds} \tag{3.17.a}$$

$$\lambda_{qr} = L_r i_{qr} + L_m i_{ds} \tag{3.17.b}$$

where, $L_s = L_{ls} + L_m$

$$L_r = L_{lr} + L_m$$

where ω_e is the rotational speed of the synchronous reference frame; $\omega_s = (\omega_e - \omega_r)$ is the slip frequency [71] and s is the slip; ω_r is the generator electrical speed in [rad/s], which is related to the generator mechanical speed by means of the pole numbers $\omega_r = \frac{p}{2}\omega_m$, $v_{ds}, v_{qs}, v_{dr}, v_{qr}; i_{ds}, i_{qs}, i_{dr}, i_{qr}; \lambda_{ds}, \lambda_{qs}, \lambda_{dr}, \lambda_{qr}$ are voltages, currents and flux linkages of the stator and rotor in *d* and *q* axis, R_s, R_r, L_s and L_r are the stator and rotor

resistances and inductances; L_m is the mutual inductance; and ω_m is the angular rotor speed.

The mutual flux between rotor and stator produces magnetic energy, which is stored in the magnetic field. This energy produces an electromagnetic torque which is calculated by [72]:

$$T_e = \frac{3}{2} p(\lambda_{dr} i_{qs} - \lambda_{qr} i_{ds}) = \frac{3}{2} pL_m (i_{dr} i_{qs} - i_{qr} i_{ds}) \tag{3.18}$$

where p is the number of pole pairs and $L_M = \frac{3}{2} L_m$

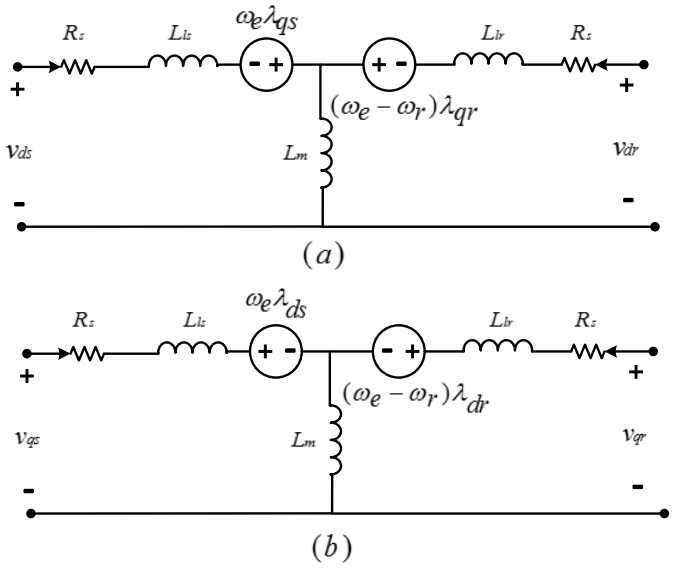

Figure 3.2: Equivalent circuit of the (*d*, *q*) model in the arbitrary reference frame. (a) *d*-axis equivalent circuit; (b) *q*-axis equivalent circuit

The active and reactive stator and rotor powers for the DFIG are given by [73]:

$$P_s = \frac{3}{2}(v_{ds} i_{ds} + v_{qs} i_{qs}) \tag{3.19}$$

$$Q_s = \frac{3}{2}(v_{qs} i_{ds} - v_{ds} i_{qs}) \tag{3.20}$$

$$P_r = \frac{3}{2}(v_{dr} i_{dr} + v_{qr} i_{qr}) \tag{3.21}$$

$$Q_r = \frac{3}{2}(v_{qr} i_{dr} - v_{dr} i_{qr}) \tag{3.22}$$

In the above power modeling, the power losses associated with the stator and rotor resistances are neglected.

An equivalent circuit may be set up by means of the voltage and flux linkage equations of the arbitrary reference frame, as shown in Figure 3.3.

3.6.2. (α,β) Reference Frame

In order to describe the alpha-beta reference frame it must be considered that it resembles the *dq0* but it is stationary. Equations (3.14.a), (3.14.b) and (3.15.a), (3.15.b), taking into account the previous assumptions, are analyzed below.

Stator voltages and fluxes in (α,β) reference frame:

$$v_{\alpha s} = R_s i_{\alpha s} + \frac{d}{dt}\lambda_{\alpha s} \tag{3.23.a}$$

$$v_{\beta s} = R_s i_{\beta s} + \frac{d}{dt}\lambda_{\beta s} \tag{3.23.b}$$

$$\lambda_{\alpha s} = \int (v_{\alpha s} - R_s i_{\alpha s}) \tag{3.24.a}$$

$$\lambda_{\beta s} = \int (v_{\beta s} - R_s i_{\beta s}) \tag{3.24.b}$$

The stator currents are:

$$i_{\alpha s} = \frac{L_{lr} + L_m}{L_{lr}L_{ls} + L_m(L_{lr} + L_{ls})}\lambda_{\alpha s} - \frac{L_m}{L_{lr}L_{ls} + L_m(L_{lr} + L_{ls})}\lambda_{\alpha r} \qquad (3.25.a)$$

$$i_{\beta s} = \frac{L_{lr} + L_m}{L_{lr}L_{ls} + L_m(L_{lr} + L_{ls})}\lambda_{\beta s} - \frac{L_m}{L_{lr}L_{ls} + L_m(L_{lr} + L_{ls})}\lambda_{\beta r} \qquad (3.25.b)$$

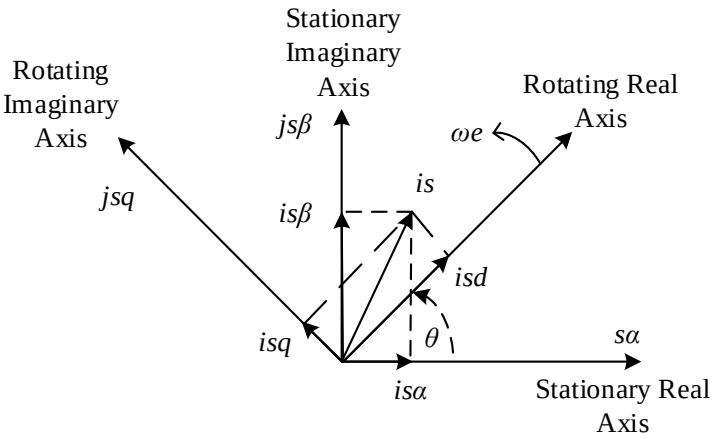

Figure 3.3: Relationship of current space vector components between (α, β) and (d, q) reference frames

Rotor voltages and fluxes in (α, β) reference frame:

$$v_{\alpha r} = R_r i_{\alpha r} + \frac{d}{dt}\lambda_{\alpha r} + \omega_r \lambda_{\beta r} \qquad (3.26.a)$$

$$v_{\beta r} = R_r i_{\beta r} + \frac{d}{dt}\lambda_{\beta r} - \omega_r \lambda_{\alpha r} \qquad (3.26.b)$$

$$\lambda_{\alpha r} = \int \left(v_{\alpha r} - R_r i_{\alpha r} - \omega_r \lambda_{\beta r}\right) \qquad (3.27.a)$$

$$\lambda_{\beta r} = \int \left(v_{\beta r} - R_r i_{\beta r} + \omega_r \lambda_{\alpha r}\right) \qquad (3.27.b)$$

The rotor currents are:

$$i_{\alpha r} = \frac{L_{lr} + L_m}{L_{lr}L_{ls} + L_m(L_{lr} + L_{ls})}\lambda_{\alpha r} - \frac{L_m}{L_{lr}L_{ls} + L_m(L_{lr} + L_{ls})}\lambda_{\alpha s} \quad (3.28.a)$$

$$i_{\beta r} = \frac{L_{lr} + L_m}{L_{lr}L_{ls} + L_m(L_{lr} + L_{ls})}\lambda_{\beta r} - \frac{L_m}{L_{lr}L_{ls} + L_m(L_{lr} + L_{ls})}\lambda_{\beta s} \quad (3.28.b)$$

The electromagnetic torque is represented by the following equation:

$$T_e = \frac{3}{2}p\left(\lambda_{\alpha r}i_{\beta r} - \lambda_{\beta r}i_{\alpha r}\right) \quad (3.29)$$

Conclusion

Induction generators are increasingly being used in nonconventional energy systems such as wind, micro/mini hydro, etc. The advantages of using an induction generator instead of a synchronous generator were introduced. Classification of induction generators are using in wind energy conversion system were presented for better understanding the reasons of their various use in wind energy conversion system. Dynamic modeling of induction machine was presented for development of the subsequent machine control. During this chapter the algebraic equations describing the operation of a DFIG over two different reference frames were introduced. Further, the independent control of the stator active-reactive power and their correlation with the rotor current was specified. Therefore, a solid background over the electrical characteristics of the generator has been achieved. Next chapter will focus on controlling of DFIG.

Chapter 4

Control Systems for DFIG

4.1. Introduction

Induction machines are almost entirely used in producing electricity from wind turbine. So, the importance of accurately controlled machine drives is increasing day by day. Controllers can provide probably the best control properties for a wide variety of processes in wind energy conversion system. The variable torque of wind turbine induced from the fluctuating wind speed can be controlled accurately, increase the efficiencies of the power electronic and electromechanical conversion processes and the most important is that a properly controlled wind turbine may save considerable amounts of energy [74].

Therefore, in this chapter, the basic control overview of grid tied variable speed wind turbine is presented. The control of doubly fed induction generator (DFIG) concepts related to the back-to-back converter are analyzed, paying particular attention to the grid side and the rotor side controllers as well. Thus, not only the grid side and rotor side is studied but also its closely associated elements such as the DC link control, the control of grid side frequency and amplitude, model reference adaptive system (MRAS) based speed estimator by artificial neural network (ANN) for sensorless operation are also discussed. Controllers are developed for controlling the active and reactive power in

DFIG based wind energy conversion system. Two controlling methods of active and reactive power, mainly by varying rotor current and by controlling the rotor speed has presented in details.

4.2. Control System Overview

In this section the overall control system of DFIG based wind turbine has presented. The general control strategy of this variable speed wind turbine has explained into three different control levels.

The controlling of wind turbine is very important especially for variable speed operation to make the wind energy conversion system efficient, reliable and feasible. The major control goals of a variable speed wind turbine, thus a DFIG based wind turbine are:

- maximum power extraction and active power control at the *Point of Common Coupling*
- reactive power control at the *Point of Common Coupling*

The general control strategy of a variable speed wind turbine can be divided into three different control levels [75], as depicted in Figure 4.1.

I. the DFIG control level

II. the Wind turbine control level

III. the Wind turbine Grid integration control level

The DFIG control level contains the electrical control (converters and machine) of the DFIG and has a fast dynamic response, its aim is to control the active and reactive power, owing from the DFIG into the grid.

The wind turbine control level, which has slower dynamics, controls the pitch angle and provides the active power reference for the DFIG control level.

The wind turbine-grid integration control level, its aim to fulfill the grid code requirements. A brief description of the two control levels is provided next.

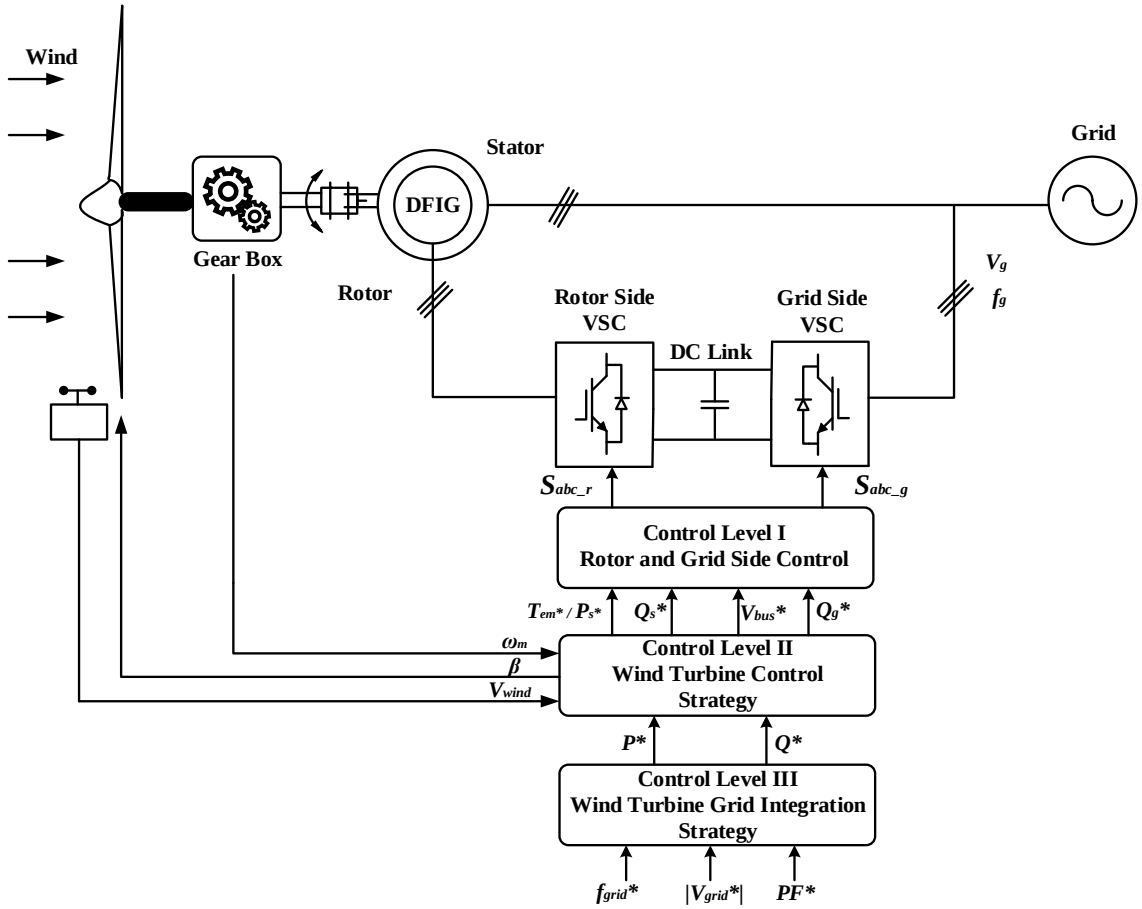

Figure 4.1: General wind turbine control strategy based on DFIG

4.2.1. DFIG Control Level

At this level, the control of active and reactive power is performed independently. This is achieved by decoupling the voltage and currents related to the active and reactive power, respectively. The decoupling can be made with the use of a special reference frame.

Two sub-control levels, one for each converter in the back-to-back configuration, can be found at this control level:

- Rotor side converter controller.
- Grid side converter controller.

The purpose of the rotor side converter is to control the active and the reactive power in the stator winding of the DFIG [76], whilst the grid side converter control aims to keep the DC-Link voltage level constant and to assure zero reactive power at the output of the converter [77]. Both the grid side and the converter side controllers will be treated thoroughly in the following sections.

4.2.2. Wind Turbine Control Level

The control strategies for the turbine are based on the power vs. wind curve, as presented in detail in [78], having the main control goals of power optimization and power limitation. For this, two cross-coupled controllers are used, one speed controller and one power controller.

The main task of the speed controller is to achieve optimum power by adapting

the generator speed by rotor magnetizing current to the wind speed/reference speed. For wind speeds above rated value, the speed controller needs to prevent the speed of the generator from becoming too large.

The power controller has the purpose to limit the generator power at rated power for wind speeds at and above rated value. This is achieved by increasing or decreasing the pitching angle β based on the measured actual generated power. Since the time constants of the wind turbine controllers are much slower compared to the dynamics of the DFIG controllers and electrical system, they can be considered constant for the time ranges relevant for fault ride through (FRT), thus the wind turbine control level will not be detailed any further.

4.2.3. Wind Turbine-Grid Integration Control Level

This control level is dedicated to wind turbine-grid integration. This control level performs as same functionalities as the wind farm control. The purpose of this level is to fulfill the grid demand. It confirms that wind turbine is under control in terms of the grid frequency, amplitude and power factor.

4.3. Control Strategy of Doubly Fed Induction Generator

This section contains the control techniques of Doubly Fed Induction Generator in wind energy conversion system. The working principle and characteristics of DFIG in terms of grid connected system has described briefly. Two types controllers has developed based on mathematical modeling and presented for controlling of Active and

Reactive Power in wind power generation. One is designed for controlling the Active and Reactive Power by varying the rotor current where the generated power does not depend on the variation of rotor speed when the machine runs at around ±30% of synchronous speed. On the other hand, the other one is built to track the wind speed profile so that the generated power will follow the wind speed profile when the machine runs at around ±30% of synchronous speed.

Field oriented vector control in synchronous reference frame strategy is chosen for implementing the control strategies for the rotor and grid side converter. A reference frame oriented with the stator flux is used so that the active and reactive power of the stator can be controlled independently by means of the quadrature and the direct current, respectively. The advantages that this method possess [79]:

- wide range of bibliographic material available
- good dynamic response in normal and fault operation
- fixed switching frequency
- robust to parameter variation
- robust to measurement noise

Other DFIG control strategies currently employed are:

- Vector oriented control in rotor/stationary reference frame [76,80,85]
- Direct torque control [81-83]
- Direct power control [84-85]

DPC/DTC has several drawbacks which make it difficult to be applied in the DFIG-based wind power generation system. For example, the rotor voltages generated by a fixed and discrete switching table cannot satisfy the control precision of the active and reactive powers during maximum wind energy capturing. Furthermore, the electromagnetic torque vibration caused by the traditional DTC is much more significant than that in the vector control with the same sampling frequency. Some disadvantages of the vector oriented control in synchronous reference frame strategy, in comparisons with the other methods are [79]:

- slower response time compared to the direct methods
- higher complexity
- need to estimate the flux angle

4.3.1. Active and Reactive Power Control by Controlling Rotor Current

A doubly fed induction generator (DFIG) is one of the most widely used generators in wind turbines due to its variable speed operation, power control, improving power quality, smaller converter capacity, and grid tie feasibility. The DFIG is able to control its active and reactive power outputs as required by system operators. Although the active power depends on the energy transferred from the wind, it can be controlled in a transient manner by resorting to the mechanical system kinetic energy. This will allow more renewable energy resources with DFIG as a combined system to be connected to the grid. When two or more renewable energy resources generate maximum power by controlling the active power of DFIG, the total system power can be controlled to fulfill

the grid requirement. In the case of a weak grid, where the voltage may fluctuate, the DFIG may be ordered to produce or absorb an amount of reactive power to or from the grid, with the purpose of voltage control. Therefore, the control technologies and the dynamic characteristics of the variable-speed constant-frequency (VSCF) doubly fed induction generator are important topics in wind energy research [86].

The control design uses the field-oriented control (FOC) theory to regulate the rotor side converter (RSC) and the hysteresis control approach to regulate the grid side converter (GSC). The most challenging task in DFIG operation is to keep the DC-link voltage constant. Here, a hysteresis controller is developed for the voltage side controller, which has a fast dynamic response [87]. The traditional current control strategies are mostly proportional-integral (PI) based on a linearized model; they are difficult to obtain and may not give satisfactory performance under parameter variations, load disturbances, and a large-scale wind changes. The RSC control scheme leads to an independent control of the DFIG active and reactive power by controlling the rotor currents [88]. For its implementation, this type of control heavily relies on the electrical parameters of the machine and multiple reference frame transformations of the electrical signals (voltages and currents). However, the FOC approach delivers a great control performance in terms of robustness, transitory and steady state response, and instrumentation specifications. The grid side converter (GSC) facilitates the power exchange through the rotor converter, and also provides additional reactive power support. GSC is controlled by a hysteresis current controller in such a way as to guarantee a smooth DC-link voltage and ensure

sinusoidal current in the grid side [89]. This thesis investigates DFIG power generation and converter control characteristics through a dynamic steady-state approach, which provides better and effective understanding of DFIG in wind energy applications under different control conditions in a broader spectrum.

4.3.1.1. Wind Turbine Modeling

Wind turbines produce electricity by using the power of the wind to drive an electrical generator. Wind passes over the blades, generating lift and exerting a turning force. The rotating blades turn a shaft inside the nacelle, which goes into a gearbox. The gearbox increases the rotational speed to that which is appropriate for the generator, which uses magnetic fields to convert the rotational energy into electrical energy.

The expression of power produced by the wind is given by:

$$P_m = 0.5 C_p(\lambda, \beta) \rho \pi r^2 v^3 \tag{4.1}$$

where ρ is the air density; r is the radius of the turbine blades, v is the wind speed, and C is the power coefficient, which is a function of tip speed ratio λ and pitch angle β.

The tip speed ratio is defined as:

$$\lambda = \frac{\omega_r r}{v} \tag{4.2}$$

where ω_r is the rotational speed of generator. From Equation (4.2), it can be observed that the tip speed ratio λ can be adjusted by controlling the speed ω, leading to the control of the power coefficient C, as well as the generated output power of the wind turbine.

In this work, a dynamometer, based on a squirrel cage induction motor, is used to emulate the wind turbine by changing its speed to produce the variable wind speed effects.

4.3.1.2. Grid Side Controller

The main objective of the grid side controller is to keep a constant DC-link voltage independent of the value and direction of the rotor power flow [87]. To fulfill the objective, a hysteresis current control strategy with a reference frame aligned with the stator voltage position is used as shown in Figure 4.2. This allows independent control of the DC-link voltage and the reactive power between the converter and the grid.

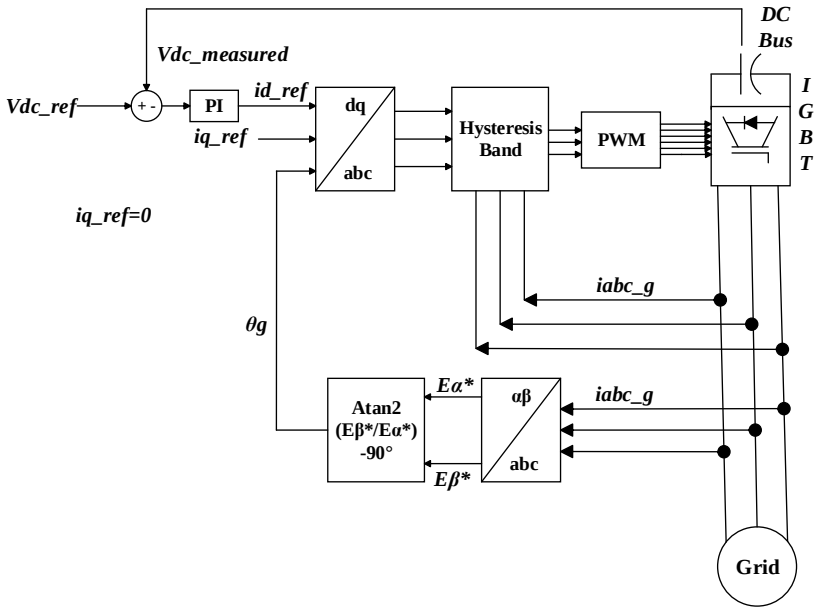

Figure 4.2: The block diagram of proposed method for GSC

The rotor side converter requires a DC power supply. The DC voltage is usually generated using another voltage source converter connected to the AC grid at the

generator stator terminals. A DC capacitor is used in order to remove ripple and keep the DC-link voltage relatively smooth. This grid PWM converter is operated to keep the DC-link voltage at a constant value. In effect, this means that the grid side converter is supplying the real power demands of the rotor side converter. It is possible to operate this converter using a current reference approach.

Therefore, a hysteresis controller is used in which the error between the desired and actual currents is passed through a controller, which controls the output voltage of a conventional Sinusoidal PWM Converter and ensures the required power factor [90]. The grid side converter control diagram is shown in figure 4.2.

The DC-link voltage error is given by:

$$e = v_{dc\_ref} - v_{dc} \tag{4.3}$$

Also, its variation is expressed by:

$$\Delta e = \left(1 - z^{-1}\right) \tag{4.4}$$

The voltage components, in the (*d*-*q*) reference frame, at the grid side are given by:

$$v_d = -Ri_d - L\frac{di_d}{dt} + L\omega i_q + v_{dl} \tag{4.5}$$

$$v_q = -Ri_q - L\frac{di_q}{dt} + L\omega i_d + v_{ql} \tag{4.6}$$

where v_d, v_q are the grid voltage (*d*-*q*) components; v_{dl}, v_{ql} are the grid inverter voltage (*d*-*q*) components; i_d, i_q are the grid current (*d*-*q*) components; *L* and *R* are the in-

ductance and resistance of the filter; and ω is the grid angular frequency.

The active and reactive power flows are then [91]:

$$P = 3\left(v_d i_d + v_q i_q\right) \tag{4.7}$$

$$Q = 3\left(v_d i_q + v_q i_d\right) \tag{4.8}$$

The detection of the reference angular position of the grid voltage is computed as

$$\theta_e = \int \omega_e dt = \tan^{-1}\left(\frac{v_\beta}{v_\alpha}\right) \tag{4.9}$$

where v_α and v_β are the (α-β) components of the grid voltage. Aligning with the d component of the voltage v_d makes v_q = 0. Also, since the grid voltage has constant amplitude, v_d also has constant amplitude.

The active power, to balance at the DC-link, can be expressed by (neglecting harmonics):

$$v_{dc} i_{os} = 3 v_d i_d \tag{4.10}$$

The DC-link voltage v_{dc} is controlled by the current i_d in the voltage vector-oriented reference frame. Thus, a reference current i_{d_ref} is derived from the DC-link voltage error Δe and the variation of the error e by tuning a PI controller, as shown in Figure 4.2. To guarantee a unity factor power at the grid side converter, the reactive

power must be zero, so $i_{q\_ref} = 0$. After a *dq-abc* transformation of these reference currents, hysteresis modulation may then be implemented.

4.3.1.3. Rotor Side Controller

The doubly fed induction generator allows power output into the stator winding as well as the rotor winding of an induction machine with a wound rotor winding. Using such a generator, it is possible to get a good power factor even when the machine speed is quite different from the synchronous speed. Such machines can therefore operate without the need for excessive shunt compensation.

The rotor currents i_{abc_r} of the machine can be resolved into the (*d-q*) components i_{dr} and i_{qr}. The component i_{dr} produces a flux in the air gap, which is aligned with the rotating flux vector linking the stator, whereas the component i_{qr} produces flux at right angles to this vector. The torque in the machine is the vector cross product of these two vectors, and hence only the component i_{qr} contributes to the machine torque and thus to the power. The component i_{dr} then controls the reactive power entering the machine. The precise control of the currents i_{dr} and i_{qr} allows the control of the stator side real and reactive powers.

The important step is to obtain the instantaneous position of the rotating flux vector in space in order to obtain the rotating reference frame. This can be achieved by realizing that, on account of Lenz's law of electromagnetism, the stator voltage is simply

the derivative of the stator flux linkage.

The three phase stator voltages and currents are converted into the (α-β) components v_α, v_β, i_α and i_β. The stator flux in the stationary (α-β) reference frame is given by [92]:

$$\psi_{\alpha\beta s} = \int v_{\alpha\beta s} - R_s i_{\alpha\beta s} dt = \left(\psi_{\alpha s}, \psi_{\beta s}\right) \tag{4.11}$$

In order to align the synchronously rotating (d-q) reference frame with the stator flux, information about the angle stator flux can be extracted using the following expressions:

$$\psi_s = \left|\psi_{\alpha\beta s}\right| angle\left(\psi_{\alpha\beta s}\right) \tag{4.12}$$

$$angle\left(\psi_{\alpha\beta s}\right) = \theta_e = \tan^{-1}\left(\psi_{\alpha s} \Big/ \psi_{\beta s}\right); \quad \left|\psi_{\alpha\beta s}\right| = \sqrt{{\psi_{\alpha s}}^2 + {\psi_{\beta s}}^2} \tag{4.13}$$

The angle θ_e gives the instantaneous location of the stator's rotating magnetic field. The rotor itself is rotating and is instantaneously located at angle θ_r. Thus, with a reference frame attached to the rotor, the stator's magnetic field vector is at the location $\theta_e - \theta_r$, which is referred to as the "slip angle."

From Equations (3.14.a)–(3.14.b), the alignment of the reference frame leads to a simplified model:

$$v_{qs} = \omega_e \psi_{ds} = v_s; \quad v_{ds} = 0 \tag{4.14}$$

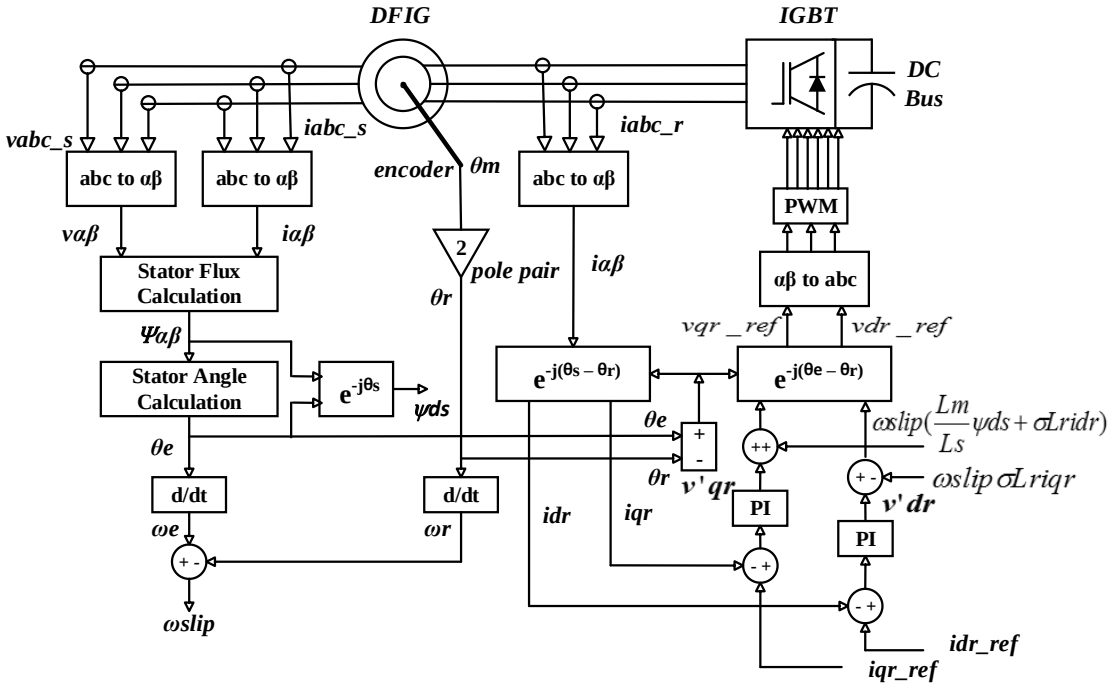

Figure 4.3: Control algorithm for the DFIG-based WECS

It can be observed that the electromagnetic torque depends on the i_{qr} current and can be controlled by the v'_{qr}. Also, the rotor magnetizing current i_{dr} can be controlled by the v'_{dr} voltage component. The controller is shown in Figure 4.3, where the errors between the currents i_{dr} and i_{qr} and the reference currents i_{dr_ref} and i_{qr_ref} are applied to the PI controllers to obtain the voltages v'_{dr} and v'_{qr} respectively. The controller output should be compensated with two decoupling terms in order to get the appropriate reference voltages, v_{dr_ref} and v_{qr_ref} as follows:

$$v_{dr\_ref} = R_r i_{dr} + \sigma L_r \frac{di_{dr}}{dt} - \omega_{slip} \sigma L_r i_{qr} \tag{4.15}$$

$$v_{qr\_ref} = R_r i_{qr} + \sigma L_r \frac{di_{qr}}{dt} + \omega_{slip}\left(\frac{L_m}{L_s}\psi_{ds} + \sigma L_r i_{dr}\right) \tag{4.16}$$

where,

$\psi_{ds} = \psi_s = L_M I_{ms}$; $I_{ms} = \psi_{ds} / L_M$; $\psi_{\mathrm{dr}} = L_M{}^2 I_{ms} / L_s + \sigma L_r i_{dr}$; $\psi_{qr} = \sigma \mathrm{L_r i_{qr}}$;

$\omega_{slip} = \omega_e - \omega_r$; $\sigma = 1 - \left(L_M{}^2 / L_s L_r\right)$

In this control approach, both rotor currents (i_{dr}, i_{qr}) are to be controlled in order to follow their respective references, i_{dr_ref} and i_{qr_ref}. Given the alignment of the reference frame with the stator flux, the *q*-current controls the active power of the machine whereas the direct current controls its reactive power. Thus, the *q*-current can be related to the electrical torque of the machine and the *d*-current can be related to the voltage value at the Point of Common Coupling (PCC) as indicated by:

$$i_{dr\_ref} = v_{qs} / \omega_e L_M \tag{4.17}$$

$$i_{qr\_ref} = -2T_e L_s / \left(3pL_M{}^2 i_{dr\_ref}\right) \tag{4.18}$$

The PWM converter acts on the rotor of the generator and the control is done by means of the signals of the rotor and the stator currents, the stator voltage, and the rotor position [93].

4.3.2. Speed Control of DFIG in Wind Energy Conversion System

The control of the variable speed wind turbines based on the doubly fed induction generator (DFIG) is a difficult engineering problem since: the induction machines are highly coupled, fast dynamics and nonlinear multi-variable system. On the other hand, the wind turbine has strong nonlinear characteristics and the aerodynamic torque change frequently. Among a variety of wind turbines, variable speed constant-frequency (VSCF) wind turbines with DFIG has many advantages including variable speed operation, and four-quadrant active and reactive power capabilities [94]. As shown in figure 4.1, the stator of the DFIG stator connects the grid directly and the rotor connects the grid by a dual PWM converter, the rated capacity of which is only a small part of wind turbine rated power. Compared with fixed speed wind turbine, the VSCF wind turbine can better capture the maximum wind energy in low wind velocity because of its adjustability of rotating speed. For the characteristic of wind energy is low energy density and strong randomness, wind turbine system requires efficient control strategy to utilize wind energy. So the maximum wind energy tracking in low wind velocity is the focus of research for wind energy conversion.

The Field-oriented vector control using cascaded PI controllers is widely using, in DFIG-based wind turbines, for reasons of simplicity and applicability [95]. It consists of controlling the stator currents represented by a vector. This control is based on projections which transform a three phase time and speed dependent system into a two co-ordinate (d and q co-ordinates) time invariant system. These projections lead to a

structure similar to that of a DC machine control. Field orientated controlled machines need two constants as input references: the torque component (aligned with the *q* co-ordinate) and the flux/reactive power component (aligned with *d* co-ordinate). As Field orientated control is simply based on projections the control structure handles instantaneous electrical quantities. This makes the control accurate in every working operation (steady state and transient) and independent of the limited bandwidth mathematical model. The technological development of semiconductors in both power and signal electronics has really enabled the application of field oriented control for accurate controlling of AC drives. In this system, field oriented control technique has chosen for controlling rotor side converter.

A hysteresis controller has proposed for controlling the grid side converter. The hysteresis control algorithm helps to maintain the constant frequency of the generated power from the wind turbine by matching with the grid frequency, generated voltage with the grid voltage. Constant frequency and voltage level are most important for grid connected/standalone system as well as one of the most difficult task to restrain from variation in wind energy conversion system. This controller can improve the power factor and try to maintain the power factor at unity so that the use of additional capacitor bank can be avoided at the power grid, which ultimately reduce the cost of power generation. As this controller is designed based on hysteresis current concept so it can protect the wind turbine from any fault occurred at grid side or in transmission line. When any fault happens in transmission line such as line to line or line to ground fault, line current

increases infinitely. In this controller the hysteresis band is designed such a way so that by comparing the abnormal current due to fault with its rated current limit, it can generate a pulse which drives the wind turbine like in normal condition. The performance of this controller has tested by implementing in various types of machines like PMSG, IG based wind turbine and the purpose of this controller is experimentally validated.

In this paper, the electromagnetic torque by means of rotor speed and reactive power are controlled by the rotor side converter (RSC), while the power transited to the grid is controlled by the grid side converter (GSC).

4.3.2.1. Adaptive Band Hysteresis (ABH) control for GSC

Hysteresis control is known to exhibit high dynamic response as the concept is to minimize the error in one sample. As the typically sampling frequencies are in the range of 50-100 kHz, which means a higher bandwidth. A constant band for the hysteresis comparator leads to variable switching frequency. An on-line adaptation of the band can be done in order to keep the switching frequency quasi-constant. The unit vector is generated from the grid voltage to estimate the flux and then angle in order to orientate the output reference currents with grid angle and for grid monitoring. This also exhibits improved performances under grid voltage variations due to the higher bandwidth of the current controller that help in order to keep the currents under the trip limits.

The DC-link voltage error is given by:

$$e = v_{dc\_ref} - v_{dc} \tag{4.19}$$

Also, its variation is expressed by:

$$\Delta e = \left(1 - z^{-1}\right) \tag{4.20}$$

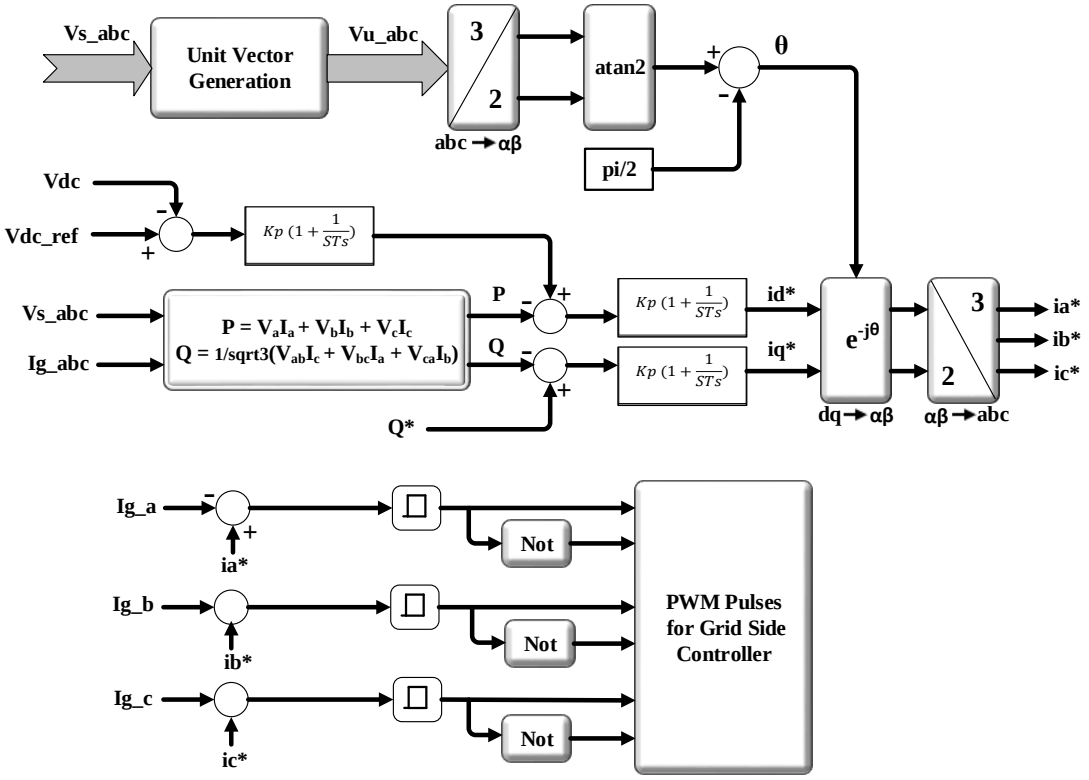

Figure 4.4: Control structure for ABH current control

The hysteresis current control system shown in Figure 4.4 is designed to maintain the DC-link voltage at a constant value and control the reactive power. This DC-link voltage magnitude is adjusted by controlling the amount of current supplied to the electrical grid. In the system, DC link voltage is maintained at 290V. The error between reference voltage *Vdc_ref* and actual voltage *Vdc* feed the PI controller to produce *id** and the error between reactive power reference Q* and actual reactive power Q through the PI produce the *iq**. The angular position θ is calculated for the transformation of rotating current *id**

and *iq** into three phase output reference current *ia*, ib*, ic** by inverse park transformation. The output reference current then compared to the actual current supplied to the electrical grid. The error difference between the signals are connected to the hysteresis current control, which produces the gate signal of the PWM. As the DC-link voltage increases, reference currents *id** produced also increase. When the current is lower than the reference current, the converter connects the positive side of the DC-link source to the load, thus the current increases. On the contrary when the current is higher than the current reference the converter connects the negative side of the DC-link source to the load, which reduces the currents. With these two operations, the error of the current can be maintained within a certain fixed band. The hysteresis controls the grid current by keeping the current wave in the range of the defined hysteresis band. When the current wave reached the band limits, the hysteresis controllers generate a control signal (0 or 1), which defines the PWM gate signal [96].

4.3.2.2. Rotor Side Controller

Mathematical model of stator and rotor circuit of doubly fed induction machine, which can be used for synthesis of control methods can be described by basic machines' equations in the excitation frame (4.21)-(4.24)

$$\bar{v}_s = R_s \bar{i}_s + \frac{d\bar{\psi}_s}{dt} + j\omega_e \bar{\psi}_s \tag{4.21}$$

$$\bar{v}_r = R_r \bar{i}_r + \frac{d\bar{\psi}_r}{dt} + j(\omega_e - \omega_r)\bar{\psi}_r \tag{4.22}$$

$$\overline{\psi}_s = L_s \bar{i}_s + L_m \bar{i}_r \tag{4.23}$$

$$\overline{\psi}_s = L_r \bar{i}_r + L_m \bar{i}_s \tag{4.24}$$

in which v_s, v_r are the vectors of stator and rotor voltage; ψ_s, ψ_r are the vectors of stator and rotor flux; i_s, i_r are the vectors of stator and rotor current; R_s, R_r, L_s, L_r are stator and rotor resistance and inductance; L_m represents mutual inductance; and ω_r, ω_e are rotor and synchronous angular speed where the frequency of rotor current, $\omega_s = \omega_e - \omega_r$ is called "slip frequency". It is needed in order for the rotor current vector in synchronization with the stator current vector.

The stator flux can also be calculated by converting the three phase stator voltage and current into the stationary (α, β) components according to (4.29)

$$\overline{\psi}_{\alpha\beta s} = \int \left(\bar{v}_{\alpha\beta s} - R_s \bar{i}_{\alpha\beta s} \right) dt = \left(\overline{\psi}_{\alpha s}, \overline{\psi}_{\beta s} \right) \tag{4.25}$$

In order to align the synchronously rotating (d-q) reference frame with the stator flux, information about the angle stator flux can be extracted using the following expressions:

$$\overline{\psi}_s = \left| \overline{\psi}_{\alpha\beta s} \right| angle\left(\overline{\psi}_{\alpha\beta s} \right) \tag{4.26}$$

$$angle\left(\overline{\psi}_{\alpha\beta s} \right) = \theta_e = \tan^{-1}\left(\overline{\psi}_{\beta s} \Big/ \overline{\psi}_{\alpha s} \right); \quad \left| \overline{\psi}_{\alpha\beta s} \right| = \sqrt{\left(\overline{\psi}_{\alpha s}{}^2 + \overline{\psi}_{\beta s}{}^2 \right)} \tag{4.27}$$

The angle θ_e gives the instantaneous location of the stator's rotating magnetic field. The rotor itself is rotating and is instantaneously located at angle θ_r. Thus, with a reference frame attached to the rotor, the stator's magnetic field vector is at the location $\theta_s = \theta e - \theta r$, which is referred to as the "slip angle".

The electromagnetic torque can be calculated from the stator flux vector in (α, β) components as:

$$T_{em} = \frac{3}{2} p\left(\overline{\psi}_{\alpha s} \bar{i}_{\beta s} - \overline{\psi}_{\beta s} \bar{i}_{\alpha s}\right) \tag{4.28}$$

This can also be conveniently analyzed by the classical rotating field theory with the well-known (d, q) transformation of rotor equation at synchronous reference frame as:

$$T_{em} = \frac{3}{2} p\left|\overline{\psi}_{dqm}\right|\left|\bar{i}_{dqr}\right| \sin\delta \tag{4.29}$$

where,

$$\overline{\psi}_{dqm} = \overline{\psi}_{dqr} - \bar{i}_{dqr} L_{lr} \tag{4.30}$$

δ is the spatial angle between the airgap flux and rotor current vectors seen in the synchronous reference frame. With the alignment of the airgap flux to the d axis of the reference frame, we can get

$$\overline{\psi}_{dqm} = \overline{\psi}_{dm} \quad \text{and} \quad \overline{\psi}_{qm} = 0 \tag{4.31}$$

The torque equation is reduced to

$$T_{em} = \frac{3}{2} p\left|\overline{\psi}_{dm}\right|\left|\bar{i}_{qr}\right| \tag{4.32}$$

Finally, according to the instantaneous power theory, which is useful for control of power conversion systems, instantaneous stator power components P_s, Q_s can be calculated as:

$$P_s = \frac{3}{2}\left(\bar{v}_{\alpha s}\bar{i}_{\alpha s} + \bar{v}_{\beta s}\bar{i}_{\beta s}\right) \tag{4.33}$$

$$Q_s = \frac{3}{2}\left(\bar{v}_{\beta s}\bar{i}_{\alpha s} - \bar{v}_{\alpha s}\bar{i}_{\beta s}\right) \tag{4.34}$$

The objective of the RSC controller is to keep the machine rotor speed near the optimum wind energy capture point on the wind turbine characteristic by controlling active and reactive power flows at the stator [97]. The doubly fed induction machine is controlled in a synchronously rotating (*d, q*) axis frame with the *d*-axis aligned along the stator flux position. This permits decoupled control of the electromagnetic torque and rotor excitation currents [98]. The PWM converter acts on the rotor of the generator and the control is done by means of the signals of the rotor and the stator currents, the stator voltage and the rotor position.

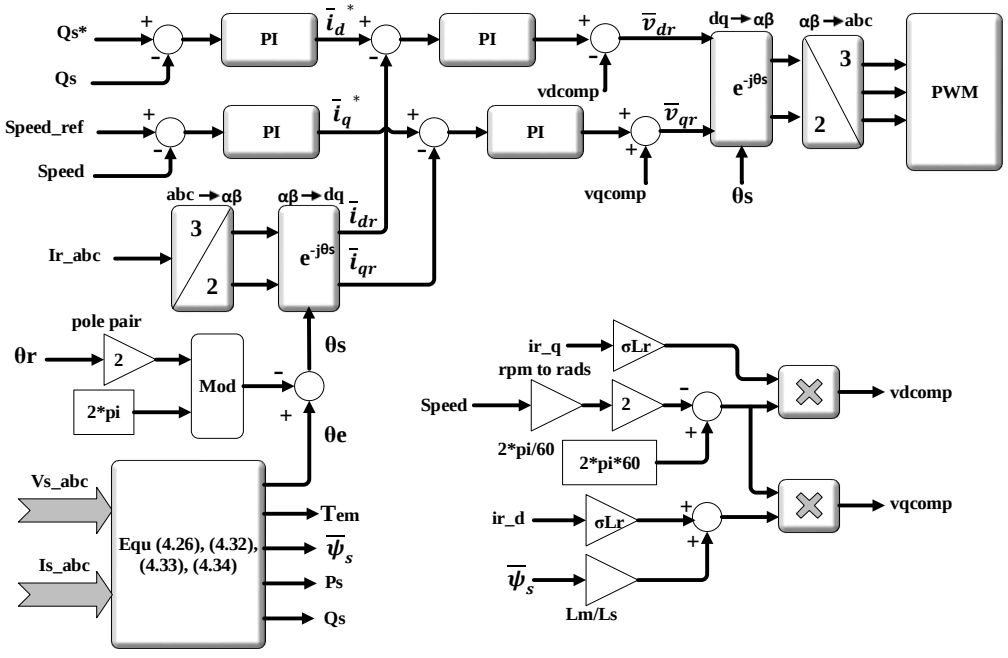

Figure 4.5: Control structure for Torque and Reactive power control

The rotor voltage in the (*d*, *q*) reference frame can be obtained from

$$\bar{v}_{dr} = R_r \bar{i}_{dr} + \partial L_r \frac{d\bar{i}_{dr}}{dt} \tag{4.35}$$

$$\bar{v}_{qr} = R_r \bar{i}_{qr} + \partial L_r \frac{d\bar{i}_{qr}}{dt} \tag{4.36}$$

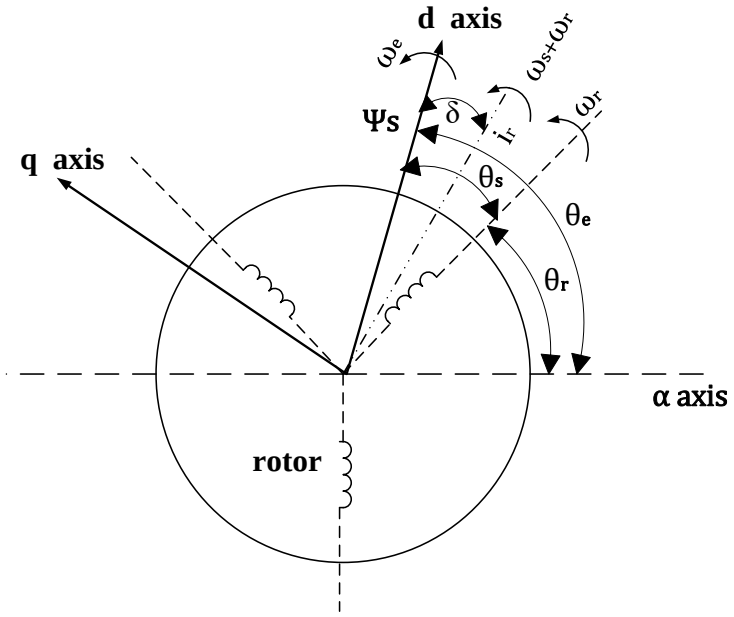

Figure 4.6: Phasor diagram of spatial angle control

It can be observed that the electromagnetic torque depends on the $\bar{i}_{qr}$ current and can be controlled by the $\bar{v}_{qr}$ voltage. Also, the rotor magnetizing current $\bar{i}_{dr}$ can be controlled by the $\bar{v}_{dr}$ voltage component to control the reactive power. The precise control of the currents $\bar{i}_{qr}$ and $\bar{i}_{dr}$ allows the control of the stator side real and reactive power. The controller is shown in Figure 4.5. The errors between the reference speed and the actual rotor speed and between the reference reactive power and the measured reactive power

from the system are applied to the PI controllers to obtain the reference currents $\bar{i}_q^*$ and $\bar{i}_d^*$ respectively. The rotor current $\bar{i}_{qr}$ and $\bar{i}_{dr}$ is tracking the reference currents $\bar{i}_q^*$ and to $\bar{i}_d^*$ fulfill the purpose of this controller. For this, the slip angle must be calculated as shown in Figure 4.6. Reference $\bar{i}_d^*$ current can be set to zero so that no reactive power flows into grid and obtain unity power factor. However in case of reactive power demand by grid under unbalance condition it can be changed. A compensation terms can be added in the rotor voltage equations to improve the transient response of the system which can be concluded equations (4.35) and (4.36) as below:

$$\bar{v}_{dr} = R_r \bar{i}_{dr} + \partial L_r \frac{d\bar{i}_{dr}}{dt} - \omega_{slip} \sigma L_r \bar{i}_{qr} \tag{4.37}$$

$$\bar{v}_{qr} = R_r \bar{i}_{qr} + \partial L_r \frac{d\bar{i}_{qr}}{dt} + \omega_{slip} \left(\frac{L_m}{L_s} \overline{\psi}_{ds} + \sigma L_r \bar{i}_{dr} \right) \tag{4.38}$$

where,

$$\omega_{slip} = \omega_e - \omega_r ; \quad \sigma = 1 - \frac{L_M^{\ 2}}{L_s L_r}$$

PI algorithm computes and transmits a controller output signal every sample time, Ts, to the final control element (e.g., $\bar{i}_{qr}$ and $\bar{i}_{dr}$). The computed controlled output from the PI algorithm is influenced by the controller tuning parameters and the controller error, e(t). PI controllers have two tuning parameters to adjust. While this makes them more challenging to tune than a P-Only controller, they are not as complex as the three parameter PID controller. Integral action enables PI controllers to eliminate offset, a

major weakness of a P-only controller. Thus, PI controllers provide a balance of complexity and capability that makes them by far the most widely used algorithm in process control applications. The main reason for not using the D term is that it amplifies high frequency noise.

4.3.2.3. Speed Estimation of DFIG

In order to extract maximum power from WECS the turbine needs to be operated at optimal angular speed which varies continually with change in the wind speed throughout a day. So, most recent papers try to achieve sensorless maximum power extraction from available wind power by avoiding mechanical sensors which lead to inaccurate measurements due to mechanical parts consideration and their high priced [99].

Model reference adaptive systems (MRAS) are the most popular strategies used to estimate the rotor speed and the rotor flux due to their simplicity and low computational effort. In general, MRAS are based on a reference model (voltage model) and an adaptive model (current model) for rotor flux estimation and adaptation scheme through a PI controller to estimate the rotor speed. The accuracy of MRAS methods depends on the exactness of the reference model, which is sensitive to parameters variations, and the way of controlling the overall system [100]–[102]. Neural Network based flux observer has been used in reference model to detect the thermal variation in stator resistance or in current model to reduce the dependency on reference model at different operating

conditions though the current model is adapted through a PI controller which can reduce the reliability when operated in hostile environment [103]–[105].

In this section, MRAS based speed estimation has developed where an Artificial Neural Network (ANN) is used instead of PI to estimate the speed which adapts the current model to reduce the dependence on reference model. The adaptation mechanism is based on ANN method to improve the speed estimation performance.

1. Stator flux based MRAS-ANN speed estimator

A MRAS-ANN speed observer is used to estimate the rotational speed and rotor position of the DFIG [106]. This observer is based on two models: a voltage model as a reference model and a current model as an adjustable model. In a stationary frame the voltage model is used to obtain the stator flux as:

$$\vec{\phi}_S = \int \left(\vec{v}_S - R_S \vec{i}_S\right) dt \tag{4.39}$$

The stator voltage drop $R_S\vec{i}_S$ will be small under rated v_s operation so that the flux estimate of (4.39) is relatively insensitive to R_s. Using a stationary frame, the stator flux is obtained from the current model as:

$$\hat{\vec{\phi}}_s = L_s \vec{i}_s + L_m \vec{i}_r e^{j\hat{\theta}_r} \tag{4.40}$$

where $\hat{\omega}_r$ is an estimation of the rotational speed. The current $\vec{i}_r$ is referred to the rotor frame. In the MRAS-ANN observer, the flux obtained from (4.39) is used as the reference flux. By adjusting the estimated rotational speed, the error between the

reference flux and the flux estimated from (4.40) is reduced. The error in (α, β) coordinates is defined as

$$\xi = \vec{\hat{\phi}}_{\alpha s}.\vec{\phi}_{\beta s} - \vec{\phi}_{\alpha s}.\vec{\hat{\phi}}_{\beta s} \tag{4.41}$$

Equations (4.39)–(4.41) are used to implement the MRAS-ANN speed observer. The error calculated using (4.41) is driven to zero by a backpopagration algorithm. The output of ANN is the estimated rotational speed used in (4.40) which is further integrated to get the rotor position. The implementation of MRAS-ANN observer is shown in Figure 4.7.

2. Rotor current based MRAS-ANN speed estimator

MRAS-ANN observers for sensorless operation of the DFIG can also be implemented using the rotor current vector. This type of MRAS-ANN observer has the advantage that $\vec{i}_s$ and $\vec{i}_r$ are both measured quantities. The implementation of estimation technique is given in [106]. For this, the reference model is the rotor current $\vec{i}_r$ measured from rotor windings by the sensors and for the adaptive model the rotor current $\vec{\hat{i}}_r$ is estimated from stator reference frame. The error between estimated and actual rotor current goes to the ANN to estimate the speed $\hat{\omega}_r$ and adaptive model is updated by the rotor angle $\hat{\theta}_r$ comes from further integrating the estimated speed.

An estimation of $\vec{\hat{i}}_r$ is obtained using $\vec{i}_s$ and $\vec{v}_s$. In the stationary frame the stator flux can be written as:

$$\vec{\phi}_s = L_s\vec{i}_s + L_m\vec{i}_r e^{j\theta r} \tag{4.42}$$

From (4.42) the rotor current is obtained as:

$$\vec{i}_r = \frac{\vec{\phi}_s - L_s\vec{i}_s}{L_m} e^{-j\theta r}; \qquad \text{where,} \quad \vec{\phi}_s = \int \left(\vec{v}_s - R_s\vec{i}_s\right)dt \tag{4.43}$$

Replacing θ_r by $\hat{\theta}_r$ in (4.43), an estimation of rotor current is obtained as:

$$\hat{\vec{i}}_r = \frac{\vec{\phi}_s - L_s\vec{i}_s}{L_m} e^{-j\hat{\theta}r} \tag{4.44}$$

The MRAS error is now defined as the cross product between:

$$\xi = \hat{\vec{i}}_{\alpha r}\vec{i}_{\beta r} - \vec{i}_{\alpha r}\hat{\vec{i}}_{\beta r} \tag{4.45}$$

Using equations (4.42)–(4.45) rotor current based MRAS-ANN speed estimator is implemented. The error calculated using (4.45) is driven to zero by a backpopagration algorithm. The output of ANN is the estimated rotational speed, which is further integrated to get the rotor position.

3. Artificial Neural Network Based Rotor Speed Estimator

The ANN used for the rotor speed estimation is a recurrent multilayer network, shown in Figure 4.8, with two external inputs (the rotor flux from the voltage model and the estimated rotor flux from the current model), the delayed output as a feedback. Its structure has one hidden layer. In this hidden layer there are five neurons which are activated by a tanh (hyperbolic tangent) function and the output layer is activated by the linear function [107]. The weight from input to hidden layer and hidden layer to output

are updated online by backpropagation algorithm.

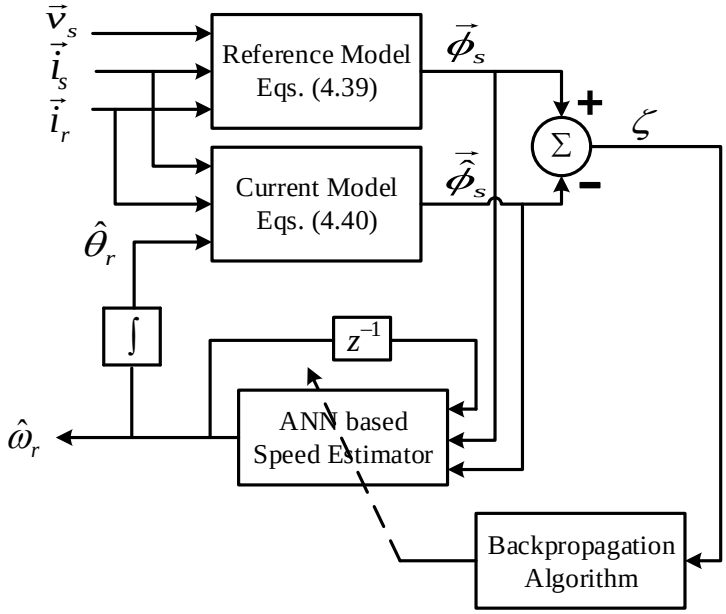

Figure 4.7: ANN based MRAS speed estimator

The estimated speed (ANN output) is given by the following equations

$$\hat{\omega}_r(k) = \sum_{i=1}^{N} w_i \tanh\big(h(k,i)\big) \tag{4.46.a}$$

$$h(k,i) = w_{1i}\hat{\omega}_r(k-1) + w_{2i}\vec{\phi}_s(k) + w_{3i}\vec{\hat{\phi}}_s(k) \tag{4.46.b}$$

where, $\hat{\omega}_r$ is the estimated rotor speed, w_{ji} are the weights between the input layer and the hidden layer, w_i are the weights between the hidden layer and the outputs layer, N is the number of neurons in the hidden layer, j= 1:3 and i = 1: N.

The training of the ANN, to update its weights and biases, is done online by a backpropagation method based on the error between the rotor flux generated by the voltage model and the rotor flux estimated by the current/adaptive model.

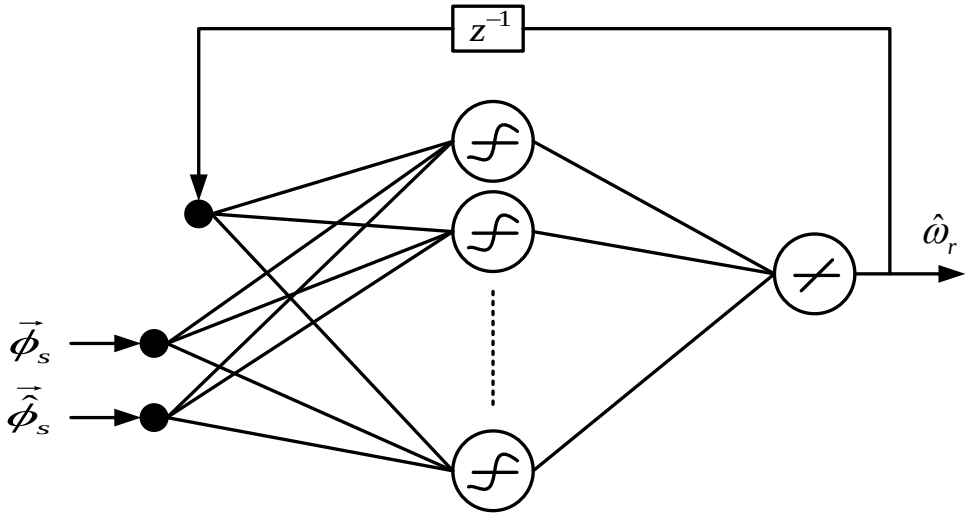

Figure 4.8: Neural network structure for the rotor speed estimation

The online training algorithm operates as follows:

- Step 1: Initialize the values of the inputs $x_{j=1\cdots3}$ = ($\hat{\omega}_r$, $\vec{\phi}_s$, $\vec{\hat{\phi}}_s$) and the weights (w_i, w_{ji}).
- Step 2: Calculate $h(k-1,i)$ for i =1: N and the error $e(k-1) = \vec{\phi}_r - \vec{\hat{\phi}}_s$
- Step 3: update the weights

$$w_i(k) = w_i(k-1) + \mu \cdot h(k-1,i) \cdot e(k-1) \tag{4.47}$$

$$w_{ji}(k) = w_{ji}(k-1) + \mu \cdot x_j(k-1) \cdot \left(w_i(k-1)\left(1-h(k-1,i)\right) \cdot e(k-1)\right) \tag{4.48}$$

- Step 4: $k=k+1$ and go to step 2, where, μ is the learning rate (good learning rate has found 0.001)

Conclusion

In this chapter, detailed wind turbine control system at variable speed operation was illustrated. Further, two control methods were presented to control grid tied DFIG based wind turbine control. Mainly, controllers were proposed to control the power generated by the DFIG itself in wind energy conversion system while power transmitted to the grid by fulfilling the grid code requirements. Rotor side controllers were built to control the rotor excitation by controlling magnetizing current. In the same time, grid side controller was designed to control the DC-Link voltage and to control the reactive power injected into the grid. Usually the grid side converter is operated at unity power factor, but it can be used for voltage support during grid faults, by injecting reactive power in the grid. It also supports the DFIG by providing the reactive power back and forth from grid when it necessary. Finally, the MRAS-ANN based speed estimator presented with state estimation process (rotor flux, rotor speed) to estimate the rotor speed for controlling of sensorless DFIG in grid tied wind energy conversion system.

Chapter 5

Real-Time Simulation Environment

5.1. Introduction

The Real-Time Simulation (RTS) has been used extensively in the planning and design of electrical systems for decades. Real-time simulation technology can be defined as a computer model building from a real physical system that can be run in the computer at the same rate as actual time [108]. Therefore, the RTS brought many advantages for engineers such as cost avoidance, increase quality, complete physical testing, reuse of simulator, more tests in the lab, early faults detection, increase productivity, and less test on the site. Simulation tools have got a rapid evolution from the analog simulators at the beginning to the digital simulators in the past decades. Unlike the simulators with limited capability and high cost at the early stage, the modern simulators not only possess more powerful capability that can solve more complicated problems in less time, but also become affordable by wider users and make digital simulators available in more areas. At present, the digital simulators have been used widely in a number of industries. Especially, the real-time simulation, based on automatic code generation, has played vital role in many engineering field and applications, such as aircraft flight control design & validation, industrial motor drive design, complex robotic controller design and power gri

-d statistical protection tests [109].

5.2. Functions of Real-Time Simulation

The real-time simulation can be defined as a virtual model established by computer on the basis of the objective physical system. It can work at the same rate as actual time, namely, the actual physical time. With this capability in nature, a real-time simulator can bring benefits to industrial design in many aspects. Generally, the functions of the real-time simulation can be classified into three applications categories as shown in Figure 5.1 [109-110]

- Rapid control prototyping (RCP)
- Hardware-in-the-loop (HIL)
- Pure Simulation (PS)

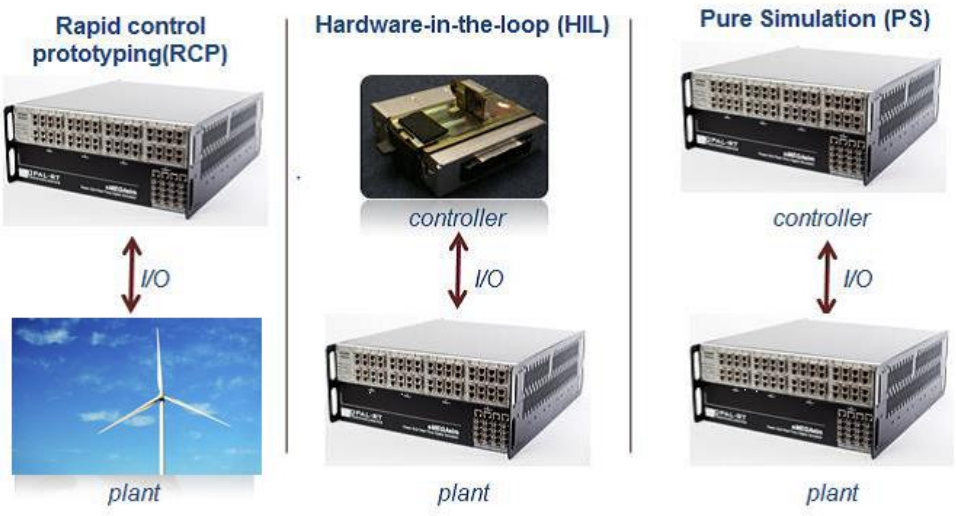

Figure 5.1: Applications categories of real-time simulation

In the RCP function, a proposed controller archetype is established into a virtual model by a real-time simulator and connected with physical plant by I/O port. Instead of testing a physical controller, a virtual model provides a more flexible, faster and more economical way for controller debug [110]. Since the controller prototype is a virtual model implemented by the simulator, any tuning and modification can be easily completed by a few mouse clicks. Especially in a very big system, such as a large power grid or an aircraft, the virtual controller archetype can be tested by external physical plant and make adjustment accordingly. On the contrast, it will be a nightmare that some problems are found after the entire physical prototype is established.

The HIL simulation aims to provide an effective platform for developing and testing physical controller. When the current hardware is much more complicated than before, the complexity of the embedded system, which is designed to control hardware, also has a great improvement. Through HIL simulation, the designed controller no longer needs to wait for a physical plant to write or test code. The plant is able to be replaced by a virtual model established by a real-time simulator, in which the testing can include the simulation for large versions of the plant, such as a high power generator. Usually, it is risky to test a controller in a large physical plant. Especially, testing the physical controller in some extreme case, such as simulation of over burdening, would likely destroy a physical plant [111]. For these facts, the HIL simulation is introduced to work as an effective platform in a controller testing, especially for the case of some very complicated plants which are hardly achieved in physical model.

Unlike RCP and HIL involving physical model in test, PS mode employs virtual models to take the places of both controller and plant in the real-time simulation. Since there is no input and output signals between virtual model and physical model, the signal loss existed in RCP and HIL is able to be eliminated in PS mode. As a result, the test in PS mode will be more accurate than RCP and HIL mode without the influence of signal loss. Moreover, PS mode can also provide a faster simulating speed than real-time with no impact on the validity of results. Because of the higher simulating rate and more powerful calculation capability than other simulators, the design period of a controller can be effectively shortened.

5.3. Time-Step in Real-Time Simulation

Simulation can be simply defined as an imitation of the operation in a real-world process or system over time [112]. In order to simulate a system in a valid way, it is necessary to set every components of the system in an appropriate rate and guarantee signals transferring between subsystems with a correct timing. In a real-time system, a constant duration is decided as a discrete time interval in advance. The processor of a real-time simulator has to repeatedly complete three procedures in each predetermined time interval as shown in Figure 5.2. The processor first receives input data from other systems and then computes all the functions and equations representing a system in accordance with the data. After the computation is completed, the result will be written and output from the processor. All these three steps should be finished during the predet-

ermined time interval which is normally known as fixed-step simulation.

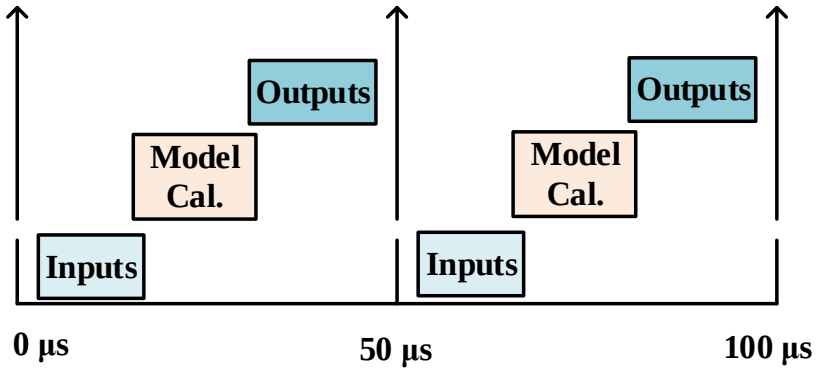

Figure 5.2: Fixed time step simulation

Depending on the different complicacy of a virtual system, the time spent on calculating functions and equations of the virtual system could be variable. Once the time step of a simulation is determined in advance, the actual time that a processor takes could be either longer or shorter than the time step. In order to make sure that a real-time simulation works validly, a simulator has to take less time than the predetermined time step, otherwise, the simulation would be working on an inaccurate state which is called "overrun". Figure 5.3 illustrates the overrun phenomenon, in which the predetermined time step is too short and the simulator spends longer time on computation than the predetermined time interval. In this case, the simulator not only occupies the first time step, but also takes part of the second steps. Then all the tasks of simulator in the second time-step, including signal input, computation and result output, are omitted. Meanwhile, the simulator directly jumps over the rest of the idle time step and waits until the clock ticks to the next time-step. Especially in the HIL and RCP modes of real-time simulation, the simulator has to have a same operating rate as the actual physical devices since the

simulator aims to swap data through inputs and outputs (I/O) with externally physical devices. If a simulator cannot complete the three tasks in time, which may be caused by a too complicated virtual system or lack of computation capability in simulator, the real-time simulation result is considered erroneous.

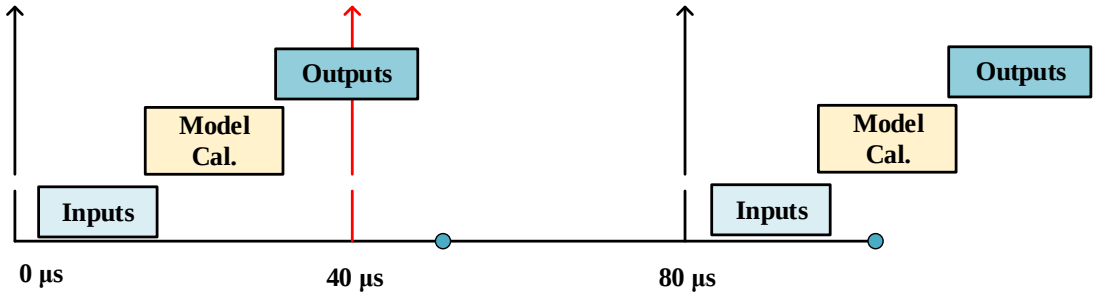

Figure 5.3: Overrun phenomenon in real time simulation

5.4. RT-LAB™ for Real-Time Simulation

As a real-time simulation platform, the RT-LAB™ software is used to achieve high-fidelity plant simulation control system prototyping, and embedded data acquisition and control. Meanwhile, its distributed processing capability also allows users to quickly convert Simulink™ or Systembuild™ models to high-speed, real-time simulations, over one or more target PC processors. It is flexible enough to be applied to the most complex simulation and control problem no matter whether it is for real-time hardware-in-the-loop applications or for speeding up model execution, control and test. [111, 113]

The real-time simulation aims to get smaller maximum time step and maintain the simulation accuracy to a certain level with fixed-time step solver. Comparing with the typical variable-step solvers, the utilization of the fixed-time step solver can lead to some

inaccuracies because there is no built-in accuracy check within the solvers [114]. In order to realize complicated electrical systems in real-time simulation and improve accuracy of the result, the RT-LAB^{TM} Electrical Drive Simulator comes with some special Simulink-based modeling tools, such as ARTEMiS and RT-Events, which permits the real-time simulation of an electrical system at practical time step of 10μs.

5.4.1. ARTEMiS

ARTEMiS works as a plug-in blockset under the SimPowerSystem and helps to improve distributed simulation of power systems over multiple processors. Other than normal simulations whose objective is to minimize total simulation time or the smallest average simulation time step, a real time simulation is proposed to get a smaller maximum time step to fulfill the operating rate of the external physical devices in the simulation while keeping the accuracy in a certain extent. For these purposes, Artemis is introduced to satisfy real-time simulation requirements in several aspects [114]. First, ARTEMiS can extend the range of time step to achieve both speed and precision for a specific real-time application. Second, some oscillations caused by network switching are hardly damped under minimum hardware limits. To solve this fact, ARTEMiS solvers' good damping properties are able to damp the spurious oscillations efficiently. Third, in applications where some underdamped or high frequency components, relative to the fastest possible sampling time, must be taken into account, ARTEMIS improves the precision of those components comparing to the trapezoidal or Tustin methods. Moreover, ARTEMiS also offers a new solver called State-Space Nodal which combines

the accuracy potential of state-space methods with the natural ability of the nodal approach to handle circuit with a large number of switches.

5.4.2. RT-Events

Similar to ARTEMiS, RT-Events is another blockset that can be used with the Simulink software and that enables the simulation of event-based systems that comprise continuous- and discrete-time subsystems whose dynamics changes due to discrete events [115]. Generally, RT-Event is introduced to solve following problem encountered in the simulation of event-based systems. During a simulation, errors would be introduced by the situations that some switching events may occur between the sampling instances or multiple events occur in a single time step. Although the standard Simulink blocks are able to compensate the errors through the variable time step solver, it is still inaccurate due to the lack of the timing information.

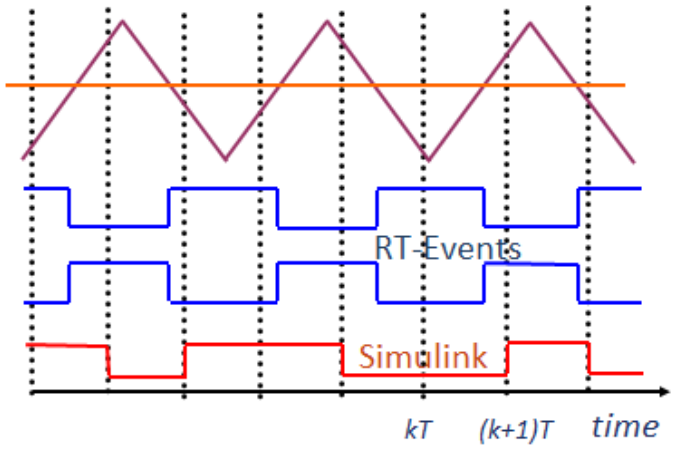

Figure 5.4: Comparison between RT-Event and Standard Simulink

This problem would be worse when the fixed-time step in the order of 10-100 us.

In the terms of the RT-Event, although the switching signal is updated in every sampling instant as same as standard SimPowerSystem, the accuracy of simulation result is highly increased for the same time-step since the switching and state transition information are concurrently kept in the time stamp as shown in Figure 5.4.

5.5. Model Building & Execution in RT-LAB^{TM} for Real-Time Simulation

Simulink model has built into RT-LAB^{TM} with rapid controller prototyping (RCP) for real time simulation and control of a grid connected doubly fed induction generator (DFIG) based laboratory size wind turbine emulator for wind energy conversation system. RT-LAB^{TM} uses Simulink to define models and corresponding parameters which will be executed by the real-time multi-processing system. DFIG based wind turbine (DFIG-WT) Simulink model is implemented in RT-LAB^{TM} environment by performing the flowing steps.

- Regrouping into subsystems
- Adding the OpComm block(s)
- Maximizing parallel execution and state variables
- Setting the real-time parameters

In order to execute the model in different target processors, or nodes, it is separated into two subsystems:

1- Console subsystem, which must be identified by the prefix (SC_) in its name

(SC_name), is executed in the command station-PC and includes user interface blocks, such as scopes, displays and reference command;

2- Master subsystem, which must be identified by the prefix (SM_) in its name (SM_name), is executed in the CPU core processor of the OP5600 and includes all the computational elements of the model, the mathematical operations of the algorithms and the input-output blocks. As the two subsystems are executed in different targets, or nodes, the communication and synchronization between them is done through the RT-LAB^{TM} OpComm blocks as shown in Figure 5.5.

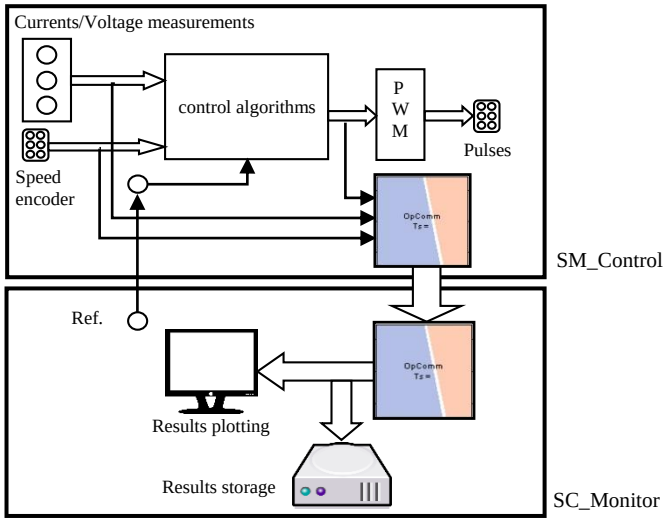

Figure 5.5: Subsystems of the model in RT-LAB

The Simulink model of the control system is opened via RT-LAB^{TM} and compiled in the real time target (OP5600), then, it is automatically loaded, by RT-LAB^{TM}, into the CPU core of the OP5600 for the master subsystem. The OP5600, real-time digital simulator, consists of analog and digital I/O signal modules, a multi-core processor and

FPGA that runs RT-LAB^{TM} real-time simulation platform. The OP8660, HIL Controller and Data Acquisition Interface, is a signal conditioning interface simplifies the connectivity between the virtual environment (the real-time simulator OP5600) and the real experimental system (Dynamometer, DFIG, power electronics inverters, grid, load) as shown in Figure 5.6. Finally, the subsystems of the model are simultaneously executed in the CPU core of the OP5600, for the SM subsystem, and the command Host-PC, for the SC subsystem to run the wind energy conversion system in real time, where all the sequencing, communication and synchronization processes are managed by RT-LAB^{TM}.

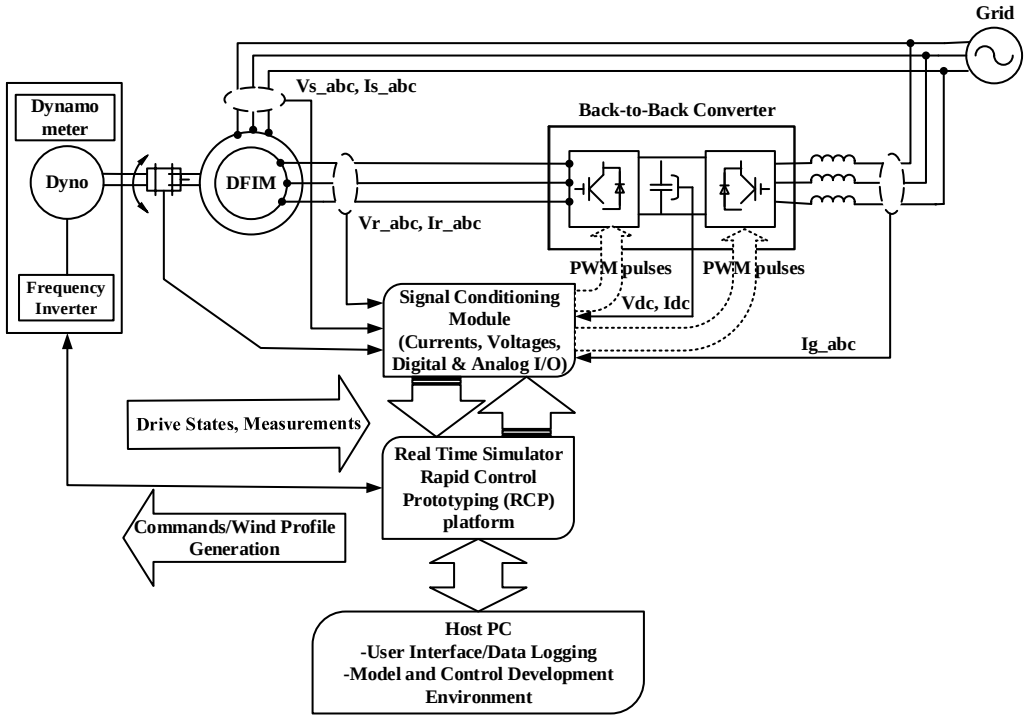

Figure 5.6: Execution of DFIG based wind energy conversion system in Real-Time Simulation

Conclusion

Simulation tools have been widely used for the design and improvement of electrical systems since the mid twentieth century. The evolution of simulation tools have progressed in step with the evolution of computing technologies. In recent years, computing technologies have improved dramatically in performance and become widely available at a steadily decreasing cost. Consequently, simulation tools have also seen dramatic performance gains and steady cost decreases. This chapter presented the overview of real-time simulation with their applications in modern technologies and the modeling and execution of laboratory scale DFIG based wind turbine emulator in wind energy conversion system.

Chapter 6

Experimentation

6.1. Introduction

A 2kW doubly fed induction machine whose parameter details given in Appendix I was emulated and validated experimentally as a real wind turbine in a laboratory scale wind energy conversion system using Opal-RT's real time digital simulator OP5600 and Data acquisition system OP8660 under Simulink/RT-Lab environment. The performance of the DFIG system is analyzed under low grid voltage. Firstly, the power control of DFIG is done by controlling the magnetizing rotor current. The effect of change in wind speed and change in supply frequency are also taken into consideration for the performance analysis of DFIG. The analysis is also done by varying the DC-Link reference voltage to show the robustness of the controller. Secondly, the performance of DFIG speed control operation in grid tied wind energy conversion system is analyzed. It generates the maximum power under the variable the wind speed and the generated power follows the wind speed profile which verify the robustness of the controller. To make the use of sensorless DFIG based power generation convenient and feasible, a conventional MRAS based speed estimation technique has improved by ANN. The performance of machine's parameters and speed estimation by Artificial Neural Network

is also analyzed using Matlab/Simulink and results are validated using Opal-RT's OP5600 real time digital simulator in RCP mode.

6.2. Experimental Rig Setup

Experiments were conducted on the platform shown in Figure 6.1, following the schematic of all connected modules is shown in Figure 6.2. The experimental system consists of the following modules:

1- A six-phase doubly fed induction generator fed by a controlled inverter its rotor terminal and its stator terminal are connected to the power supply. The specifications of the machine and power supply are given in Appendix I.

2- A variable frequency IGBT inverter operated by the rotor side controller, where the PWM pulses are generated from the controller outputs to act as switch control inputs.

3- A variable frequency IGBT inverter works as a DC-AC converter operated by the hysteresis controller, where the PWM pulses are generated from the controller outputs to act as switch control inputs.

4- A four quadrant dynamometer is coupled with the doubly fed induction generator to emulate the effect of real bladed wind energy turbine in a laboratory scale wind energy conversion system.

5- Data acquisition interface (OPAL-RT OP8660) to measure voltage and current.

6- The OPAL-RT real-time digital simulator (OPAL-RT OP5600) is a powerful tool

for rapid control prototyping and hardware-in-the-loop applications and is equipped with Intel® Xeon Quad Core 2.4 GHz Processor.

6.2.1. Hardware Components

The experimental system shown in Figure 6.1 consists of a 4-pole three-phase wound-rotor induction machine. Each phase of the stator winding is accessible via the connection module to allow wye or delta connections.

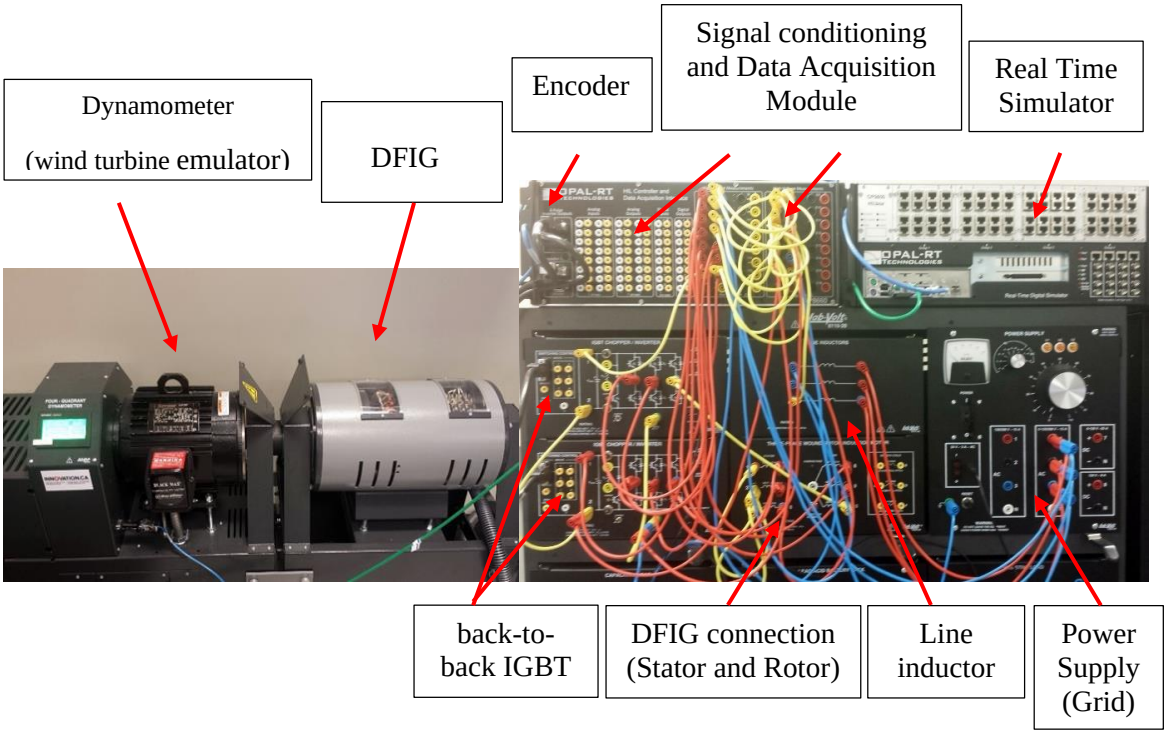

Figure 6.1: Experimental setup to emulate WECS

The rotor is wye connected to four slip rings to give access to all windings, including neutral; a four quadrant dynamometer, type of squirrel cage induction motor with an encoder feedback; two back-to-back 6 pulse IGBT inverters, the switching frequency

(here 3kHz) should be chosen in a way that the balance between switching losses and accuracy of the desired signals achieved; a line inductor, a 2 kW variable power supply, Opal RT's data acquisition system OP8660, and real-time digital simulator OP5600, which is a powerful tool for rapid control prototyping with Intel® Xeon Quad Core 2.4 GHz Processor.

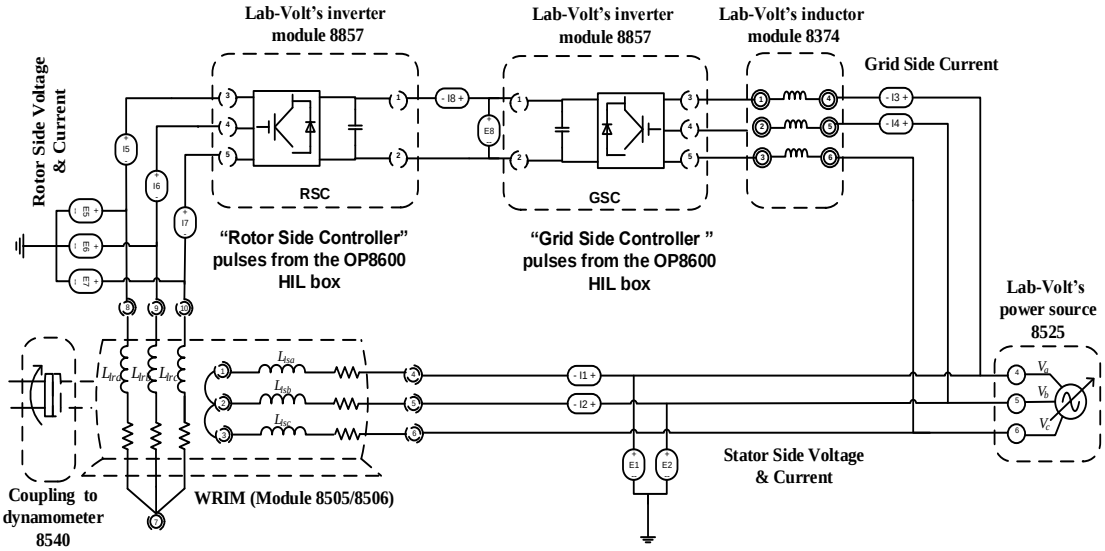

Figure 6.2: Schematic of the connected experimental setup to emulate WECS

6.2.2. Software Components

RT-LAB™ represents a complete software environment that integrates OP5600 simulator with the powerful graphical, model-based capabilities of Matlab/Simulink. The control and mathematical model is created in Simulink where it is compiled in C code using the Real time Workshop tool integrated in Matlab. The code is then loaded into the real time simulator. Once the model is running in the real time simulator, a Simulink-based interface (i.e. console) is created to give the user access in real time to the signals

and parameters within the model. This interface is used for monitoring different measurements, adjusting system parameters and operation modes of the experimental rig as shown in Figure 6.3. At any time while the model is running RT-LAB allows: fully configuring the data acquisition properties; modifying; monitoring the simulator's real time performance.

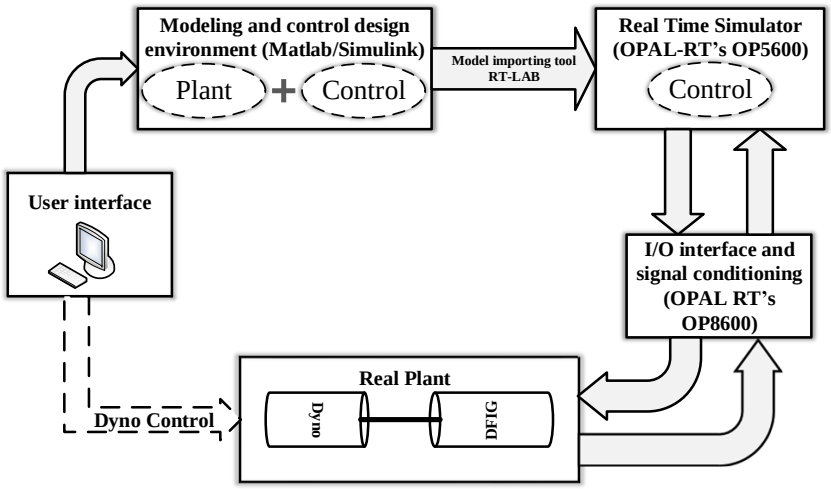

Figure 6.3: Schematic of monitoring and control the experiment from RT-LAB™

6.3. Active and Reactive Power Control by Controlling Rotor Current

In this experimental rig, a 60Hz, 2kW, 120V, 2-pole pairs slip ring wound rotor induction generator is driven at a variable speed by a standard 4-pole squirrel cage induction motor works as a real wind turbine emulator to generate the effect of wind on the bladed rotor of a wind turbine. This driving motor is controlled by a commercial variable frequency converter. The voltage level of the DFIG is limited to 60V due to saturation effects in the generator. Thus the whole DFIG system has a rated power of

2kW including grid side converter. OP8660 data acquisition system with analog and digital I/O is used to measure the voltages and currents of the real experimental system as shown in Figure 6.1. Finally, OP5600 real time digital simulator is used to run the developed control algorithm (discussed in section 4.3.1) inside in it for emulating the laboratory scale wind energy conversion system with rapid control prototyping.

6.3.1. *Power Control by Rotor D-Current*

In this test, the dynamometer (wind turbine emulator) is running at constant speed, as shown in Figure 6.4, and the active power can be controlled by controlling the rotor *d*-current i_{dr} to follow a reference i_{dr_ref} , while reactive power can be controlled by regulating the rotor *q*-current i_{qr} to be constant at i_{qr_ref} . Responses of the controlled rotor *d*- and *q*-currents are illustrated in Figures 6.5 and 6.6, respectively, and it can be seen that the current tracking for both currents is successfully achieved. From the rotor power response, shown in Figure 6.7, it can be observed that the change in active power can be controlled by varying the rotor *d*-current i_{dr_ref} . The change in active power makes slightly effect on the reactive power changes. The reactive power increases while the active power decreases to balance the total power at rotor side. In Figure 6.8, it can be seen that due to the controlled rotor currents i_{dr} and i_{qr}, the induced active and reactive power at the stator side are fulfilling the grid demand as it is directly connected with the grid. Figure 6.9 illustrates the overall response of active and reactive power from DFIG are being controlled by controlling the rotor currents i_{dr} and i_{qr}. It is

clear that the rotor *d*-current i_{dr} controlling the generated active power (shown in positive region) of DFIG which is transmitting to the grid and rotor q-current controlling the reactive power which will be either transmitted to the grid or consumed from the grid. In this case, the reactive power is being consumed from the grid (shown in negative region). This is a practical controller that supports the reactive power to the grid to improve the power factor. Furthermore, the DC-link voltage is successfully regulated to follow a constant reference, as shown in figure 6.10, by the grid side controller despite the variation of the rotor *d*-current at the machine side.

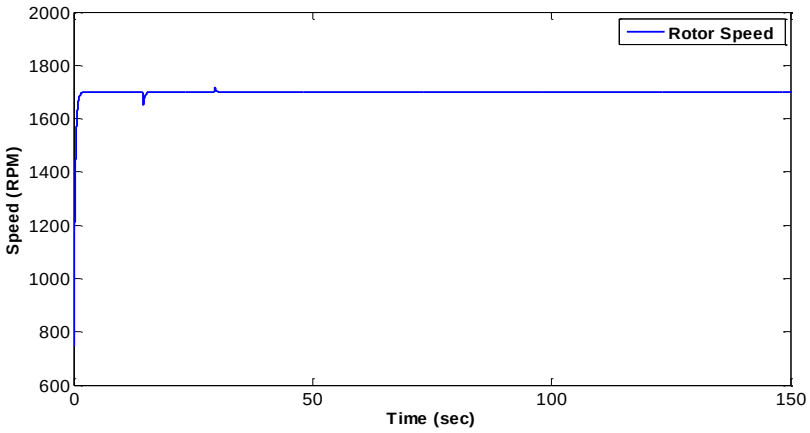

Figure 6.4: Rotor speed of DFIG

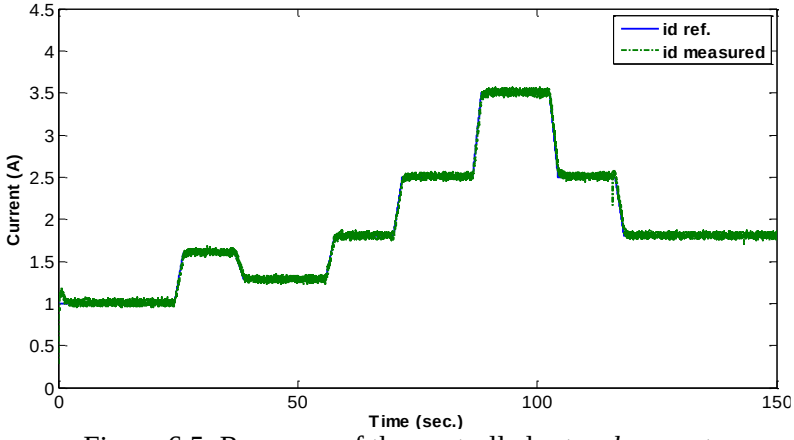

Figure 6.5: Response of the controlled rotor *d*-current

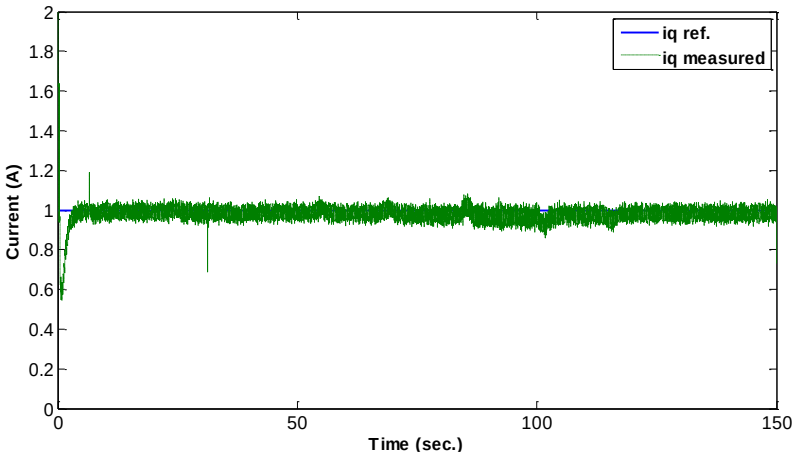

Figure 6.6: Response of the controlled rotor *q*-current

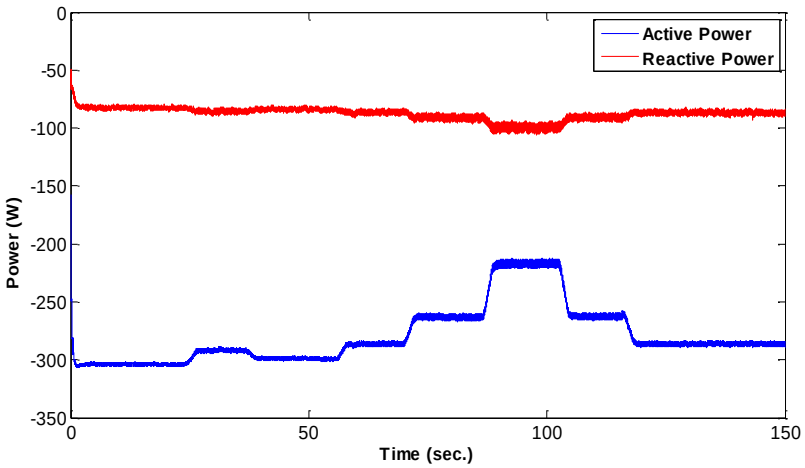

Figure 6.7: Rotor Power response by varying the rotor *d*-current

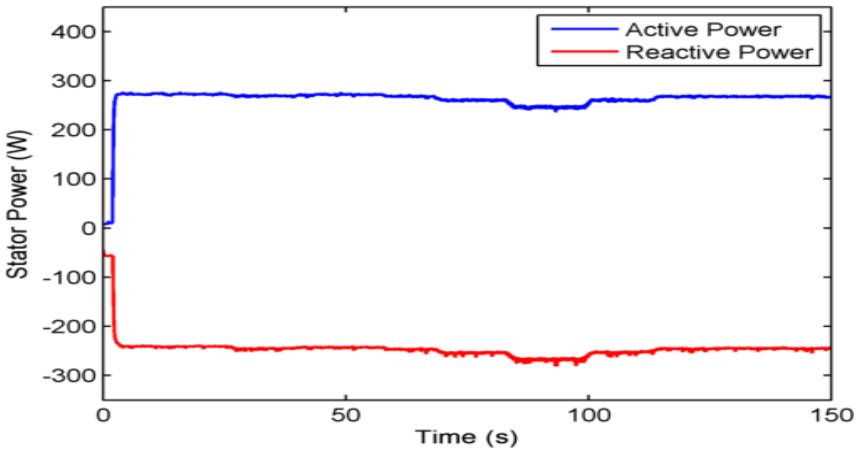

Figure 6.8: Stator Power response by varying the rotor *d*-current

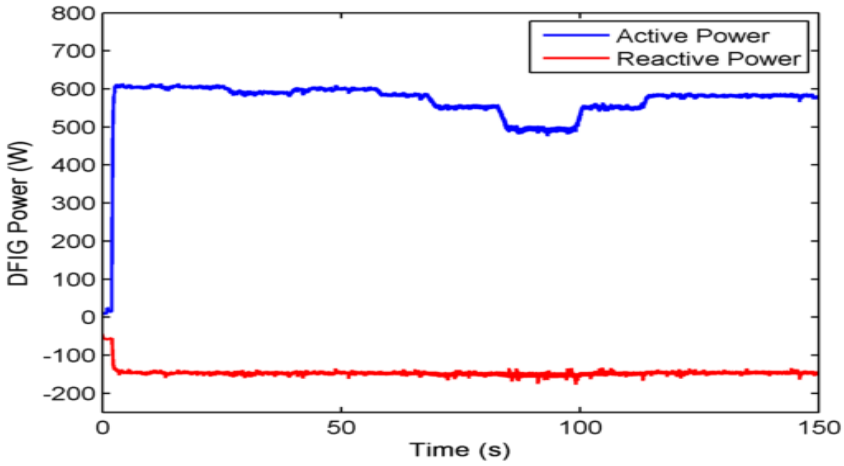

Figure 6.9: DFIG Power response by varying the rotor *d*-current

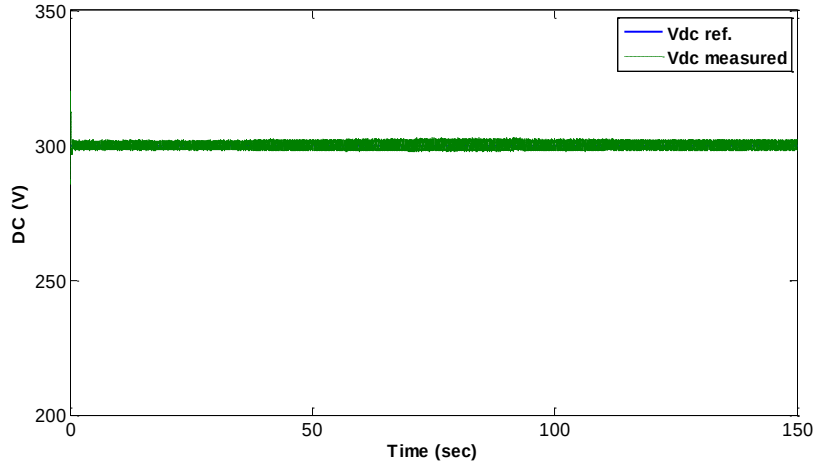

Figure 6.10: DC-link voltage regulation

6.3.2. *Power Control by Rotor Q-Current*

Now, the active power can be controlled by controlling the rotor *q*-current i_{qr} to follow a reference i_{qr_ref}, while reactive power can be regulated by the rotor *d*-current i_{dr} to be constant at i_{dr_ref} as shown in Figures 6.11 and 6.12, respectively. It can be observed that the current tracking performance is good. From the power response at rotor side, shown in Figure 6.13, it can be observed that the active power can be varied by

controlling the rotor *q*-current to follow a reference i_{qr_ref} equivalent to the desired active power, while the reactive power increases to balance the power. Figure 6.14 illustrates the power response at stator side. As stator terminal directly connected with grid, the voltage induced at the stator terminal will match the grid requirements. I has fixed amplitude and frequency. This figure shows the power transmitted to the grid is as per the grid requirement. In Figure 6.15 shows, the rotor *q*-current i_{qr} is controlling the actual active power generated and the rotor *d*-current i_{dr} is controlling the reactive power consumed by the DFIG under this operation.

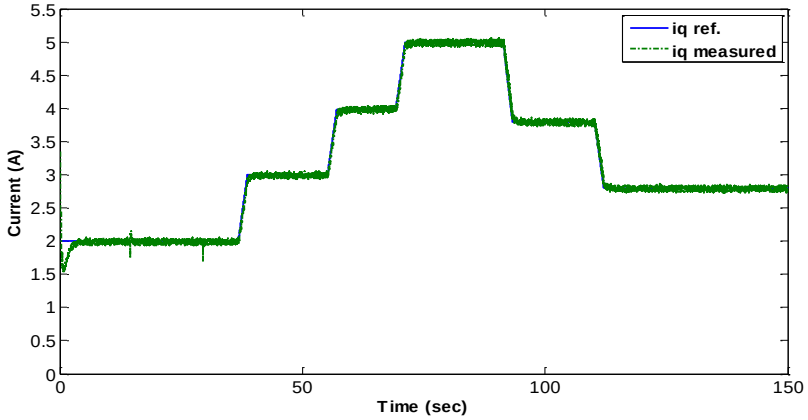

Figure 6.11: Response of the controlled rotor *q*-current

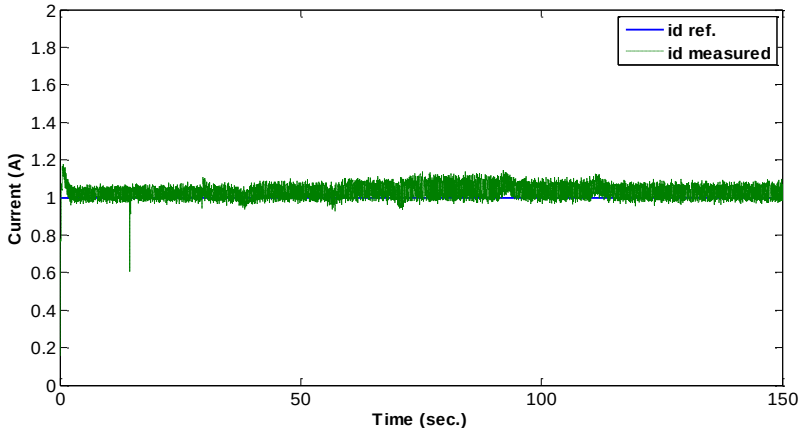

Figure 6.12: Response of the controlled rotor *d*-current

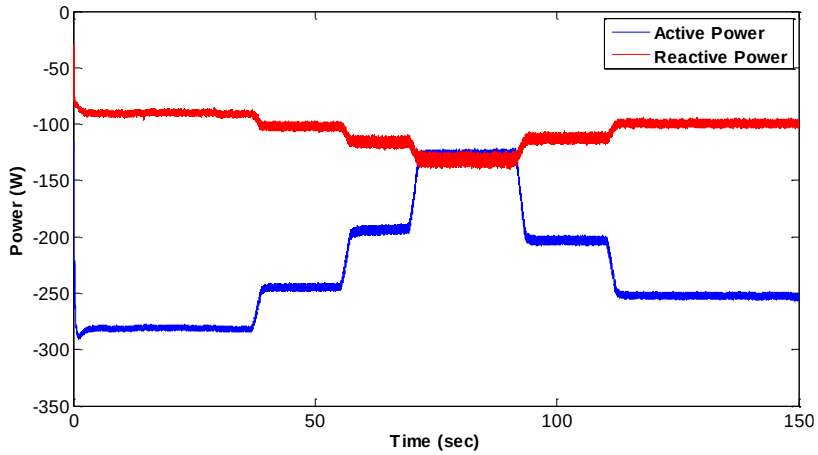

Figure 6.13: Rotor Power response by varying the rotor *q*-current

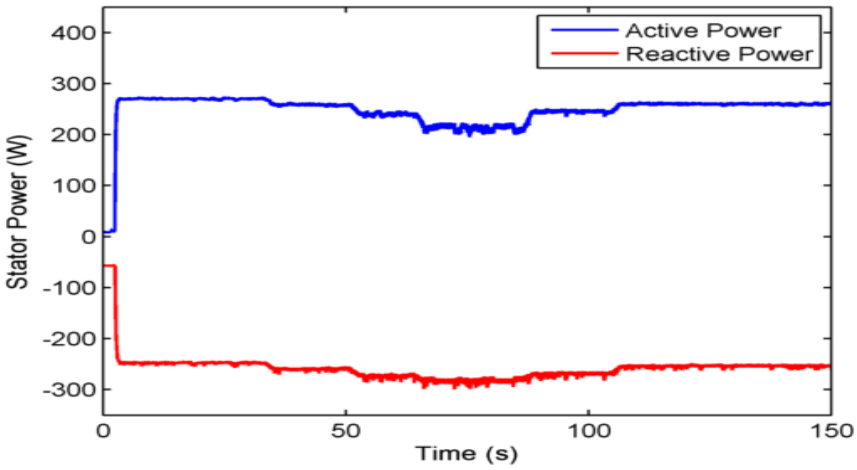

Figure 6.14: Stator Power response by varying the rotor *q*-current

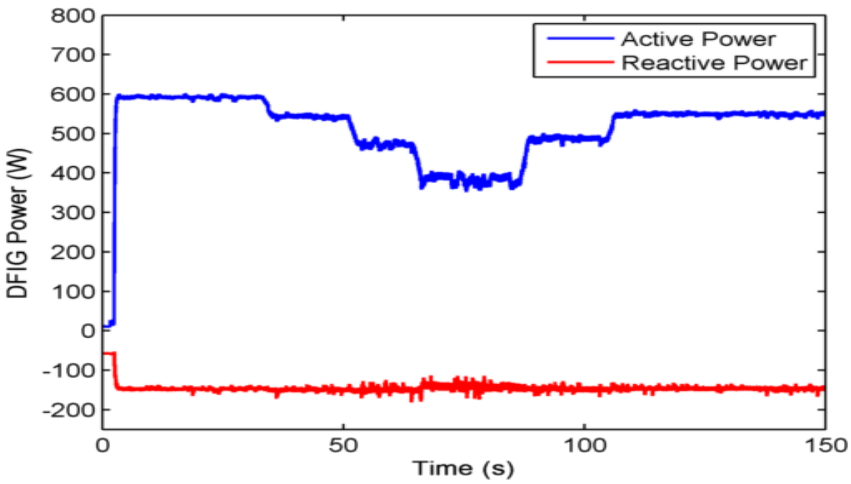

Figure 6.15: DFIG Power response by varying the rotor *q*-current

6.3.3. *Effect of the DC-Link Voltage Variation on the Rotor Current Control*

In this section, the effect of a variable DC-link voltage on the performance of the RSC current controllers is tested. The DC-link voltage is controlled to follow a varying reference, as shown in Figure 6.16, at the grid side, while the *d*-*q* currents are controlled to track the desired references, as shown in Figures 6.17 and 6.18, at the machine side simultaneously. It can be observed that the current tracking performance is well established despite the variation of the DC-link voltage, which ensures the high tracking performance of the overall control system at the grid and machine sides.

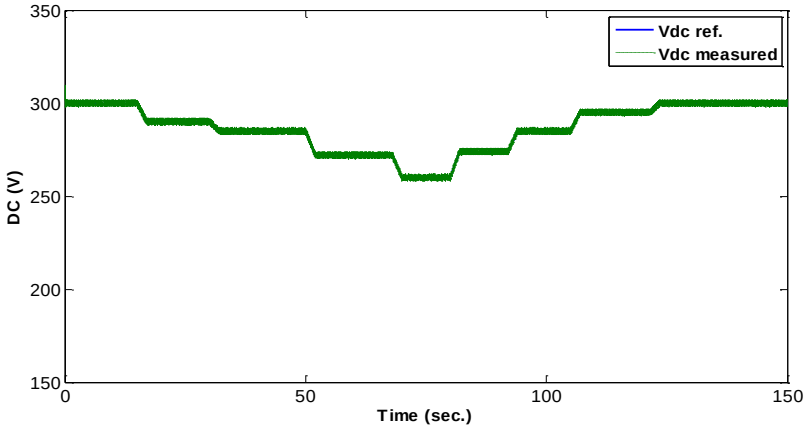

Figure 6.16: Response of the DC-link voltage controller

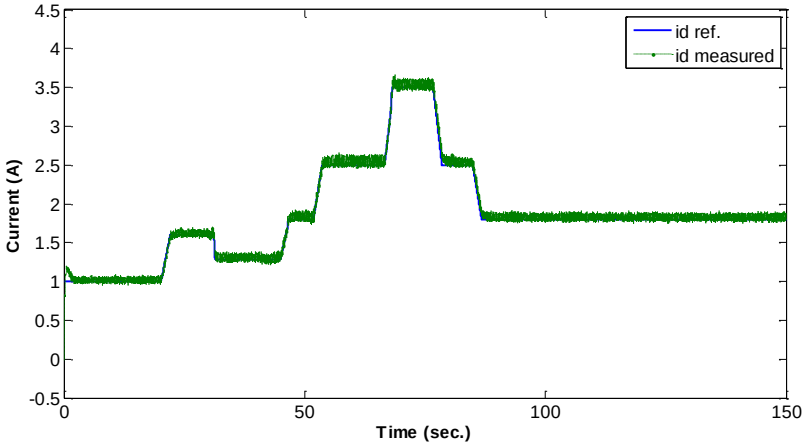

Figure 6.17: Response of the controlled rotor *d*-current

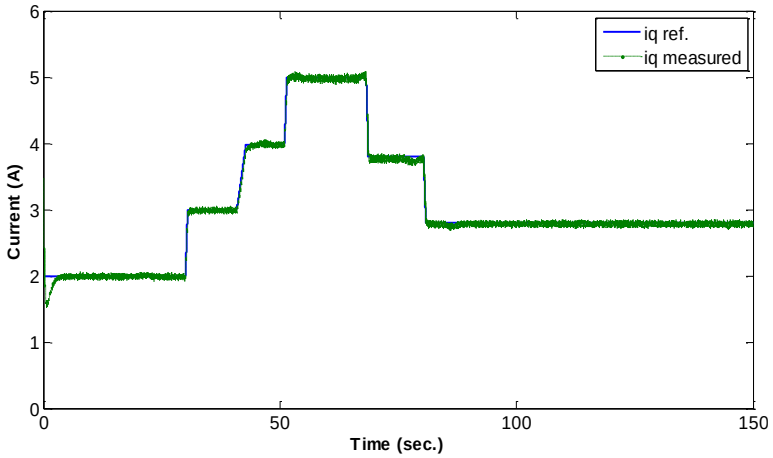

Figure 6.18: Response of the controlled rotor *q*-current

6.3.4. *Effects of Variable Rotor Speed on the Rotor Current Control*

In wind energy conversion system, the speed variation of the wind turbine causes variation of the rotor current which ultimately vary the generated power from the wind turbine. In large scale power plant, the most challenging part of the grid tied wind turbine system is to making sure the generated power is free from variation. For this reason, power controlling is necessary. Power control can be done by controlling the blade pitch or rotor current. In this scenario, the effect of wind speed variation, emulated by varying the rotor speed at sub-synchronous and super-synchronous mood through the dynamometer, on the rotor *d*-*q* currents is tested by regulating the currents to follow constant references while changing the rotor speed as shown in Figure 6.19. It can be observed from the *d*-*q* current responses, shown in Figures 6.20 and 6.21, that the *d*-current component is well regulated with no effects from the rotor speed variation and the *q*-current component is affected by the rotor speed; however a zero-steady state tracking error is quickly established, which ensures the robustness of the control system. This type

of controller doesn't require blade pitch control for power control. The rotor *q*-current i_{qr} is derived from the equation of machine's torque. So, the variation of torque due to the rotor speed variation makes the spike shape of controlled i_{qr} current. The responses for active and reactive power are shown in Figure 6.22, 6.23, 6.24 and it can be observed that they follow the controlled *d*-*q* rotor currents. Therefore, the rotor side controller can be used to regulate the power by tracking appropriate rotor currents. This experiment demonstrates that the power can be controlled to track a desired reference despite the variation of the rotor speed during variable wind speeds.

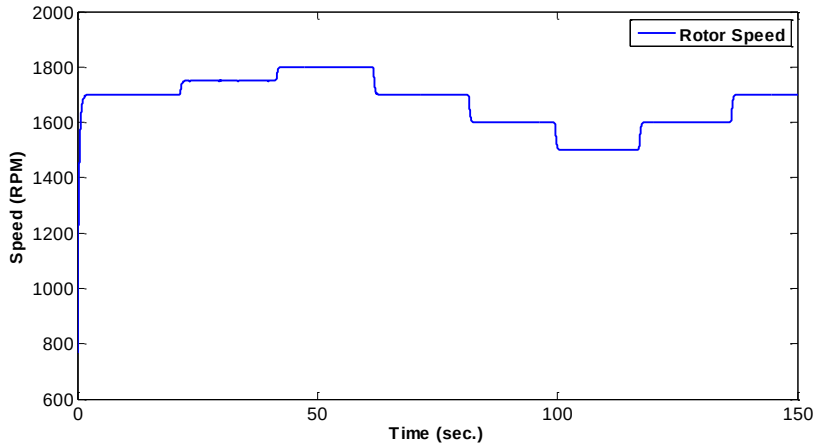

Figure 6.19: Variable rotor speed of DFIG

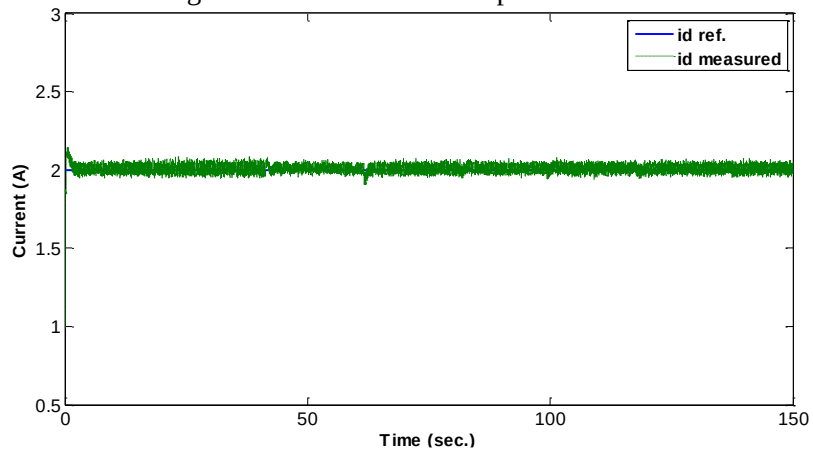

Figure 6.20: Response of the controlled rotor *d*-current

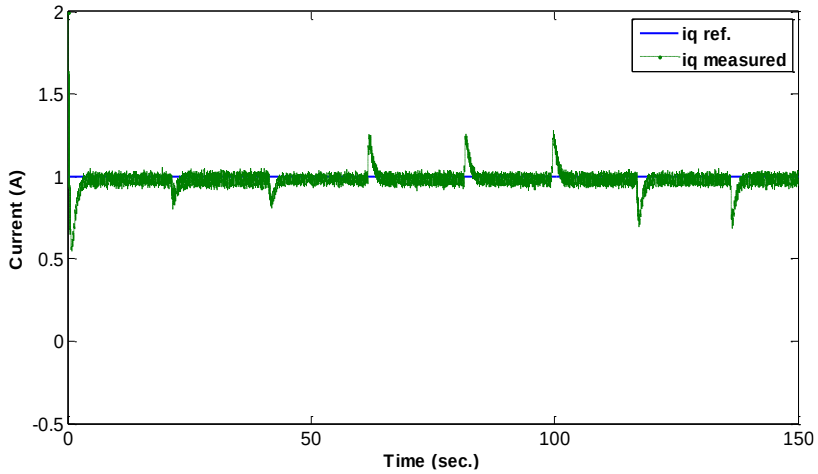

Figure 6.21: Response of the controlled rotor *q*-current

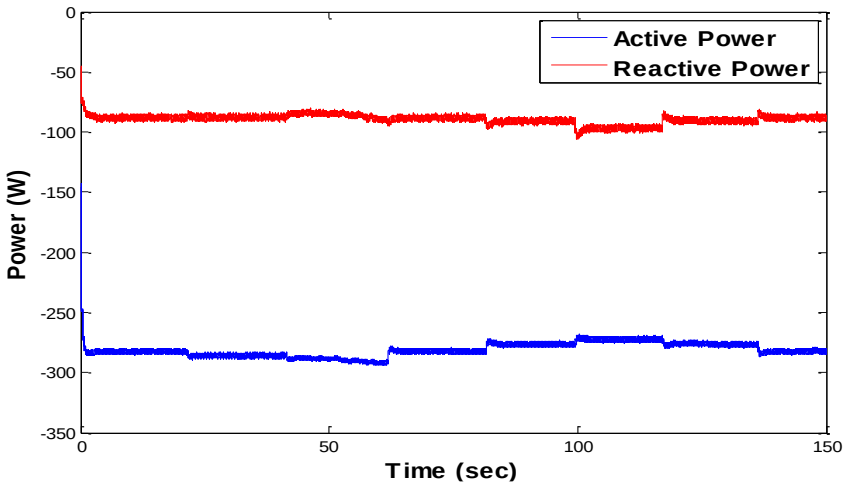

Figure 6.22: Rotor Power response for rotor speed variation

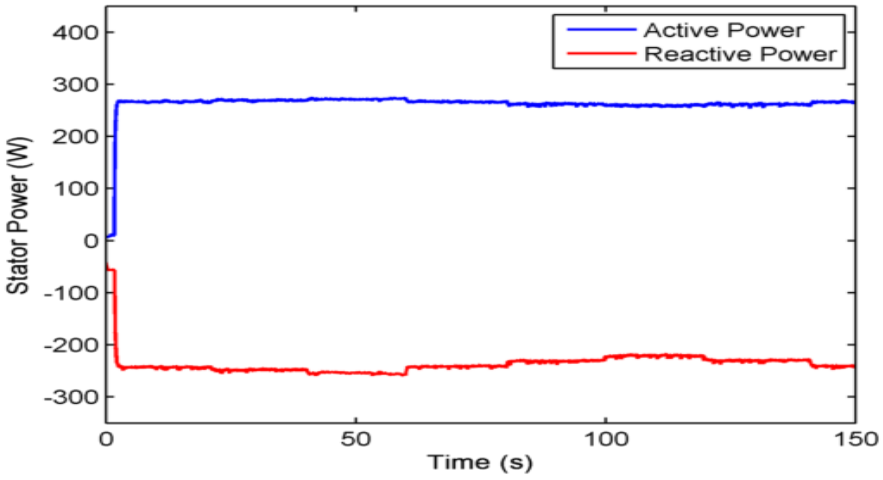

Figure 6.23: Stator Power response for rotor speed variation

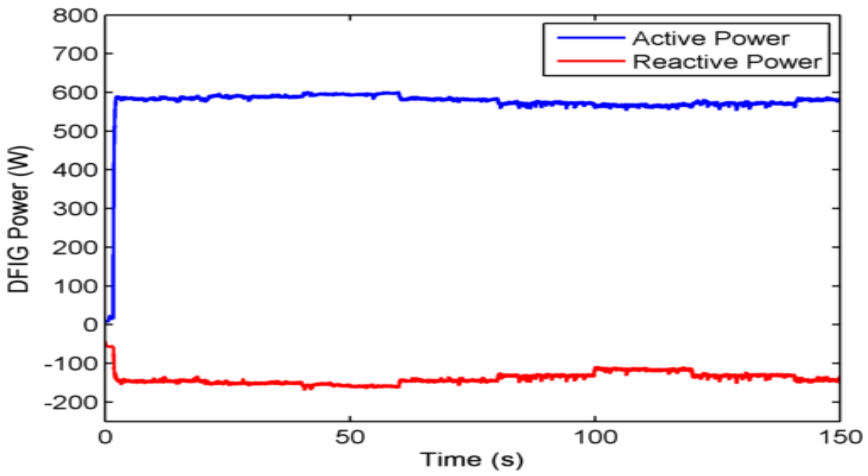

Figure 6.24: DFIG Power response for rotor speed variation

6.4. Speed Control of DFIG in Wind Energy Conversion System

This experiment is executed to validate the developed speed controller in the platform as shown in Figure 6.1 and schematic of all connected modules is shown in Figure 6.2. The objective is to make the rotor speed track the desired speed to capture the maximum power from the variable wind speed. To make the variable speed wind turbine system reliable, efficient and cost effective a MRAS-ANN based estimator has designed for rotor speed estimation and combined with the controllers. Normally, in the wind turbine rotor speed is measured by encoder which is expensive and sensitive in hostile environment. Among the conventional estimator MRAS based speed estimator is highly popular where PI is used to estimate the speed. PI based speed estimation takes time to reach the peak of the speed signal and it requires continuous tuning it's parameter at high frequency speed signal. By comparing with PI, ANN comprise a powerful tool to approximate the complicated behavior and response of the peak of speed signal allowing

considerable reduction in computation time during time-consuming optimization runs. In this test, the dynamometer (wind turbine emulator) is running at variable speed, as shown in Figure 6.25 the estimated rotor speed tracking the reference speed. The generated power response at stator side due to the rotor speed variation is shown in Figure 6.26. It is noticed that the active power is following the rotor speed profile which verifies the purpose of controller. The active and reactive power at rotor side is shown in Figure 6.27. The measured rotor torque and estimated rotor torque are illustrated in Figure 6.28. Estimated rotor is similar to the actual rotor torque measured by the encoder. The torque profile matches the stator active power profile which also validates that the accurateness of rotor side controller (RSC) and estimator. In this experiment, the DC-link voltage is regulated at the required voltage level which is the main intension of grid side controller (GSC). Figure 6.29 shows the DC-link voltage is following the reference which ultimately validates the robustness of the controller.

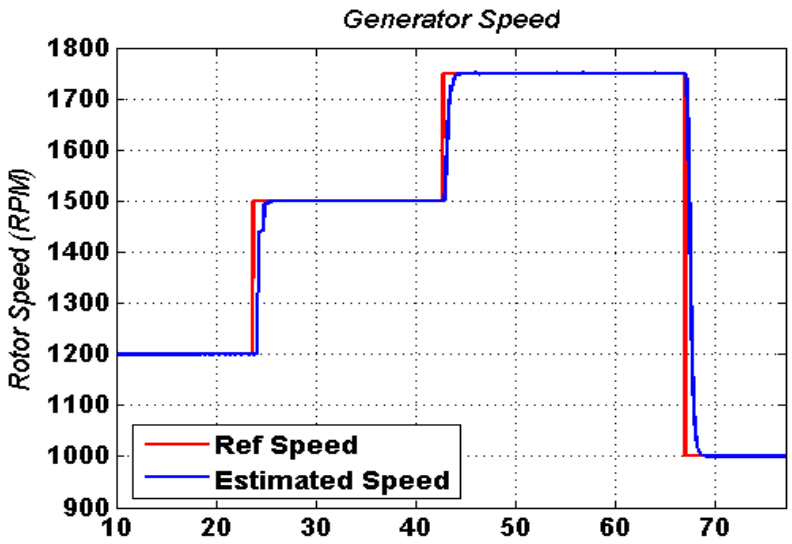

Figure 6.25: rotor speed variation of DFIG

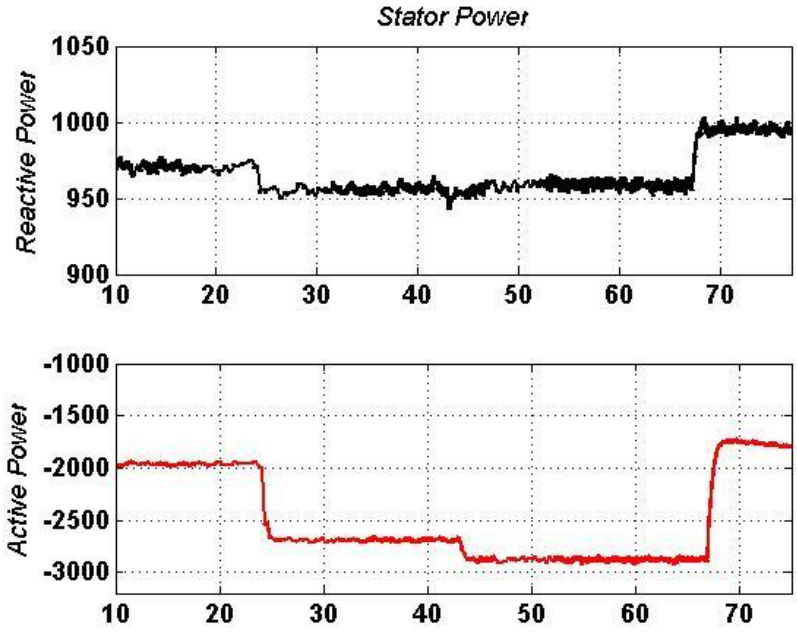

Figure 6.26: Stator reactive and active power response for rotor speed variation

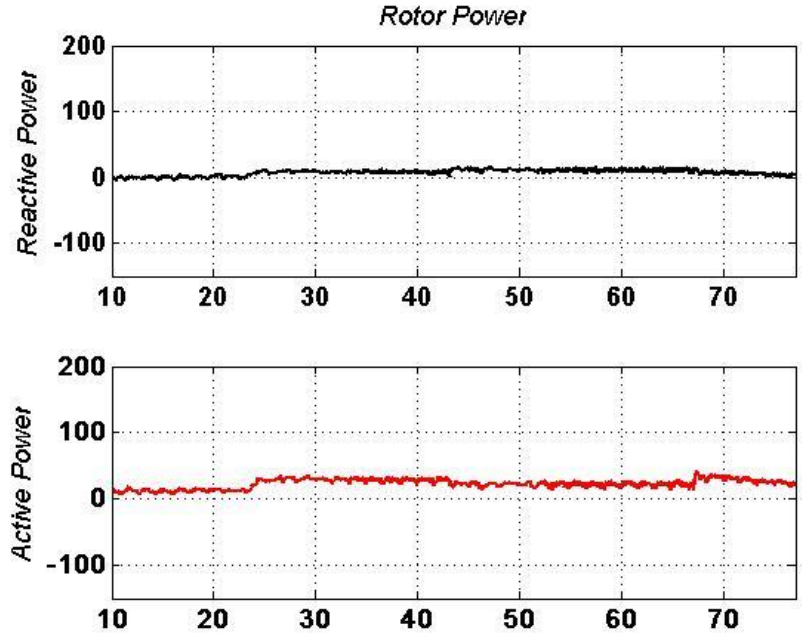

Figure 6.27: Rotor reactive and active power response for rotor speed variation

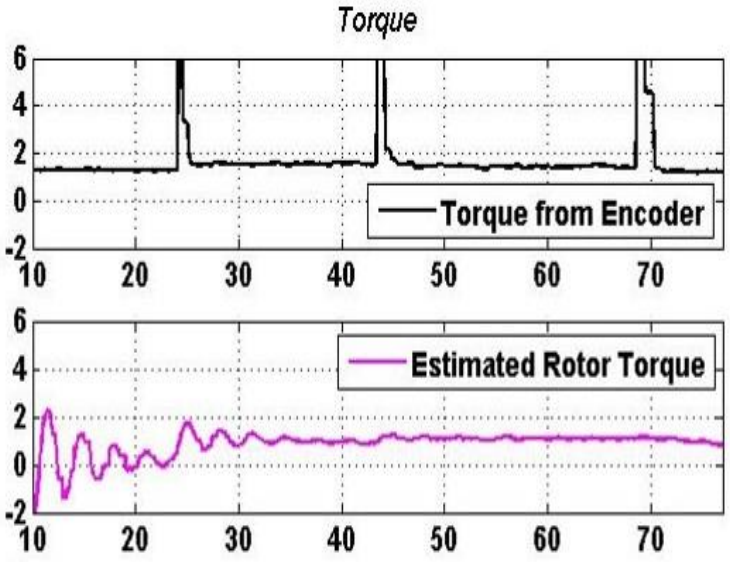

Figure 6.28: a) measured rotor torque by encoder b) estimated rotor torque

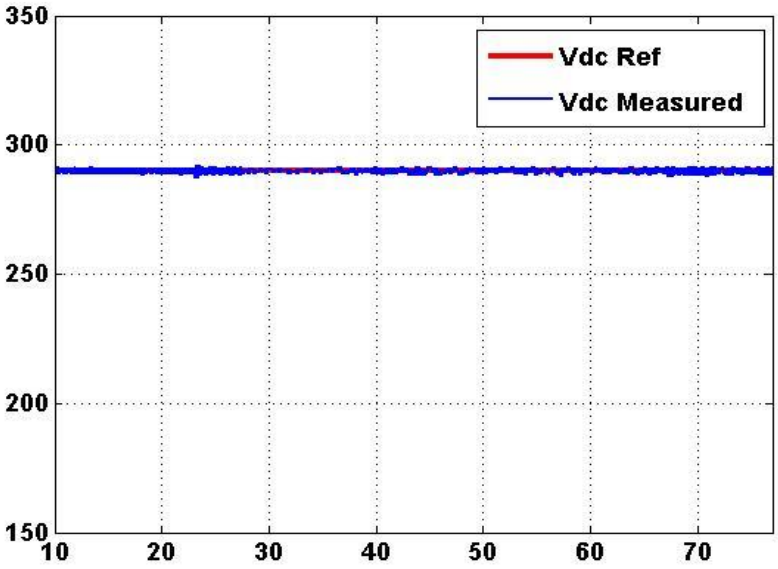

Figure 6.29: DC-Link voltage regulation

Conclusion

Automatic control represents one of the most important factors responsible for the efficiency and reliability of wind power conversion systems. The control scheme proposed for section 6.3 in this thesis assures the constant power output for the grid connected DFIG under varying speed by optimally controlling the active and reactive power flow. This method adequately controls the slip power by regulating the reactive power. Another control scheme proposed for section 6.4 where the speed at which a wind turbine rotates must be controlled for efficient power generation and to keep the turbine components within designed speed and torque limits. In addition, the proposed designing of MRAS-ANN has significantly improved the performance of conventional MRAS based speed estimation technique for sensorless operation of DFIG. The performed experimental results serve as proof of concept for the developed control strategies.

Chapter 7

Conclusion & Future Work

The doubly-fed induction generator wind turbine is a variable speed wind turbine widely used in the modern wind power industry. At present, commercial DFIG wind turbines primarily make use of the technology that was developed a decade ago. But, it is found in the literature review that there is a limitation in the conventional vector control technique. In this thesis, the doubly fed machine was introduced. The electrical energy efficiency of wind turbine systems equipped with doubly-fed induction generators in comparison to other wind turbine generator systems has been investigated. Functioning, equivalent circuits and mathematical models were presented for the doubly fed induction machine in both $\alpha\beta$ and $dq0$ (stator flux oriented) reference frames in order to provide the reader with a better understanding of the operational behavior of the machine. The proper designing of two methods for improving the control strategy of the rotor side converter controller were proposed, implemented and tested for wind energy extraction, reactive power, and grid voltage support controls of the wind turbine, namely the active and reactive power control by controlling rotor current and the speed control of DFIG with improved rotor position estimation MRAS-ANN method. Using the measured stator voltages, stator currents, and rotor currents, the proposed algorithm can generates the rotor position and speed by ANN. The speed is estimated independently of the machine

parameters and the algorithm avoids using differentiation, which results in a substantial improvement in control robustness and improves its immunity to noise. A hysteresis controller was proposed and tested for controlling the grid side converter. It helps to maintain the constant frequency of the generated power from the wind turbine by matching with the grid frequency, generated voltage with the grid voltage. This controller can improve the power factor and try to maintain the power factor at unity so that the use of additional capacitor bank can be avoided at the power grid, which ultimately reduce the cost of power generation. As this controller is designed based on hysteresis current concept so it can protect the wind turbine if any fault occur at power grid or in transmission line by comparing the abnormal current due to fault with its rated current limit. Experimental results from a laboratory scale system were presented and thoroughly analyzed in Chapter 6 where DFIG wind turbine system was found with a superior performance in various aspects.

The next challenge is to design the controllers for stand-alone DFIG based wind energy conversion system with storage. A new control algorithm will be developed to control the system for isolated area, small community, hill tracks that means where the grid extension is not possible or grid connection is not economical. It is also important to step up for the new era of offshore wind energy conversion system using Double Fed Induction Generator (DFIG). Moreover, the overall control scheme is complicated. The main problems are the unaccepted load voltage distortion due to unbalanced load demand, variation of frequency as load varies, battery charging/discharging operation.

So, the developed controller will ensure the constant supply voltage and frequency regardless of voltage distortion as well as it will maintain the battery/charging discharging operation when required by the system. Stability analysis will also be made using modern control techniques.

Appendix

Parameters of DFIG Wind Turbine System

Quantity	Value
DFIG machine	
Power	2 kW
Stator voltage	120 V
Rotor voltage	360 V
Stator current	10 A
Rotor current	3.3 A
Speed	1800 RPM
Pole pairs	2
Ls	0.0662
Lr	0.0662
Lm	0.0945
Dynamometer machine	
Required voltage (3 phase)	208 V
Required current (3 phase)	12 A
Speed range	0–3600 RPM
IGBT inverter	
DC-bus voltage	420 V
DC-bus current	10 A
Switching Frequency	0–20 kHz
Grid side controller gains	
Kp = 0.5, Ki = 7, Current regulator = 0.0001 A	
Rotor side controller gains (for i_{dr} and i_{qr})	
Kp = 4.5, Ki = 7.5	

Publications

1. Aman. A. Tanvir; A. Merabet; R. Beguenane, “Real-Time Control of Active and Reactive Power for Doubly Fed Induction Generator (DFIG)-Based Wind Energy Conversion System”, Energies vol. 8, no. 9, pp. 10389-10408, 2015

2. Aman. A. Tanvir; A. Merabet; R. Beguenane, “Artificial Neural Network Based Speed Estimator for Controlled DFIG Wind Energy Conversion System”, underwork for IEEE Transactions

References

[1] Wind energy facts (http://www.ewea.org/wind-energy-basics/facts/)

[2] End-use Energy Demand, National Energy Board, 2015-09-16 (https://www.neb-one.gc.ca/nrg/ntgrtd/ftr/2013/ppndcs/pxndsdmnd-eng.html)

[3] Global Wind Report 2015 – Annual market update (http://www.gwec.net/publications/global-wind-report-2/global-wind-report-2015-annual-market-update/)

[4] T. Burton, D. Sharpe, N. Jenkins, and E. Bossanyi, Wind Energy Handbook. John Wiley & Sons, Ltd, 2001

[5] T. Ackermann and L. S¨oder, “An overview of wind energy-status 2002,” Renew. Sustain. Energy Rev., vol. 6, no. 1–2, pp. 67–128, Feb./Apr. 2002.

[6] DEWIND. The D8.2 series. Brochure. [Online]. Available: (http://www.dewindco.com/eng/product/summary.asp)

[7] K. Thorborg, Power Electronics – in Theory and Practice. Lund, Sweden: Studentlitteratur, 1997.

[8] L. Xu and C. Wei, “Torque and reactive power control of a doubly fed induction machine by position sensorless scheme,” IEEE Trans. Ind. Applicat., vol. 31, no. 3, pp. 636–642, May/June 1995.

[9] B. Singh and N. K. Swami Naidu, "Direct Power Control of Single VSC-Based DFIG Without Rotor Position Sensor," Industry Applications, IEEE Transactions on, vol. 50, pp. 4152-4163, 2014.

[10] O. Carlson, J. Hylander and K. Thorborg, “Survey of variable speed operation of wind turbines”. In 1996 European Union Wind Energy Conference, Goteborg, Sweden

pp. 406-409. 20-24 May, 1996.

[11] D. S. Zinger and E. Muljadi, “Annualized wind energy improvement using variable speeds”. Industry Applications, IEEE Transactions on, 33(6):1444-1447, 1997.

[12] DeWind. D8 Series. Brochure. www.dewind.de.

[13] G. L. Johnson. Wind Energy Systems. Prentice-Hall, Englewood Cliffs, New Jersey, 1985.

[14] B. Rabelo and W. Hofmann. “Optimal active and reactive power control with the doubly-fed induction generator in the MW-class wind-turbines.” Proceedings of International Conference on Power Electronics and Drives Systems (PEDS), pp.53-8 vol.1, 2001.

[15] Y. Tang and L. Xu. “Flexible active and reactive power control strategy for a variable speed constant frequency generating system”. Power Electronics, IEEE Transactions on, 10(4):472-478, 1995.

[16] R. Datta and V. T. Ranganathan. “Variable-speed wind power generation using doubly fed wound rotor induction machine-a comparison with alternative schemes.” Energy Conversion, IEEE Transactions on 17(3):414-21, Sept. 2002.

[17] C. S. Brune, R. Spee, & A. K. Wallace, “Experimental Evaluation of a Variable-Speed, Doubly-Fed Wind-Power Generation System.” Ind. Applications, IEEE Trans. on, 30, 648-655, 1994.

[18] L. Liao, & C. Sun, “A Novel Position Sensorless Control Scheme for Doubly Fed Reluctance Motor Drives.” Ind. Applications, IEEE Trans. on 30 noo.5, 1210 – 1218, 1994

[19] Y. Tang, & L. Xu, “Vector Control and Fuzzy Logic Control of Doubly Fed Variable Speed Drives with DSP Implementation.” Energy Conversion 10, IEEE Transactions on, 661-668. 1995.

[20] R. Pena, J.C. Clare & G. M. Asher, “Doubly fed induction generator using back-to-back PWM converters and its application to variable-speed wind-energy generation.” IEEE Proc.-Electr. Power Appl., 143, No.3, 231-241. 1996.

[21] R. Cárdenas, R. Peña, J. Proboste, G. Asher, & J. Clare, “MRAS Observer for Sensorless Control of Standalone Doubly Fed Induction Generators”. Energy Conversion, 20, IEEE Trans. on, no. 4, 710-718, 2005.

[22] A. Petersson, T. O. Thiringer, L. Harnefors, & T. A. Petru°, “Modeling and Experimental Verification of Grid Interaction of a DFIG Wind Turbine”. Energy Conversion, 20, IEEE Trans. on, no. 4, 878-886, 2005.

[23] P. Ledesma, & J. Usaola, “Doubly Fed Induction Generator Model for Transient Stability Analysis.” Energy Conversion, 20, IEEE Trans. on No. 2, 388-397, 2005.

[24] B. H. Chowdhury, & S. Chellapilla, “Double-fed induction generator control for variable speed wind power generation.” Electric Power Systems Research, 76, 786-800, 2006.

[25] L. Xu, “Coordinated Control of DFIG’s Rotor and Grid Side Converters During Network Unbalance.” Power Electronics, IEEE Transactions on 23, no. 3, 1041-1049, 2008a.

[26] S. Seman, J. Niiranen, & A. Arkkio, “Ride-Through Analysis of Doubly Fed Induction Wind-Power Generator Under Unsymmetrical Network Disturbance.” Power Systems, 21, IEEE Transactions on no. 4, 1782-1789, 2006.

[27] M. Mesbah, S. Islam, & M. A. S. Masoum, “A novel direct active power control method for DFIG wind turbine applications.” IEEE PES ISGT. USA, 2011.

[28] D. Xiang, L. Ran, P. J. Tavner, & S. Yang, “Control of a Doubly Fed Induction Generator in a Wind Turbine during Grid Fault Ride-Through.” Energy Conversion, 21, IEEE Trans. on no. 3, 652-662, 2006.

[29] P. S. Jesús López, X. Roboam, & L. Marroyo. “Dynamic Behavior of the Doubly Fed Induction Generator During Three-Phase Voltage Dips.” Energy Conversion, 22, IEEE Trans. on no. 3, 709-717.

[30] L. Xu, & P. Cartwright, “Direct Active and Reactive Power Control of DFIG for Wind Energy Generation.” Energy Conversion, 21, IEEE trans. on no. 3, 750-758. 2006.

[31] A. Luna, F. K. D. A. Lima, D. Santos, P. Rodríguez, E. H. Watanabe, & S. Arnaltes, “Simplified Modeling of a DFIG for Transient Studies in Wind Power Applications.”Ind. Electron., 58, IEEE Trans. on no. 1, 2011.

[32] J. Hu, H. Nian, H. Xu, & Y. He, “Dynamic Modeling and Improved Control of DFIG Under Distorted Grid Voltage Conditions.” Energy Conversion, 26, IEEE trans. on no. 1, 163-175, 2011.

[33] D. Zhi, L. Xu, & B. W. Williams, “Model-Based Predictive Direct Power Control of Doubly Fed Induction Generators.” Power Electron., 25, IEEE Trans. on no. 2, 341-351. 2010.

[34] A. J. S. Filho, M. E. D. O. Filho, & E. R. Filho, “A Predictive Power Control for Wind Energy”. Sust. Eenergy. , 2, IEEE Trans. on, no. 1, 97-105, 2011.

[35] G. Abad, M. Á. Rodríguez, & J. Poza, “Two-Level VSC Based Predictive Direct Torque Control of the Doubly Fed Induction Machine With Reduced Torque and Flux Ripples at Low Constant Switching Frequency." Power Electron., 23, IEEE Trans. on no. 3, 1050-1061, 2008.

[36] M. Mohseni, & S. Islam, “A New Vector-Based Hysteresis Current Control Scheme for Three-Phase PWM Voltage-Source Inverters”. Power Electronics, 25, IEEE Trans. On no. 9, 2299-2309, 2010.

[37] M. Mohseni, M. Mesbah, S. Islam, & M.A.S. Masoum, “Vector-Based Hysteresis Current Regulator for DFIG Wind Turbines under Non-Ideal Supply Conditions”.

Australian Journal of Electrical and Electronic Engineering (AJEEE), 8 , no.1 27-38, 2011

[38] S. Z. Chen, N. C. Cheung, K. C. Wong, & J. Wu, “Integral variable structure direct torque control of doubly fed induction generator. IET Renew. Power Gener., 5, 18-25. 2011

[39] G. D. Marques, V. F. A. Pires, S. E. Sousa, & D. M. Sousa, “A DFIG Sensorless Rotor-Position Detector Based on a Hysteresis Controller”. IEEE Trans. on Energy Conversion, 26, no. 1, 9-17, 2011.

[40] B. Shen, B. Mwinyiwiwa, Y. Zhang, & B.-T. Ooi, “Sensorless Maximum Power Point Tracking of Wind by DFIG Using Rotor Position Phase Lock Loop (PLL). IEEE Trans. on Power Electron., 24, no. 4, 942-951, 2009.

[41] D. G. Forchetti, G. O. García, & M. I. Valla, “Adaptive Observer for Sensorless Control of Stand-Alone Doubly Fed Induction Generator”. IEEE Transactions on Industrial Electronics, 56, no. 10, 4174-4180, 2009.

[42] W. Qiao, W. Zhou, J. M. Aller, & R. G. Harley, “Wind Speed Estimation Based Sensorless Output Maximization Control for a Wind Turbine Driving a DFIG”. IEEE Transactions on Power Electronics, 23, no. 3, 1156-1169, 2008.

[43] E. Tremblay, S. Atayde, & A. Chandra, “Comparative study of control strategies for the Doubly Fed Induction Generator in Wind Energy Conversion Systems: a DSP-based implementation approach”. IEEE Transactions on Sustainable Energy, early access, 2011.

[44] A. Balogun, O. Ojo and F. Okafor, "Decoupled Direct Control of Natural and Power Variables of Doubly Fed Induction Generator for Extended Wind Speed Range Using Feedback Linearization," Emerging and Selected Topics in Power Electronics, IEEE Journal of, vol. 1, pp. 226-237, 2013.

[45] B. Singh and N. K. Swami Naidu, "Direct Power Control of Single VSC-Based

DFIG Without Rotor Position Sensor," Industry Applications, IEEE Transactions on, vol. 50, pp. 4152-4163, 2014.

[46] M. E. Zarei and B. Asaei, "Combined vector control and direct power control methods for DFIG under normal and unbalanced and distorted grid voltage conditions," in Power Electronics, Drive Systems and Technologies Conference (PEDSTC), 2013 4th, pp. 107-112, 2013.

[47] R. Dev Shukla and R. K. Tripathi, "Speed-sensorless voltage & frequency control in autonomous DFIG based wind energy systems," in Power Engineering Conference (AUPEC), 2014 Australasian Universities, pp. 1-6, 2014.

[48] T. Burton, D. Sharpe, N. Jenkins, and E. Bossanyi, Wind Energy Handbook, Wiley, 2001

[49] E. Hau, Wind Turbines: Fundamentals, Technologies, Application, Economics, 2nd edition, Springer, 2005.

[50] G. L. Johnson. Wind Energy Systems. Prentice-Hall, Englewood Cliffs, New Jersey, 1985.

[51] Wind Resource Map of a Section of New Brunswick (http://www2.gnb.ca/content/dam/gnb/Departments/en/pdf/Maps-Cartes/CarteSpd_80m_nb_en_tuile_05_06.pdf)

[52] Averaged Wind Speed Data (Environment Canada) (https://www.halifax.ca/regionalplanning/documents/FigureA14AverageWindSpeed.pdf)

[53] T. Burton, D. Sharpe, N. Jenkins, and E. Bossanyi, Wind Energy Handbook. John Wiley & Sons, Ltd, 2001.

[54] G. L. Johnsson, Wind Energy Systems. Englewood Cliffs, N.J., USA.: Prentice-Hall, 1985.

[55] B.Wu, Y. Lang, N. Zargari, S. Kouro, Power Conversion and Control of Wind

Energy System, Wiley, IEEE Press, 2011.

[56] M. P. Papadopoulos, S. A. Papathanassiou, N. G. Boulaxis, and S. T. Tentzerakis, “Voltage quality change by grid-connected wind turbines,” in European Wind Energy Conference, Nice, France, 1999, pp. 783–785.

[57] T. Petru and T. Thiringer, “Active flicker reduction from a sea-based 2.5 MW wind park connected to a weak grid,” in Proc. Nordic Workshop on Power and Industrial Electronics, Aalborg, Denmark, June, 13–16, 2002.

[58] A°. Larsson, P. Sørensen, and F. Santjer, “Grid impact of variable speed wind turbines,” in Proc. of European Wind Energy Conference and Exhibition (EWEC´99), Nice, France, Mar., 1–5, 1999

[59] F. Blaabjerg and Z. Chen, Power Electronics for Modern Wind Turbines, Morgan & Claypool Publishers, 2006.

[60] D. Burnham, S. Santoso, and E. Muljadi, Variable Rotor-Resistance Control of Wind Turbine Generators, in IEEE Power and Energy Society General Meeting (PES), 2009.

[61] F. Blaabjerg and Z. Chen, Power Electronics for Modern Wind Turbines, Morgan & Claypool Publishers, 2006.

[62] G. Abad, J. Lopez, M. Rodriguez, L. Marroyo, G. Iwanski, “Doubly Fed Induction Machine: Modeling and Control for Wind Energy Generation”, Wiley, IEEE Press, 2011

[63] P. Krause, O. Wasynczuk, and S. Sudhoff, Analysis of Electric Machinery and Drive Systems, 2nd Edition, Wiley-IEEE Press, 2002.

[64] I. Boldea, The Electric Generators Handbook: Variable Speed Generators, CRC Press, 2005

[65] P. C. Sen, Principle of Electric Machines and Power Electronics, 2nd Edition, Wiley, 1997

[66] R. C. Bansal, "Three-phase self-excited induction generators: an overview," in IEEE Transactions on Energy Conversion, vol. 20, no. 2, pp. 292-299, June 2005.

[67] R. Pena, J. C. Clare and G. M. Asher, "Doubly fed induction generator using back-to-back PWM converters and its application to variable-speed wind-energy generation," *IEE Proceedings - Electric Power Applications,* vol. 143, pp. 231-241, 1996.

[68] P. Tourou and C. Sourkounis, "Review of control strategies for DFIG-based wind turbines under unsymmetrical grid faults," in *Ecological Vehicles and Renewable Energies (EVER), 2014 Ninth International Conference on,*2014, pp. 1-9.

[69] B. Hopfensperger, D. J. Atkinson and R. A. Lakin, "Stator-flux-oriented control of a doubly-fed induction machine with and without position encoder," *IEE Proceedings - Electric Power Applications,* vol. 147, pp. 241-250, 2000.

[70] Yazhou Lei, A. Mullane, G. Lightbody and R. Yacamini, "Modeling of the wind turbine with a doubly fed induction generator for grid integration studies," *IEEE Transactions on Energy Conversion,* vol. 21, pp. 257-264, 2006.

[71] T. Lei, M. Barnes and M. Ozakturk, "Doubly-fed induction generator wind turbine modelling for detailed electromagnetic system studies," *IET Renewable Power Generation,* vol. 7, pp. 180-189, 2013.

[72] C. E. Ugalde-Loo, J. B. Ekanayake and N. Jenkins, "State-Space Modeling of Wind Turbine Generators for Power System Studies," *IEEE Transactions on Industry Applications,* vol. 49, pp. 223-232, 2013.

[73] A. Tapia, G. Tapia, J. X. Ostolaza and J. R. Saenz, "Modeling and control of a wind turbine driven doubly fed induction generator," *IEEE Transactions on Energy Conversion,* vol. 18, pp. 194-204, 2003.

[74] Modeling and Dynamic Behavior of Wind Generation as it Relates to Power System Control and Dynamic Performance, CIGRE, 2007, ISBN 2858730164, 9782858730162

[75] G. Abad, J. Lopez, M. Rodriguez, L. Marroyo, G. Iwanski, “Doubly Fed Induction Machine: Modeling and Control for Wind Energy Generation”, Wiley, IEEE Press, 2011

[76] R. Pena, J. C. Clare, and G.M. Asher. Doubly fed induction generator using back-to-back PWM converters and its application to variable-speed wind energy generation. IEE Proceedings - Electric Power Applications, 143(3):231, 1996.

[77] Andreas Petersson. Analysis, Modelling and Control of Doubly-Fed Induction Generators for Wind Turbines. PhD thesis, Chalmers University of Technology, 2005.

[78] Anca Hansen, Frede Blaabjerg, Poul Sorensen, and Florin Iov. Control of variable speed wind turbines with doubly-fed induction generators. Wind Engineering, 28(4):411{432, July 2009.

[79] E Tremblay, S Atayde, A Chandra, and Senior Member. Comparative study of control strategies for the Doubly Fed Induction Generator in Wind Energy Conversion Systems: a DSP-based implementation approach . IEEE, pages 1{13, 2011.

[80] A. Luna, A. Rolan, G. Medeiros, P. Rodriguez, and R. Teodorescu. Control Strategies for DFIG Wind Turbines Under Grid Fault Conditions, 2009.

[81] R. Zhu, Z. Chen, Y. Tang, F. Deng and X. Wu, "Dual-Loop Control Strategy for DFIG-Based Wind Turbines Under Grid Voltage Disturbances," in IEEE Transactions on Power Electronics, vol. 31, no. 3, pp. 2239-2253, March 2016.

[82] Wei Cheng and Longya Xu, "Torque and reactive power control of a doubly-fed induction machine by position sensorless scheme," Industry Applications Society Annual Meeting, 1994., Conference Record of the 1994 IEEE, Denver, CO, 1994, pp. 496-502 vol.1.

[83] Ouari Kamel1 / Ouhrouche Mohand2 / Rekioua Toufik1 / Nabil Taib1 Nonlinear Predictive Control of Wind Energy Conversion System Using Dfig with Aerodynamic Torque Observer, Journal of Electrical Engineering. Volume 65, Issue 6, Pages 333-341,

ISSN (Online) 1339-309X, DOI: 10.2478/jee-2014-0055, January 2015

[84] M. T. Hagh, S. Roozbehani, F. Najaty, S. Ghaemi, Y. Tan and K. M. Muttaqi, "Direct power control of DFIG based wind turbine based on wind speed estimation and particle swarm optimization," Power Engineering Conference (AUPEC), 2015 Australasian Universities, Wollongong, NSW, 2015, pp. 1-6

[85] J. Mohammadi, S. Vaez-Zadeh, S. Afsharnia and E. Daryabeigi, "A Combined Vector and Direct Power Control for DFIG-Based Wind Turbines," in IEEE Transactions on Sustainable Energy, vol. 5, no. 3, pp. 767-775, July 2014.

[86] M. Tazil; V. Kumar; R.C. Bansal; S. Kong; Z.Y. Dong; W. Freitas; H.D. Mathur, "Three-phase doubly fed induction generators: An overview.", *Electr. Power Appl. IET*, vol. 4, pp. 75–89, 2010.

[87] A. A. Tanvir; A. Merabet; R. Beguenane, "Real-Time Control of Active and Reactive Power for Doubly Fed Induction Generator (DFIG)-Based Wind Energy Conversion System", *Energies* vol. 8, no. 9, pp. 10389-10408, 2015

[88] R. Pena; J.C. Clare; G.M. Asher, "Doubly fed induction generator using back-to-back PWM converters and its application to variable-speed wind-energy generation." *in IEE Proceedings - Electric Power Applications*, vol. 143, no. 3, pp. 231-241, 1996.

[89] R. K. Soni, A. K. Chauhan, R. R. Kumar and S. K. Singh, "Comparative study of SVM and hysteresis control strategies for grid side converter of PMSG," *Annual IEEE India Conference (INDICON)*, Pune, pp. 1-6, 2014.

[90] J. Eloy-Garcia, S. Arnaltes and J. L. Rodriguez-Amenedo, "Direct power control of voltage source inverters with unbalanced grid voltages," in *IET Power Electronics*, vol. 1, no. 3, pp. 395-407, 2008.

[91] H. C. Chen, P. H. Chen, "Active and Reactive Power Control of a Doubly Fed Induction Generator", *Applied Mathematics & Information Sciences*, vol. 8, No. 1L,

pp. 117-124, 2014.

[92] M. Suwan, T. Neumann, C. Feltes and I. Erlich, "Educational experimental rig for Doubly-Fed Induction Generator based wind turbine," *IEEE Power and Energy Society General Meeting, San Diego, CA*, pp. 1-8, 2012.

[93] J. Mohammadi, S. Vaez-Zadeh, S. Afsharnia and E. Daryabeigi, "A Combined Vector and Direct Power Control for DFIG-Based Wind Turbines," in *IEEE Transactions on Sustainable Energy*, vol. 5, no. 3, pp. 767-775, 2014.

[94] S. Peresadaa, A. Tillib, A. Tonielli, "Power control of a doubly fed induction machine via output feedback" *Control Engineering Practice*, vol. 12, pp. 41-57, 2012.

[95] K. Ouari, M. Ouhrouche, T. Rekioua, T. Nabil, "Nonlinear Predictive Control of Wind Energy Conversion System Using DFIG With Aerodynamic Torque Observer", *Journal of ELECTRICAL ENGINEERING*, vol. 65, no. 6, pp. 333–341, 2014.

[96] R. C. Bansal, T. S. Bhatti, and D. P. Kothari, "Some aspects of grid connected wind electric energy conversion systems," Interdisciplinary J. Inst. Eng. (India), vol. 82, pp. 25–28, 2001

[97] J. M. Mauricio, A. E. LeÓn, A. GÓmez-ExpÓsito and J. A. Solsona, "An Adaptive Nonlinear Controller for DFIM-Based Wind Energy Conversion Systems," in *IEEE Transactions on Energy Conversion*, vol. 23, no. 4, pp. 1025-1035, 2008.

[98] W. Cheng and L. Xu, "Torque and reactive power control of a doubly-fed induction machine by position sensorless scheme," *Industry Applications Society Annual Meeting*, vol. 1, pp. 496-502, 1994.

[99] J. C. Y. Hui, A. Bakhshai and P. K. Jain, "A sensorless adaptive maximum power point extraction method with voltage feedback control for small wind turbines in off-grid applications," *IEEE Journal of Emerging and Selected Topics in Power Electronics*, vol. 3, no. 3, pp. 817-828, 2015.

[100] C. Korlinchak, M. Comanescu, “Sensorless field orientation of an induction motor drive using a time-varying observer,” *IET Electric Power Applications,* vol. 6, no. 6, pp. 353 – 361, 2012.

[101] N. Bensiali, E. Etien, N. Benalia, “Convergence analysis of back-EMF MRAS observers used in sensorless control of induction motor drives”, *Mathematics and Computers in Simulation,* vol. 115, pp. 12–23, 2015.

[102] K. Zhao; X. You, “Speed estimation of induction motor using modified voltage model flux estimation”, *IEEE 6th International Power Electronics and Motion Control Conference*, pp. 1979 – 1982, 2009.

[103] S.M. Gadoue, D. Giaouris, J.W. Finch, “Sensorless Control of Induction Motor Drives at Very Low and Zero Speeds Using Neural Network Flux Observers”, *IEEE Transactions on Industrial Electronics,* vol. 56, no. 8, pp. 3029 - 3039, 2009.

[104] S.M. Gadoue, D. Giaouris, J.W. Finch, “Stator current model reference adaptive systems speed estimator for regenerating-mode low-speed operation of sensorless induction motor drives”, *IET Electric Power Applications,* vol. 7, no. 7, pp. 597 - 606, 2013.

[105] T. Orlowska-Kowalska, M. Dybkowski,” Stator-Current-Based MRAS Estimator for a Wide Range Speed-Sensorless Induction-Motor Drive”, *IEEE Transactions on Industrial Electronics,* vol. 57, no. 4, pp. 1296 - 1308, 2010.

[106] R. Cardenas, R. Pena, J. Proboste, G. Asher and J. Clare, "MRAS observer for sensorless control of standalone doubly fed induction generators," in *IEEE Transactions on Energy Conversion,* vol. 20, no. 4, pp. 710-718, Dec. 2005.

[107] A. Merabet, M. Ouhrouche and R.T. Bui (2008), “Neural generalized predictive control with reference control model for induction motor drive”, *Control and Intelligent Systems*, vol. 36, no. 2, pp. 144-154

[108] Wikipedia, "Real-time simulation," 2013, Available at https://en.wikipedia.org/wiki/Real-time_simulation

[109] Dufour, C., Andrade, C. & Bélanger, J., Real-Time Simulation Technologies in Education: a Link to Modern Engineering Methods and Practices. Retrieved October 3, 2014, from: http://www.opal-rt.com/technical-document/real-time-simulation-technologies-education-link-modernengineering-methods-and

[110] J. Belanger, P.Venne, and J. N. Paquin, "The What, Where, and Why of Real-Time Simulation," in Planet RT, October 2010.

[111] RT-Lab Quick Guide. Retrieved June 07, 2015, from: http://www.opal-rt.com/

[112] Banks, J., Carson, J., Nelson, B. & Nicol D. (2001). Discrete-Event System Simulation. (3nd ed.). Prentice Hall.

[113] K. Bao, “Battery Charge and Discharge Control For Energy Management in Edv and Utility Integration”, University of Alabama, Tuscaloosa, Alabama

[114] ARTEMiS User Guide. Retrieved June 07, 2015, from: http://www.opal-rt.com/

[115] RT-Event Guide. Retrieved June 07, 2015, from: http://www.opal-rt.com/